TIDAL PROPAGATION

IN THE

GULF OF CARPENTARIA

by

Michele Marie Rienecker
B.Sc.(Hons.), University of Queensland

Thesis submitted for the degree of
Doctor of Philosophy

in the

University of Adelaide
Department of Applied Mathematics

December 1978

TABLE OF CONTENTS

SUMMARY

This thesis considers tidal propagation in a rectangular resonator-channel system, with specific reference to the Gulf of Carpentaria, situated to the North of Australia.

The linearized form of the two-dimensional depth-averaged equations of continuity and momentum conservation is used. An analytic solution is found by dividing the area into regions of constant depth. In this manner, a solution is found for the case of a single connecting channel and then for the extended case of two connecting channels, associated with either neglecting or including the effect of tidal flux from Torres Strait into the Gulf.

Results from the analytic model are used to provide tidal inputs for two numerical models, both of which use explicit finite-difference approximations. The first numerical model is linear and is developed to account for realistic boundary and bathymetry variations, with the emphasis on obtaining a model with small computer time and memory requirements. Since, in shallower coastal areas, the non-linear terms in the continuity and momentum equations become more important, the second numerical model developed includes these terms to determine their effect on the resonator as a whole. The two models show favourable agreement, thus verifying the usefulness of the linear model.

SIGNED STATEMENT

I hereby declare that this thesis contains no material which has been accepted for the award of any other degree or diploma in any University and, to the best of my knowledge, it contains no material previously published by any other person, except where due reference is made in the text of the thesis.

M.M. RIENECKER.

ACKNOWLEDGEMENTS

I would like to thank my supervisor, Dr. B.J. Noye, for his advice and guidance in completing this thesis.

Many thanks are also due to Dr. Michael Teubner for his help and encouragement throughout, to Mrs. Angela McKay for her excellent, accurate typing, to Mr. G. de Vries for preparing the diagrams and to Mr. Phil Leppard for his advice on computing.

The work associated with this thesis was carried out from February 1975 to November 1978, during which time I was financed by a Commonwealth Postgraduate Research Award.

M.M. Rienecker.

CHAPTER 1

INTRODUCTION

The Gulf of Carpentaria, located in the North-Eastern part of Australia, is an area of difficult access by either land or water and hence remains relatively uncharted and unstudied. However, over the past few years, there has been an increase in the number of research programs in the area as its potential for the lucrative mining and fishing industries has been recognized. Limited sectors, such as at Weipa, Port McArthur, Groote Eylandt and Gove Peninsular, have been surveyed as port facilities were required by mining companies. The C.S.I.R.O. has reported on the hydrology of the region (Rochford (1966), Newell (1973)) and has made a preliminary study of the circulation in the Gulf (Cresswell (1971)). Further work by this organization is currently under way. The Gulf was also chosen by Teleki et al (1973), as the test site for assessing the usefulness of satellite imagery to the mapping of hydrological parameters in areas of difficult access.

Tides and wind are the only two mechanisms which generate the currents in the area. For several months of the year it is the influence of the strong, steady trade winds which drive the circulation. However, overall, the circulation and mixing of waters in the Gulf are governed by the clockwise motion of tides and by density gradients resulting from the stratification of the water masses. Stratification is partly induced by differential evaporation rates between the Northern and Southern halves of the bay (Teleki et al (1973)). According to Newell (1973), "the annual evaporation/precipitation budget of the Gulf forms a very small part of

the total water exchange but is of great importance in influencing water movement."

One example of the effect, in the Gulf, of winds and precipitation/evaporation is the striking feature of the annual cycle of about .7m in the tides, the lowest tides being recorded at the end of the dry season and the highest during the wet season. It is during the wet season, which occurs in the summer months, that the activity of cyclones sometimes has a disastrous effect, causing large surges. Some description of this is given by Easton (1970) who outlines the general tidal features of the Gulf.

Realistic and accurate modelling of the water movement in the Gulf of Carpentaria is obviously an intricate affair, it being necessary to incorporate the effects of tide, wind, stratification, precipitation/evaporation and pressure surges, not to mention river run-off and sediment transport. However, whereas the effects of the other mechanisms diminish at certain times of the year, tidal forcing is always present; and it is only the response of the Gulf to tidal forcing which is investigated in this thesis. Once the tidal response is understood, it is easier to study the coupling of the tide with other effects.

The tides are caused by the movement of the sun and the moon and their changing gravitational pull on the water of the earth; however, in coastal areas, such as gulfs and estuaries, away from the deep oceans, astronomical tidal forcing can usually be neglected compared to the direct forcing from the motion of adjacent waters. From the results of Hamblin (1976) for different size basins, the maximum amplitude of the response of the Gulf of Carpentaria to direct astronomical forcing could be expected to be only about 3 cm, a very small contribution to the response as a whole.

In this thesis, tidal propagation in Gulf systems is investigated by finding the response of the system to tidal forcing on an open boundary.

One of the main problems in ascertaining the accuracy or limitations of any model of an area is that reliable input data across the open boundary is rarely available, especially if the boundary is wide. Data is usually available from coastal areas, but this may be disturbed by local effects and is not always representative for the open sea. Values may be interpolated between coastal areas, but this does not normally take into account the distribution of depth (see Hansen (1962)). A more accurate input may be obtained from the results of an analytic model which produces the input from the solution to the model equations. This still does not account for the true distribution of depth, but avoids the need to interpolate over wide areas.

Analytic models have their limitations in that they provide solutions only for simplified situations; however, they can be very useful in providing an insight into the important features of a model area. As well as providing the tidal forcing data along an open boundary for numerical models, they may also act as a guideline to the accuracy or validity of these more complicated models.

With this in mind, two analytic models of the tidal propagation in the Gulf of Carpentaria are developed. They are essentially extensions of Taylor's (1920a) problem of the reflection of a Kelvin wave by an end barrier in a semi-infinite channel.

Williams (1972) modelled the Gulf as a rectangular resonator on a semi-infinite channel. His first model neglects the effect of the Coriolis force; his second considers the frequency of rotation of the earth to be small compared to the frequency of the tidal motion.

The models in this thesis are extensions of his work, incorporating, amongst other things, the dissipation of energy by bottom friction. Although the Coriolis parameter is taken to be a constant, no assumption is made as

to its value relative to the forcing frequency and, hence, this model is applicable to more general situations.

The solutions are found for the linearized form of the two-dimensional depth-integrated equations of continuity and momentum conservation. When it is impossible to find a solution which satisfies a boundary condition exactly, a Galerkin technique is used to find an approximate solution.

The first model, in keeping with Williams (1972), considers no flux through Torres Strait, while the second allows for the presence of tidal forcing through this Strait by incorporating a second semi-infinite channel in the model. Torres Strait is a shallow region with an intricate array of islands, reefs and atolls. It is not considered that the tides in this area have been modelled accurately; only the effect of motion through the Strait on the tides in the Gulf is of interest.

The results from the second model are used as input for a linear numerical model which accounts for more complicated boundaries and bottom topography. This numerical model is a frequency-response scheme, based on the EVP method described by Roache (1972), rather than a time-stepping model, and has the asset of requiring very little computer time and storage. Its results also compare very well with a more complicated non-linear numerical scheme which is developed to determine the effects of the non-linear terms on the tidal motion in the Gulf and to assess the usefulness of the more simple linear model. Both numerical models use a finite-difference approximation to the two-dimensional depth-integrated form of the equations of continuity and momentum conservation which govern fluid motion.

CHAPTER 2

THE PROBLEM: A RECTANGULAR RESONATOR ON A SEMI-INFINITE CHANNEL

2.1 The Tidal Equations

The general two-dimensional depth-averaged equations governing fluid motion have been derived by such authors as Dronkers (1964) and Nihoul (1975). These equations, as given by Nihoul, may be written in vector form as

$$\frac{\partial}{\partial t}(h+Z) + \nabla.\{(h+Z)\underset{\sim}{q}\} = 0 \qquad 2.1.1a$$

$$\frac{\partial \underset{\sim}{q}}{\partial t} + \underset{\sim}{q}.\nabla\underset{\sim}{q} + f\ \underset{\sim}{k}\wedge\underset{\sim}{q} = -\nabla(gZ) - \frac{\gamma}{h+Z}\,\underset{\sim}{q}\|\underset{\sim}{q}\| + \underset{\sim}{\xi} \qquad 2.1.1b$$

where $\underset{\sim}{q} = (U,V)$ is the depth-averaged horizontal velocity,

h is the depth at mean-sea-level,

Z is the surface elevation above mean-sea-level,

t is the time coordinate,

f is the Coriolis parameter,

$\underset{\sim}{k}$ is the unit vector in the vertical direction,

g is the acceleration due to gravity,

γ is a bottom friction parameter,

$\nabla \equiv (\frac{\partial}{\partial x}, \frac{\partial}{\partial y})$

x,y are orthogonal Cartesian coordinates, positively increasing to the East and North respectively,

and $\underset{\sim}{\xi}$ represents the contribution from other factors such as external forces, atmospheric pressure gradients, wind stress effects and turbulence and shear effects.

In this study of the response of some systems to tidal forcing on an open boundary, the effects of the term $\underset{\sim}{\xi}$ are neglected. The equations 2.1.1 can be further simplified to yield linear equations which have the advantage of superposition of solutions. The assumptions (and a discussion of their validity) implicit in such an approximation may be found, for example, in Hendershott and Munk (1970) and Noye and Tronson (1978).

The linearized shallow water wave equations may then be written

$$\frac{\partial}{\partial x}(hU) + \frac{\partial}{\partial y}(hV) = - \frac{\partial Z}{\partial t} \qquad 2.1.2a$$

$$\frac{\partial U}{\partial t} + \frac{r}{h}U - f V = - g \frac{\partial Z}{\partial x} \qquad 2.1.2b$$

$$\frac{\partial V}{\partial t} + \frac{r}{h}V + f U = - g \frac{\partial Z}{\partial y} \qquad 2.1.2c$$

in which the Coriolis parameter is considered to be constant and the friction parameter, r, is some linear approximation to $\gamma \| \underset{\sim}{q} \|$. A discussion of this linearization of the quadratic friction term is given in Appendix 1 along with different forms which may be used to model γ .

2.2 Frequency Response Analysis

Equations 2.1.2 are used to model the tidal propagation in a channel-resonator system, as shown in Figure 2.1, where the motion is produced in response to an input $\mathrm{Re}\{\zeta_0(x,y)e^{-i\omega t}\}$, of period $T = 2\pi/\omega$, travelling along the channel in the positive x-direction. The equations are solved subject to the input $\zeta_0 e^{-i\omega t}$ and the real parts of the solutions for Z, U and V will give the elevation and velocity fields at any instant in time. $(i = \sqrt{-1})$.

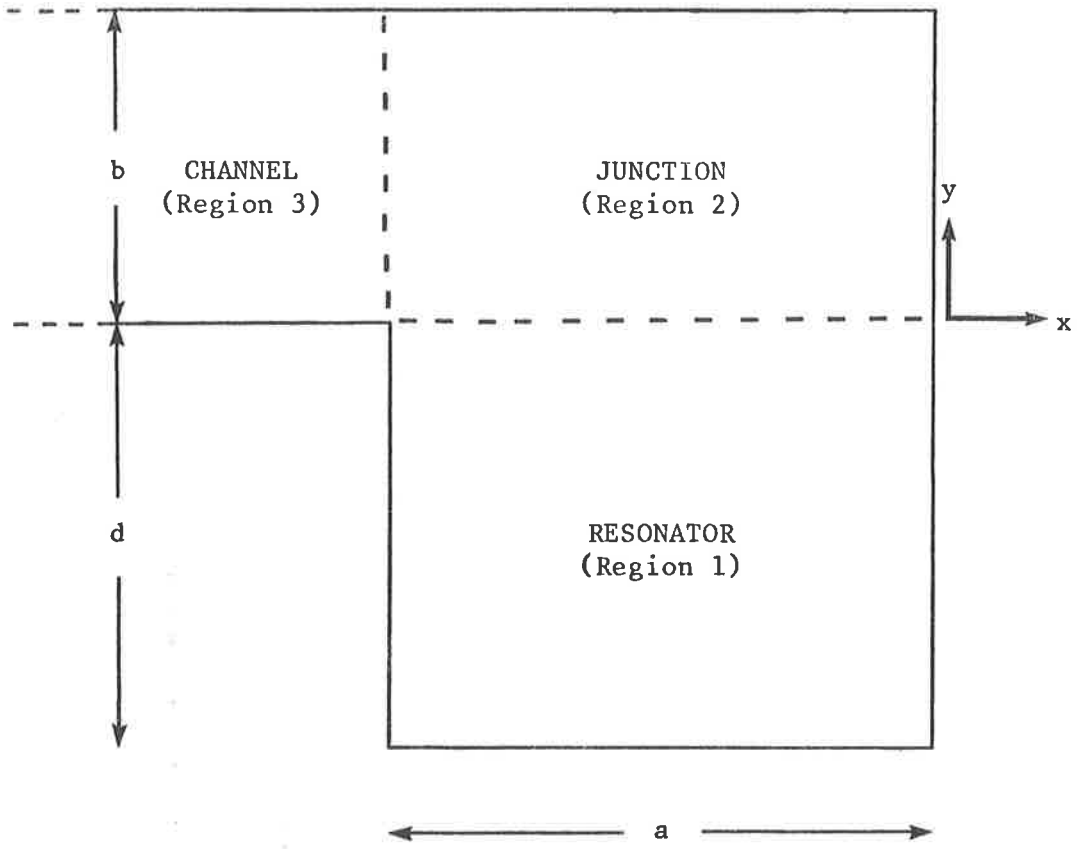

Figure 2.1 A rectangular resonator on a semi-infinite channel. The area is divided into three regions with a depth-step at the common boundaries of each region.

Since the equations are linear, it follows that

$$Z(x,y,t) = \zeta(x,y)e^{-i\omega t}$$

$$U(x,y,t) = u(x,y)e^{-i\omega t}$$

$$V(x,y,t) = v(x,y)e^{-i\omega t}$$

so that the explicit time dependence in 2.1.2 may be removed. The equations governing the spatial variation of the fluid motion are therefore

$$(-i\omega+r/h)u - fv = -g\frac{\partial\zeta}{\partial x} \qquad 2.2.1a$$

$$(-i\omega+r/h)v + fu = -g\frac{\partial\zeta}{\partial y} \qquad 2.2.1b$$

$$\frac{\partial}{\partial x}(hu) + \frac{\partial}{\partial y}(hv) = i\omega\zeta \qquad 2.2.1c$$

subject to the boundary conditions

$$u(0,y) = 0, \quad -d \leq y \leq b \qquad 2.2.2a$$

$$u(-a,y) = 0, \quad -d \leq y < 0 \qquad 2.2.2b$$

$$v(x,-d) = 0, \quad -a \leq x \leq 0 \qquad 2.2.2c$$

$$v(x,b) = 0, \quad x \leq 0 \qquad 2.2.2d$$

$$v(x,0) = 0, \quad x < -a \qquad 2.2.2e$$

and a radiation condition that the input wave does not excite other waves travelling in the same direction.

2.3 Reformulation of the Equations for an Analytic Model

The equations 2.2.1 can be solved analytically if it is assumed that the depth is a constant; the equations being formulated in terms of $\zeta(x,y)$ only and the solution found by a separation of variables technique. Manipulation of equations 2.2.1a and b yields the relations

$$u(x,y) = -g\{(-i\omega+r/h)^2 + f^2\}^{-1}\{(-i\omega+r/h)\frac{\partial\zeta}{\partial x} + f\frac{\partial\zeta}{\partial y}\} \qquad 2.3.1a$$

$$v(x,y) = -g\{(-i\omega+r/h)^2 + f^2\}^{-1}\{-f\frac{\partial\zeta}{\partial x} + (-i\omega+r/h)\frac{\partial\zeta}{\partial y}\} \qquad 2.3.1b$$

and substitution of these expressions into 2.2.1c yields the differential equation governing ζ :-

$$\nabla^2\zeta + \frac{i\omega}{gh}\frac{\{(-i\omega+r/h)^2+f^2\}}{(-i\omega+r/h)}\zeta = 0 \qquad 2.3.2$$

Defining

$$\phi = r/h\omega \qquad 2.3.3a$$

$$\theta = f/\omega \qquad 2.3.3b$$

$$\chi^2 = \frac{\omega^2}{gh}\frac{\{(1+i\phi)^2-\theta^2\}}{(1+i\phi)} \quad , \qquad 2.3.3c$$

these equations may be rewritten as

$$u(x,y) = -\frac{g}{\omega}\{(1+i\phi)^2-\theta^2\}^{-1}\{i(1+i\phi)\frac{\partial\zeta}{\partial x} - \theta\frac{\partial\zeta}{\partial y}\} \qquad 2.3.4a$$

$$v(x,y) = -\frac{g}{\omega}\{(1+i\phi)^2-\theta^2\}^{-1}\{\theta\frac{\partial\zeta}{\partial x} + i(1+i\phi)\frac{\partial\zeta}{\partial y}\} \qquad 2.3.4b$$

$$\nabla^2\zeta + \chi^2\zeta = 0 \qquad 2.3.5$$

and solved subject to the conditions 2.2.2.

CHAPTER 3

THE ANALYTIC SOLUTION

3.1 The Method of Solution and the Boundary Conditions

To find the solution to equations 2.3.4 and 2.3.5 in the area depicted in Figure 2.1, the system is divided into three constant depth regions as shown - the channel, the junction and the resonator. The equations are solved (as far as possible) in each separate region and then the elevations and volume transports are matched at the common boundaries of adjacent regions.

Thus, the solutions are required to the equations

$$(\nabla^2 + \chi_j^2)\zeta_j = 0, \quad j = 1,2,3$$

subject to the conditions

(i) $v_3(x,0) = v_3(x,b) = 0, \quad x \leq -a$

(ii) $v_2(x,b) = 0, \quad -a \leq x \leq 0$

(iii) $u_2(0,y) = 0, \quad 0 \leq y \leq b$

(iv) $v_1(x,-d) = 0, \quad -a \leq x \leq 0$

(v) $u_1(0,y) = u_1(-a,y) = 0, \quad -d \leq y \leq 0$

(vi) $\zeta_1(x,0) = \zeta_2(x,0), \quad -a \leq x \leq 0$

(vii) $h_1v_1(x,0) = h_2v_2(x,0), \quad -a \leq x \leq 0$

(viii) $\zeta_2(-a,y) = \zeta_3(-a,y), \quad 0 \leq y \leq b$

(ix) $h_2u_2(-a,y) = h_3u_3(-a,y), \quad 0 \leq y \leq b$

and (x) a radiation condition in the channel region.

(In the above, $j = 1$ refers to the resonator, $j = 2$ to the junction and $j = 3$ to the channel, and each of the $u_j(x,y)$, $v_j(x,y)$ may be found from the appropriate forms of 2.3.4.)

The condition at the corner $(-a,0)$ is given as $v_3(-a,0) = u_1(-a,0) = 0$, while the restrictions $v_2(-a,0) = h_1 v_1(-a,0)/h_2$ and $u_2(-a,0) = h_3 u_3(-a,0)/h_2$ do not necessarily drive these latter velocities to zero and hence could provide a shear effect. Whereas it is recognised that this may be erroneous, the exact condition on the velocity at such corners is not known and the use of the above condition is not considered to be too detrimental to the solution as a whole.

The inclusion of the Coriolis force $(\theta \neq 0)$ prohibits the finding of an exact solution to this system. Even for the simpler problem of a constant depth channel with a barrier at one end (Taylor (1920a), Defant (1961)) one has to resort to an approximate method to find a solution which satisfies the zero normal velocity condition at the closed end of the channel. Here, for those boundary or matching conditions which cannot be satisfied exactly, a Galerkin method, which is an approximation technique, is used. This technique is discussed in Appendix 2.

3.2 Solution for the Channel Region

In the channel region, the equation which governs the surface elevation is

$$\nabla^2 \zeta_3 + \chi_3^2 \zeta_3 = 0, \qquad 3.2.1$$

where

$$\chi_3^2 = \frac{\omega^2}{gh_3} \frac{\{(1+i\phi_3)^2-\theta^2\}}{(1+i\phi_3)}, \qquad 3.2.2$$

subject to

$$v_3(x,0) = v_3(x,b) = 0, \quad \text{for} \quad x \leq -a \qquad 3.2.3$$

and the radiation condition.

The general solution, found by separation of variables, is

$$\zeta_3(x,y) = \zeta_0(x,y) + A_0 e^{-i k_3^{(0)} x + K_3 y}$$

$$+ \sum_{\ell=1}^{\infty} A_\ell \, e^{-i k_3^{(\ell)} x} \left\{ \cos\frac{\ell\pi y}{b} + \frac{\theta}{(1+i\phi_3)} \, k_3^{(\ell)} \frac{b}{\ell\pi} \sin\frac{\ell\pi y}{b} \right\}, \quad 3.2.4$$

where $\zeta_0(x,y)$ is the input described in Section 2.2 and

$$K_3 = \theta \left\{ \frac{\omega^2}{g h_3} \frac{1}{(1+i\phi_3)} \right\}^{1/2} \quad 3.2.5$$

$$k_3^{(0)} = \left\{ \frac{\omega^2}{g h_3} (1+i\phi_3) \right\}^{1/2} \quad 3.2.6a$$

$$k_3^{(\ell)} = \left\{ \chi_3^2 - (\ell\pi/b)^2 \right\}^{1/2}, \ \ell \in \mathbb{Z}^+ \quad 3.2.6b$$

with $\mathrm{Re}\{k_3^{(\ell)}\} > 0$ so that the radiation condition is satisfied. It immediately follows that $\mathrm{Im}\{k_3^{(\ell)}\} > 0$ so that the waves with coefficient A_ℓ, which travel back up the channel, have a finite amplitude as $x \to -\infty$.

The input wave must also satisfy 3.2.1 and 3.2.3, so that

$$\zeta_0(x,y) = \alpha_0 e^{i k_3^{(0)} x - K_3 y}$$

$$+ \sum_{\ell=1}^{\infty} \alpha_\ell \, e^{i k_3^{(\ell)} x} \left\{ \cos\frac{\ell\pi y}{b} - \frac{\theta}{(1+i\phi_3)} \, k_3^{(\ell)} \frac{b}{\ell\pi} \sin\frac{\ell\pi y}{b} \right\}. \quad 3.2.7$$

Each component in 3.2.7 decays exponentially as x increases. If the rate of decay of the zeroth mode is less than that of the higher modes and the channel is sufficiently long, the contribution to $\zeta_0(x,y)$ from the higher modes ($\ell > 0$) can be neglected relative to the contribution from the wave corresponding to $\ell = 0$. Hence, the input wave is approximated as

$$\zeta_0(x,y) = e^{i k_3^{(0)} x - K_3 y} \quad 3.2.8$$

and the surface elevation in the channel region may be written

$$\zeta_3(x,y) = e^{i k_3^{(0)} x - K_3 y} + A_0\, e^{-i k_3^{(0)} x + K_3 y}$$

$$+ \sum_{\ell=1}^{\infty} A_\ell\, e^{-i k_3^{(\ell)} x}\left\{\cos\frac{\ell\pi y}{b} + \frac{\theta}{(1+i\phi_3)}\, k_3^{(\ell)}\, \frac{b}{\ell\pi}\, \sin\frac{\ell\pi y}{b}\right\} \qquad 3.2.9$$

The coefficient α_0 is omitted in 3.2.8 and 3.2.9 since the system is linear and α_0 serves only as a scaling factor. Relative amplitudes and phases at different locations may be obtained by using 3.2.8 as input, and the actual amplitude or phase at any location may be found if the results are scaled according to some reference point.

Using the relations 2.3.4, the velocities are found to be

$$u_3(x,y) = \frac{-g}{\omega(1+i\phi_3)}\left[- k_3^{(0)}\, e^{i k_3^{(0)} x - K_3 y} + A_0 k_3^{(0)}\, e^{-i k_3^{(0)} x + K_3 y}\right.$$

$$\left. + \sum_{\ell=1}^{\infty} A_\ell\, e^{-i k_3^{(\ell)} x}\left\{k_3^{(\ell)}\, \cos\frac{\ell\pi y}{b} + \theta\, \frac{b}{\ell\pi}\, \frac{\omega^2}{g h_3}\, \sin\frac{\ell\pi y}{b}\right\}\right]. \qquad 3.2.10$$

$$v_3(x,y) = \frac{ig}{\omega(1+i\phi_3)} \sum_{\ell=1}^{\infty} A_\ell\, e^{-i k_3^{(\ell)} x}\, \frac{b}{\ell\pi}\left[K_3^2 + \left(\frac{\ell\pi}{b}\right)^2\right]\sin\frac{\ell\pi y}{b} \quad . \qquad 3.2.11$$

3.3 Solution for the Resonator Region

To determine the surface elevation in the resonator, the equation

$$\nabla^2\zeta_1 + \chi_1^2\zeta_1 = 0, \qquad 3.3.1$$

where

$$\chi_1^2 = \frac{\omega^2}{g h_1}\, \frac{\{(1+i\phi_1)^2 - \theta^2\}}{(1+i\phi_1)}\ , \qquad 3.3.2$$

must be solved, subject to the conditions

$$u_1(-a,y) = u_1(0,y) = 0, \quad -d \leq y \leq 0 \qquad 3.3.3$$

$$v_1(x,-d) = 0, \quad -a \leq x \leq 0. \qquad 3.3.4$$

The separation of variables technique is used once again to obtain a solution which satisfies 3.3.3, resulting in the expression

$$\begin{aligned}\zeta_1(x,y) = {} & B_0\left\{\cosh K_1x \cos p_0(y+d) + i \sinh K_1x \sin p_0(y+d)\right\} \\ & + \sum_{\ell=1}^{\infty} B_\ell\left\{\cos\frac{\ell\pi x}{a} \cos p_\ell(y+d) + \frac{i\theta}{(1+i\phi_1)} \frac{a}{\ell\pi} p_\ell \sin\frac{\ell\pi x}{a} \sin p_\ell(y+d)\right\} \\ & + C_0\left\{\cosh K_1x \sin p_0(y+d) - i \sinh K_1x \cos p_0(y+d)\right\} \\ & + \sum_{\ell=1}^{\infty} C_\ell\left\{\cos\frac{\ell\pi x}{a} \sin p_\ell(y+d) - \frac{i\theta}{(1+i\phi_1)} \frac{a}{\ell\pi} p_\ell \sin\frac{\ell\pi x}{a} \cos p_\ell(y+d)\right\},\end{aligned} \tag{3.3.5}$$

where

$$K_1 = \theta\left\{\frac{\omega^2}{gh_1} \frac{1}{(1+i\phi_1)}\right\}^{\frac{1}{2}} \tag{3.3.6}$$

$$p_0 = \left\{\frac{\omega^2}{gh_1} (1+i\phi_1)\right\}^{\frac{1}{2}} \tag{3.3.7a}$$

$$p_\ell = \left\{\chi_1^2 - \left(\frac{\ell\pi}{a}\right)^2\right\}^{\frac{1}{2}}, \quad \ell \in \mathbb{Z}^+ . \tag{3.3.7b}$$

The condition 3.3.4, which cannot be satisfied exactly, is treated, using the Galerkin process, in Section 3.5.

The velocities may be found from 2.3.4 and are

$$\begin{aligned}u_1(x,y) = {} & \frac{ig}{\omega(1+i\phi_1)} \sum_{\ell=1}^{\infty} \frac{a}{\ell\pi}\left\{K_1^2 + \left(\frac{\ell\pi}{a}\right)^2\right\}\left\{B_\ell \cos p_\ell(y+d)\right. \\ & \left. + C_\ell \sin p_\ell(y+d)\right\}\sin\frac{\ell\pi x}{a}\end{aligned} \tag{3.3.8}$$

$$\begin{aligned}v_1(x,y) = {} & \frac{-g}{\omega(1+i\phi_1)}\Big[- B_0p_0\left\{\sinh K_1x \cos p_0(y+d) + i \cosh K_1x \sin p_0(y+d)\right\} \\ & - \sum_{\ell=1}^{\infty} B_\ell\left\{\theta\frac{\omega^2}{gh_1} \frac{a}{\ell\pi} \sin\frac{\ell\pi x}{a} \cos p_\ell(y+d) + i\, p_\ell \cos\frac{\ell\pi x}{a} \sin p_\ell(y+d)\right\} \\ & + C_0p_0\left\{- \sinh K_1x \sin p_0(y+d) + i \cosh K_1x \cos p_0(y+d)\right\} \\ & - \sum_{\ell=1}^{\infty} C_\ell\left\{\theta\frac{\omega^2}{gh_1} \frac{a}{\ell\pi} \sin\frac{\ell\pi x}{a} \sin p_\ell(y+d) - i\, p_\ell \cos\frac{\ell\pi x}{a} \cos p_\ell(y+d)\right\}\Big].\end{aligned} \tag{3.3.9}$$

3.4 Solution for the Junction Region

The surface elevation in the junction must satisfy the equation

$$\nabla^2\zeta_2 + \chi_2^2\zeta_2 = 0, \qquad 3.4.1$$

where

$$\chi_2^2 = \frac{\omega^2}{gh_2}\,\frac{\{(1+i\phi_2)^2-\theta^2\}}{(1+i\phi_2)}\ , \qquad 3.4.2$$

and the conditions

$$v_2(x,b) = 0, \quad -a \leqslant x \leqslant 0 \qquad 3.4.3$$

$$u_2(0,y) = 0, \quad 0 \leqslant y \leqslant b\ . \qquad 3.4.4$$

The solution to 3.4.1, which also satisfies 3.4.3, may be written as

$$\zeta_2(x,y) = \int_{-\infty}^{\infty} \beta(\lambda)e^{-i\lambda x}\{\lambda\theta \sinh s(y-b) + s(1+i\phi_2)\cosh s(y-b)\}d\lambda\ , \qquad 3.4.5$$

where $\lambda^2 - s^2 = \chi_2^2$ 3.4.6

and $\beta(\lambda)$ is an unknown complex function of λ .

Only a discrete set of λ-values satisfies the matching condition (vii) given in Section 3.1,

$$h_1v_1(x,0) = h_2v_2(x,0), \quad -a \leqslant x \leqslant 0. \qquad 3.4.7$$

From 3.4.5 it is found that

$$\theta\,\frac{\partial\zeta_2}{\partial x}(x,0) + i(1+i\phi_2)\frac{\partial\zeta_2}{\partial y}(x,0)$$

$$= i\int_{-\infty}^{\infty} \beta(\lambda)e^{-i\lambda x}\{\lambda^2\theta^2 - s^2(1+i\phi_2)^2\}\sinh sb\, d\lambda \qquad 3.4.8$$

so that 3.4.7 may be written as

$$i \int_{-\infty}^{\infty} \beta(\lambda) e^{-i\lambda x} \left\{\lambda^2\theta^2 - s^2(1+i\phi_2)^2\right\} \sinh sb \, d\lambda$$

$$= \Omega\Big[- B_0 p_0 \left\{\sinh K_1 x \cos p_0 d + i \cosh K_1 x \sin p_0 d\right\}$$

$$- \sum_{\ell=1}^{\infty} B_\ell \left\{\theta \frac{\omega^2}{gh_1} \frac{a}{\ell\pi} \cos p_\ell d \sin \frac{\ell\pi x}{a} + i\, p_\ell \sin p_\ell d \cos \frac{\ell\pi x}{a}\right\}$$

$$+ C_0 p_0 \left\{- \sinh K_1 x \sin p_0 d + i \cosh K_1 x \cos p_0 d\right\}$$

$$- \sum_{\ell=1}^{\infty} C_\ell \left\{\theta \frac{\omega^2}{gh_1} \frac{a}{\ell\pi} \sin p_\ell d \sin \frac{\ell\pi x}{a} - i\, p_\ell \cos p_\ell d \cos \frac{\ell\pi x}{a}\right\}\Big] , \qquad 3.4.9$$

in which

$$\Omega = \frac{h_1}{h_2} \frac{\{(1+i\phi_2)^2 - \theta^2\}}{(1+i\phi_1)} .$$

Hence

$$\frac{i}{2\pi} \int_{-a}^{0} e^{i\lambda x} \int_{-\infty}^{\infty} \beta(\mu) e^{-i\mu x} \left\{\mu^2\theta^2 - s^2(1+i\phi_2)^2\right\} \sinh sb \, d\mu \, dx$$

$$= \frac{\Omega}{2\pi} \int_{-a}^{0} e^{i\lambda x} \Big\{g_0 \cosh K_1 x + f_0 \sinh K_1 x$$

$$+ \sum_{n=1}^{\infty} g_n \cos \frac{n\pi x}{a} + \sum_{n=1}^{\infty} f_n \sin \frac{n\pi x}{a}\Big\} dx, \qquad 3.4.10$$

where

$$g_0 = i\, p_0 [- B_0 \sin p_0 d + C_0 \cos p_0 d]$$

$$f_0 = - p_0 [B_0 \cos p_0 d + C_0 \sin p_0 d]$$

$$g_n = i\, p_n [- B_n \sin p_n d + C_n \cos p_n d], \; n \in \mathbb{Z}^+$$

$$f_n = - \theta \frac{a}{n\pi} \frac{\omega^2}{gh_1} [B_n \cos p_n d + C_n \sin p_n d], \; n \in \mathbb{Z}^+ . \qquad 3.4.11$$

To evaluate the left-hand-side of the equality sign in 3.4.10, the definition of $v_2(x,0)$ is extended to the infinite domain by

$$v_2(x,0) = \begin{cases} 0 & , \; x < -a \\ v_2(x,0), & -a \leq x \leq 0 \\ 0 & , \; x > 0 \end{cases} .$$

The definition for $x < -a$ is essentially an analytic continuation into region 3. The extension for $x > 0$ is quite arbitrary, but, as long as the results are not used outside the original domain of definition of $v_2(x,y)$, this device causes no loss in generality.

Thus, equation 3.4.10 reduces to

$$\beta(\lambda)\, i\{\lambda^2\theta^2 - s^2(1+i\phi_2)^2\}\sinh sb$$

$$= \frac{\Omega}{2\pi}\left\{\frac{g_0}{\lambda^2+K_1^2}[-i\lambda + e^{-i\lambda a}\{i\lambda\cosh K_1a + K_1\sinh K_1a\}]\right.$$

$$+ \frac{f_0}{\lambda^2+K_1^2}[K_1 - e^{-i\lambda a}\{i\lambda\sinh K_1a + K_1\cosh K_1a\}]$$

$$- \sum_{n=1}^{\infty} g_n \frac{i\lambda}{\lambda^2-(\frac{n\pi}{a})^2}[1 - (-1)^n e^{-i\lambda a}]$$

$$\left. + \sum_{n=1}^{\infty} f_n \frac{n\pi/a}{\lambda^2-(\frac{n\pi}{a})^2}[1 - (-1)^n e^{-i\lambda a}]\right\} \qquad 3.4.12$$

The expression for $\beta(\lambda)$ which is obtained from 3.4.12 may be substituted into 3.4.5 to yield the new expression for $\zeta_2(x,y)$ which now satisfies 3.4.7, the condition which ensures the continuity of volume flux from region 1 to region 2:-

$$\zeta_2(x,y) = \frac{\Omega}{2\pi}\left[-\int_{-\infty}^{\infty} e^{-i\lambda x}\,\frac{\{\lambda g_0 + iK_1 f_0\}}{\lambda^2+K_1^2}\,\Phi(\lambda)d\lambda\right.$$

$$+ \int_{-\infty}^{\infty} e^{-i\lambda(x+a)}\{g_0[\lambda\cosh K_1a - iK_1\sinh K_1a]$$

$$- f_0[\lambda\sinh K_1a - iK_1\cosh K_1a]\}\frac{\Phi(\lambda)}{\lambda^2+K_1^2}d\lambda$$

$$- \sum_{n=1}^{\infty}\int_{-\infty}^{\infty} e^{-i\lambda x}\,\frac{\{\lambda g_n + i\frac{n\pi}{a}f_n\}}{\lambda^2 - (\frac{n\pi}{a})^2}\,\Phi(\lambda)\,d\lambda$$

$$\left. + \sum_{n=1}^{\infty}(-1)^n\int_{-\infty}^{\infty} e^{-i\lambda(x+a)}\,\frac{\{\lambda g_n + i\frac{n\pi}{a}f_n\}}{\lambda^2 - (\frac{n\pi}{a})^2}\,\Phi(\lambda)d\lambda\right], \qquad 3.4.13$$

where

$$\Phi(\lambda) = \frac{\lambda\theta \sinh s(y-b)+s(1+i\phi_2)\cosh s(y-b)}{\{\lambda^2\theta^2-s^2(1+i\phi_2)^2\}\sinh sb} . \qquad 3.4.14$$

The details of the contour integration used to evaluate these integrals are given in Appendix 3, the result being

$$\begin{aligned}\zeta_2(x,y) = {} & E_0 e^{ik_2^{(0)}x - K_2(y-b)} + G_0 e^{-ik_2^{(0)}x + K_2(y-b)} \\ & + \sum_{\ell=1}^{\infty} E_\ell e^{ik_2^{(\ell)}x}\left[\cos\frac{\ell\pi y}{b} - \frac{\theta}{(1+i\phi_2)}\frac{b}{\ell\pi}k_2^{(\ell)}\sin\frac{\ell\pi y}{b}\right] \\ & + \sum_{\ell=1}^{\infty} G_\ell e^{-ik_2^{(\ell)}x}\left[\cos\frac{\ell\pi y}{b} + \frac{\theta}{(1+i\phi_2)}\frac{b}{\ell\pi}k_2^{(\ell)}\sin\frac{\ell\pi y}{b}\right] \\ & + D_0\left[\cosh K_1 x \cosh s_0(y-b) + \frac{i\theta K_1}{s_0(1+i\phi_2)}\sinh K_1 x \sinh s_0(y-b)\right] \\ & + \sum_{\ell=1}^{\infty} D_\ell\left[\cos\frac{\ell\pi x}{a}\cosh s_\ell(y-b) - \frac{i\theta}{(1+i\phi_2)}\frac{\ell\pi}{as_\ell}\sin\frac{\ell\pi x}{a}\sinh s_\ell(y-b)\right] \\ & + F_0\left[\sinh K_1 x \cosh s_0(y-b) + \frac{i\theta K_1}{s_0(1+i\phi_2)}\cosh K_1 x \sinh s_0(y-b)\right] \\ & + \sum_{\ell=1}^{\infty} F_\ell\left[\sin\frac{\ell\pi x}{a}\cosh s_\ell(y-b) + \frac{i\theta}{(1+i\phi_2)}\frac{\ell\pi}{as_\ell}\cos\frac{\ell\pi x}{a}\sinh s_\ell(y-b)\right] , \end{aligned} \qquad 3.4.15$$

with

$$(D_0,F_0) = \frac{i\Omega\, s_0(1+i\phi_2)}{[\theta^2K_1^2+s_0^2(1+i\phi_2)^2]\sinh s_0 b}\,(g_0,f_0) \qquad 3.4.16a$$

$$(D_\ell,F_\ell) = -\frac{i\Omega\,(1+i\phi_2)s_\ell}{[(\frac{\ell\pi\theta}{a})^2 - s_\ell^2(1+i\phi_2)^2]\sinh s_\ell b}\,(g_\ell,f_\ell),\ \ell\in\mathbb{Z}^+ , \qquad 3.4.16b$$

where

$$
\begin{aligned}
s_0 &= i\left\{K_1^2 + \chi_2^2\right\}^{\frac{1}{2}} \\
s_\ell &= \left\{\left(\frac{\ell\pi}{a}\right)^2 - \chi_2^2\right\}^{\frac{1}{2}}, \quad \ell \in \mathbb{Z}^+ \\
k_2^{(0)} &= \left\{\frac{\omega^2}{gh_2}(1+i\phi_2)\right\}^{\frac{1}{2}} \\
k_2^{(\ell)} &= \left\{\chi_2^2 - \left(\frac{\ell\pi}{b}\right)^2\right\}^{\frac{1}{2}}, \quad \ell \in \mathbb{Z}^+ \\
K_2 &= \theta\left\{\frac{\omega^2}{gh_2}\frac{1}{(1+i\phi_2)}\right\}^{\frac{1}{2}},
\end{aligned}
\tag{3.4.17}
$$

and the f_n and g_n are as defined in 3.4.11.

The velocities, which are obtained using the relations 2.3.4, are

$$
\begin{aligned}
u_2(x,y) = \frac{-g}{\omega(1+i\phi_2)} \Bigg\{ & - E_0 k_2^{(0)} e^{i k_2^{(0)} x - K_2(y-b)} \\
& + G_0 k_2^{(0)} e^{-i k_2^{(0)} x + K_2(y-b)} \\
& + \sum_{\ell=1}^{\infty} E_\ell e^{i k_2^{(\ell)} x}\left[- k_2^{(\ell)} \cos\frac{\ell\pi y}{b} + \theta\frac{b}{\ell\pi}\frac{\omega^2}{gh_2}\sin\frac{\ell\pi y}{b}\right] \\
& + \sum_{\ell=1}^{\infty} G_\ell e^{-i k_2^{(\ell)} x}\left[k_2^{(\ell)} \cos\frac{\ell\pi y}{b} + \theta\frac{b}{\ell\pi}\frac{\omega^2}{gh_2}\sin\frac{\ell\pi y}{b}\right] \\
& + D_0\left[iK_1 \sinh K_1 x \cosh s_0(y-b) + \frac{\theta}{s_0}\frac{\omega^2}{gh_2}\cosh K_1 x \sinh s_0(y-b)\right] \\
& + \sum_{\ell=1}^{\infty} D_\ell\left[- i\frac{\ell\pi}{a}\sin\frac{\ell\pi x}{a}\cosh s_\ell(y-b) + \frac{\theta}{s_\ell}\frac{\omega^2}{gh_2}\cos\frac{\ell\pi x}{a}\sinh s_\ell(y-b)\right] \\
& + F_0\left[iK_1 \cosh K_1 x \cosh s_0(y-b) + \frac{\theta}{s_0}\frac{\omega^2}{gh_2}\sinh K_1 x \sinh s_0(y-b)\right] \\
& + \sum_{\ell=1}^{\infty} F_\ell\left[i\frac{\ell\pi}{a}\cos\frac{\ell\pi x}{a}\cosh s_\ell(y-b) + \frac{\theta}{s_\ell}\frac{\omega^2}{gh_2}\sin\frac{\ell\pi x}{a}\sinh s_\ell(y-b)\right]\Bigg\}
\end{aligned}
\tag{3.4.18}
$$

$$v_2(x,y) = \frac{ig}{\omega(1+i\phi_2)}\Bigg\{ \sum_{\ell=1}^{\infty} E_\ell\, e^{i k_2^{(\ell)} x}\, \frac{b}{\ell\pi}\left[K_2^2 + \left(\frac{\ell\pi}{b}\right)^2\right]\sin\frac{\ell\pi y}{b}$$

$$+ \sum_{\ell=1}^{\infty} G_\ell\, e^{-i k_2^{(\ell)} x}\, \frac{b}{\ell\pi}\left[K_2^2 + \left(\frac{\ell\pi}{b}\right)^2\right]\sin\frac{\ell\pi y}{b}$$

$$+ D_0\,\frac{1}{s_0}\left[K_1^2 + \left(k_2^{(0)}\right)^2\right]\cosh K_1 x \sinh s_0(y-b)$$

$$+ \sum_{\ell=1}^{\infty} D_\ell\,\frac{1}{s_\ell}\left[\left(k_2^{(0)}\right)^2 - \left(\frac{\ell\pi}{a}\right)^2\right]\cos\frac{\ell\pi x}{a}\sinh s_\ell(y-b)$$

$$+ F_0\frac{1}{s_0}\left[K_1^2 + \left(k_2^{(0)}\right)^2\right]\sinh K_1 x \sinh s_0(y-b)$$

$$+ \sum_{\ell=1}^{\infty} F_\ell\,\frac{1}{s_\ell}\left[\left(k_2^{(0)}\right)^2 - \left(\frac{\ell\pi}{a}\right)^2\right]\sin\frac{\ell\pi x}{a}\sinh s_\ell(y-b)\Bigg\}\ . \qquad 3.4.19$$

Williams (1972) has omitted the wave forms associated with the coefficients F_ℓ. Since their presence is not due to the inclusion of friction, nor to the absence of any condition on θ (Williams assumes that θ may be considered small enough to neglect, when convenient, terms of order θ^2), their omission appears to be inconsistent with his earlier analysis using $\theta = 0$.

3.5 The Remaining Matching Conditions and the Galerkin Technique

Not all the conditions listed in Section 3.1 have been satisfied by the expressions found for ζ_1, ζ_2 and ζ_3 which still involve, as yet, unknown complex coefficients. The conditions which remain to be satisfied are

(1) continuity of elevation at $x = -a$, $0 \leq y \leq b$

that is, $\zeta_2(-a,y) = \zeta_3(-a,y)$, $0 \leq y \leq b$ 3.5.1

(2) continuity of volume flux at $x = -a$, $0 \leq y \leq b$

that is, $h_2 u_2(-a,y) = h_3 u_3(-a,y)$, $0 \leq y \leq b$ 3.5.2

(3) continuity of elevation at $y = 0$, $-a \leq x \leq 0$

that is, $\zeta_1(x,0) = \zeta_2(x,0)$, $-a \leq x \leq 0$ 3.5.3

(4) zero normal velocity at the boundary $x = 0$

that is, $u_2(0,y) = 0,\ 0 \leq y \leq b$ 3.5.4

(5) zero normal velocity at the boundary $y = -d$

that is, $v_1(x,-d) = 0,\ -a \leq x \leq 0.$ 3.5.5

Since the expressions for the elevations (3.2.9, 3.3.5, 3.4.15) and velocities (3.2.10, 3.2.11, 3.3.8, 3.3.9, 3.4.18, 3.4.19) involve infinite sums, no explicit expression or value can be found for each coefficient, and it is obvious that no finite combination of terms will satisfy the above conditions exactly. Hence, some approximation technique must be used. Techniques widely used in such circumstances belong to the Method of Weighted Residuals (Finlayson, 1972), from which class, the most commonly used are probably Collocation and the Galerkin method. These, with particular emphasis on the latter, are discussed in Appendix 2. The Galerkin technique is used here.

Each of the series in the expressions for elevations or velocities is truncated after $\ell = N$; and, for each of the five conditions above, (N+1) weighting functions are used. The resulting equations, together with the appropriate 2(N+1) equations from 3.4.16, yield a system of 7(N+1) simultaneous linear equations in the 7(N+1) unknown coefficients A_ℓ, B_ℓ, C_ℓ, D_ℓ, E_ℓ, F_ℓ, G_ℓ, $\ell = 0,1,\ldots,N$.

The five conditions are now treated in turn.

(1) Continuity of elevation at $x = -a$, $0 \leq y \leq b$.

Substitution of 3.2.9 and 3.4.15 into equation 3.5.1 yields

$$E_0 e^{-ik_2^{(0)}a - K_2(y-b)} + \sum_{\ell=1}^{\infty} E_\ell e^{-ik_2^{(\ell)}a}\left[\cos\frac{\ell\pi y}{b} - \beta_\ell \sin\frac{\ell\pi y}{b}\right]$$

$$+ G_0 e^{ik_2^{(0)}a + K_2(y-b)} + \sum_{\ell=1}^{\infty} G_\ell e^{ik_2^{(\ell)}a}\left[\cos\frac{\ell\pi y}{b} + \beta_\ell \sin\frac{\ell\pi y}{b}\right]$$

$$+ D_0\left[\cosh K_1 a \cosh s_0(y-b) - \frac{i\theta K_1}{(1+i\phi_2)s_0}\sinh K_1 a \sinh s_0(y-b)\right]$$

$$+ F_0\left[-\sinh K_1 a \cosh s_0(y-b) + \frac{i\theta K_1}{(1+i\phi_2)s_0}\cosh K_1 a \sinh s_0(y-b)\right]$$

$$+ \sum_{\ell=1}^{\infty} D_\ell(-1)^\ell \cosh s_\ell(y-b) + \sum_{\ell=1}^{\infty} F_\ell \frac{i\theta}{(1+i\phi_2)} \frac{\ell\pi}{as_\ell}(-1)^\ell \sinh s_\ell(y-b)$$

$$= e^{-ik_3^{(0)}a - K_3 y} + A_0 e^{ik_3^{(0)}a + K_3 y}$$

$$+ \sum_{\ell=1}^{\infty} A_\ell e^{ik_3^{(\ell)}a}\left[\cos\frac{\ell\pi y}{b} + \rho_\ell \sin\frac{\ell\pi y}{b}\right] \quad , \qquad 3.5.6$$

where

$$\beta_\ell = \frac{\theta}{(1+i\phi_2)} \frac{b}{\ell\pi} k_2^{(\ell)}, \quad \ell \in \mathbb{Z}^+ \qquad 3.5.7a$$

$$\rho_\ell = \frac{\theta}{(1+i\phi_3)} \frac{b}{\ell\pi} k_3^{(\ell)}, \quad \ell \in \mathbb{Z}^+ \; . \qquad 3.5.7b$$

The Galerkin equations are produced using

$$\int_0^b w_m \tilde{\zeta}_2(-a,y)dy = \int_0^b w_m \tilde{\zeta}_3(-a,y)dy, \quad m = 0,1,\ldots,N, \qquad 3.5.8$$

where the w_m are chosen to be

$$w_0 = e^{K_3 y}$$

$$w_m = \cos\frac{m\pi y}{b} + \rho_m \sin\frac{m\pi y}{b} \quad , \; m > 0 \qquad 3.5.9$$

and the $\tilde{\zeta}_2(-a,y)$, $\tilde{\zeta}_3(-a,y)$ are the truncated-series forms of the expressions for $\zeta_2(-a,y)$, $\zeta_3(-a,y)$ given in 3.5.6 (this notational convention is carried throughout without further explanation).

The resulting equations are

$$E_0 \frac{1}{K_3-K_2} e^{-ik_2^{(0)}a}\left[e^{K_3 b}-e^{K_2 b}\right] + G_0 \frac{1}{K_3+K_2} e^{ik_2^{(0)}a}\left[e^{K_3 b}-e^{-K_2 b}\right]$$

$$+ \sum E_\ell \, e^{-ik_2^{(\ell)}a} \frac{1}{K_3^2+(\frac{\ell\pi}{b})^2} \left[K_3 + \beta_\ell \frac{\ell\pi}{b}\right]\left[(-1)^\ell e^{K_3 b}-1\right]$$

$$+ \sum G_\ell \, e^{ik_2^{(\ell)}a} \frac{}{K_3^2+(\frac{\ell\pi}{b})^2} \left[K_3 - \beta_\ell \frac{\ell\pi}{b}\right]\left[(-1)^\ell e^{K_3 b}-1\right]$$

$$+ D_0 \frac{1}{K_3^2-s_0^2}\left[\cosh K_1 a \; T_{10} - \frac{i\theta K_1}{(1+i\phi_2)s_0} \sinh K_1 a \; T_{20}\right]$$

$$+ F_0 \frac{1}{K_3^2-s_0^2}\left[-\sinh K_1 a \; T_{10} + \frac{i\theta K_1}{(1+i\phi_2)s_0} \cosh K_1 a \; T_{20}\right]$$

$$+ \sum D_\ell (-1)^\ell \frac{1}{K_3^2-s_\ell^2} T_{1\ell} + \sum F_\ell \frac{i\theta}{(1+i\phi_2)} \frac{\ell\pi}{as_\ell} \frac{(-1)^\ell}{K_3^2-s_\ell^2} T_{2\ell}$$

$$= b \, e^{-ik_3^{(0)}a} + A_0 \frac{1}{2K_3} e^{ik_3^{(0)}a}\left[e^{2K_3 b}-1\right]$$

$$+ \sum A_\ell \, e^{ik_3^{(\ell)}a} \frac{1}{K_3^2+(\frac{\ell\pi}{b})^2} \left[K_3 - \rho_\ell \frac{\ell\pi}{b}\right]\left[(-1)^\ell e^{K_3 b}-1\right] \quad , \qquad 3.5.10$$

(Note that, if $h_3 = h_2$, the term with coefficient E_0 is $E_0 b \, e^{-ik_2^{(0)}a + K_3 b}$)

where

$$T_{1\ell} = K_3(e^{K_3 b} - \cosh s_\ell b) - s_\ell \sinh s_\ell b \, , \quad \ell = 0,1,\ldots,N$$

$$T_{2\ell} = K_3 \sinh s_\ell b - s_\ell(e^{K_3 b} - \cosh s_\ell b), \quad \ell = 0,1,\ldots,N,$$

and

$$E_0\, e^{-i k_2^{(0)} a}\, \frac{1}{K_2^2+(\frac{m\pi}{b})^2}\left[K_2 + \rho_m \frac{m\pi}{b}\right]\left[e^{K_2 b} - (-1)^m\right]$$

$$+ G_0\, e^{i k_2^{(0)} a}\, \frac{1}{K_2^2+(\frac{m\pi}{b})^2}\left[- K_2 + \rho_m \frac{m\pi}{b}\right]\left[e^{-K_2 b} - (-1)^m\right]$$

$$+ E_m \frac{b}{2}\, e^{-i k_2^{(m)} a}\left[1 - \rho_m\beta_m\right] + \sum{}' E_\ell\, e^{-i k_2^{(\ell)} a}\left[\rho_m \hat{I}_{\ell m} - \beta_\ell \hat{I}_{m\ell}\right]$$

$$+ G_m \frac{b}{2}\, e^{i k_2^{(m)} a}\left[1 + \rho_m\beta_m\right] + \sum{}' G_\ell\, e^{i k_2^{(\ell)} a}\left[\rho_m \hat{I}_{\ell m} + \beta_\ell \hat{I}_{m\ell}\right]$$

$$+ D_0 \frac{1}{s_0^2+(\frac{m\pi}{b})^2}\left[\cosh K_1 a\, T_{30} + \frac{i\theta K_1}{(1+i\phi_2)s_0} \sinh K_1 a\, T_{40}\right]$$

$$- F_0 \frac{1}{s_0^2+(\frac{m\pi}{b})^2}\left[\sinh K_1 a\, T_{30} + \frac{i\theta K_1}{(1+i\phi_2)s_0} \cosh K_1 a\, T_{40}\right]$$

$$+ \sum D_\ell \frac{(-1)^\ell}{s_\ell^2+(\frac{m\pi}{b})^2}\, T_{3\ell} - \sum F_\ell \frac{i\theta}{(1+i\phi_2)} \frac{\ell\pi}{a s_\ell} \frac{(-1)^\ell}{s_\ell^2+(\frac{m\pi}{b})^2}\, T_{4\ell}$$

$$= e^{-i k_3^{(0)} a} \frac{1}{K_3^2+(\frac{m\pi}{b})^2}\left[K_3 + \rho_m \frac{m\pi}{b}\right]\left[1 - (-1)^m e^{-K_3 b}\right]$$

$$+ A_0\, e^{i k_3^{(0)} a}\, \frac{1}{K_3^2+(\frac{m\pi}{b})^2}\left[K_3 - \rho_m \frac{m\pi}{b}\right]\left[(-1)^m e^{K_3 b} - 1\right]$$

$$+ A_m \frac{b}{2}\, e^{i k_3^{(m)} a}\left[1+\rho_m^2\right] + \sum{}' A_\ell\, e^{i k_3^{(\ell)} a}\left[\rho_m \hat{I}_{\ell m} + \rho_\ell \hat{I}_{m\ell}\right], \quad m = 1,\ldots,N \qquad 3.5.11$$

where

$$T_{3\ell} = s_\ell \sinh s_\ell b + \rho_m \frac{m\pi}{b}(\cosh s_\ell b - (-1)^m), \quad \ell = 0,1,\ldots,N$$

$$T_{4\ell} = s_\ell(\cosh s_\ell b - (-1)^m) + \rho_m \frac{m\pi}{b} \sinh s_\ell b, \quad \ell = 0,1,\ldots,N$$

$\sum$ means $\sum_{\ell=1}^{N}$

$\sum'$ means $\sum_{\substack{\ell=1 \\ \ell\neq m}}^{N}$

and $$\hat{I}_{\ell m} = \frac{b}{\pi} \frac{m}{\ell^2-m^2}\left[(-1)^{\ell-m}-1\right], \quad \ell \neq m \,. \qquad 3.5.12$$

(2) Continuity of volume flux at $x = -a$, $0 \leq y \leq b$.

Using the expressions 3.2.10 and 3.4.18, equation 3.5.2 may be written as

$$
\begin{aligned}
&- E_0 \, k_2^{(0)} \, e^{-i k_2^{(0)} a - K_2 (y-b)} + G_0 \, k_2^{(0)} \, e^{i k_2^{(0)} a + K_2 (y-b)} \\
&- \sum_{\ell=1}^{\infty} E_\ell \, e^{-i k_2^{(\ell)} a} \, k_2^{(\ell)} \left[\cos \frac{\ell \pi y}{b} - \nu_\ell \sin \frac{\ell \pi y}{b} \right] \\
&+ \sum_{\ell=1}^{\infty} G_\ell \, e^{i k_2^{(\ell)} a} \, k_2^{(\ell)} \left[\cos \frac{\ell \pi y}{b} + \nu_\ell \sin \frac{\ell \pi y}{b} \right] \\
&+ D_0 \left[- i K_1 \sinh K_1 a \cosh s_0 (y-b) + \frac{\theta}{s_0} \frac{\omega^2}{g h_2} \cosh K_1 a \sinh s_0 (y-b) \right] \\
&+ F_0 \left[i K_1 \cosh K_1 a \cosh s_0 (y-b) - \frac{\theta}{s_0} \frac{\omega^2}{g h_2} \sinh K_1 a \sinh s_0 (y-b) \right] \\
&+ \sum_{\ell=1}^{\infty} D_\ell \frac{\theta}{s_\ell} \frac{\omega^2}{g h_2} (-1)^\ell \sinh s_\ell (y-b) + \sum_{\ell=1}^{\infty} F_\ell \, i \frac{\ell \pi}{a} (-1)^\ell \cosh s_\ell (y-b) \\
&= \frac{h_3}{h_2} \frac{(1+i\phi_2)}{(1+i\phi_3)} \left\{ - k_3^{(0)} \, e^{-i k_3^{(0)} a - K_3 y} + A_0 k_3^{(0)} e^{i k_3^{(0)} a + K_3 y} \right. \\
&\qquad \left. + \sum_{\ell=1}^{\infty} A_\ell \, e^{i k_3^{(\ell)} a} \, k_3^{(\ell)} \left[\cos \frac{\ell \pi y}{b} + \mu_\ell \sin \frac{\ell \pi y}{b} \right] \right\}, \qquad 3.5.13
\end{aligned}
$$

where

$$\nu_\ell = \frac{\omega^2}{g h_2} \frac{\theta}{k_2^{(\ell)}} \frac{b}{\ell \pi} , \quad \ell \in \mathbb{Z}^+ \qquad 3.5.14a$$

$$\mu_\ell = \frac{\omega^2}{g h_3} \frac{\theta}{k_3^{(\ell)}} \frac{b}{\ell \pi} , \quad \ell \in \mathbb{Z}^+ . \qquad 3.5.14b$$

The Galerkin equations, resulting from

$$\int_0^b w_m \, h_2 \, \tilde{u}_2(-a,y) dy = \int_0^b w_m \, h_3 \, \tilde{u}_3(-a,y) dy \qquad 3.5.15$$

with

$$w_0 = e^{K_3 y}$$

$$w_m = \cos \frac{m \pi y}{b} + \mu_m \sin \frac{m \pi y}{b} , \quad m = 1, \ldots, N, \qquad 3.5.16$$

are

$$- E_0 k_2^{(0)} e^{-i k_2^{(0)} a} \frac{1}{K_3-K_2} \left[e^{K_3 b} - e^{K_2 b} \right]$$

$$+ G_0 k_2^{(0)} e^{i k_2^{(0)} a} \frac{1}{K_3+K_2} \left[e^{K_3 b} - e^{-K_2 b} \right]$$

$$- \sum E_\ell e^{-i k_2^{(\ell)} a} k_2^{(\ell)} \frac{1}{K_3^2+(\frac{\ell\pi}{b})^2} \left[K_3 + \nu_\ell \frac{\ell\pi}{b} \right] \left[(-1)^\ell e^{K_3 b} - 1 \right]$$

$$+ \sum G_\ell e^{i k_2^{(\ell)} a} k_2^{(\ell)} \frac{1}{K_3^2+(\frac{\ell\pi}{b})^2} \left[K_3 - \nu_\ell \frac{\ell\pi}{b} \right] \left[(-1)^\ell e^{K_3 b} - 1 \right]$$

$$+ D_0 \frac{1}{K_3^2-s_0^2} \left[- iK_1 \sinh K_1 a \, T_{10} + \frac{\theta}{s_0} \frac{\omega^2}{gh_2} \cosh K_1 a \, T_{20} \right]$$

$$+ F_0 \frac{1}{K_3^2-s_0^2} \left[i K_1 \cosh K_1 a \, T_{10} - \frac{\theta}{s_0} \frac{\omega^2}{gh_2} \sinh K_1 a \, T_{20} \right]$$

$$+ \sum D_\ell \frac{\theta}{s_\ell} \frac{\omega^2}{gh_2} \frac{(-1)^\ell}{K_3^2-s_\ell^2} T_{2\ell} + \sum F_\ell \, i \frac{\ell\pi}{a} \frac{(-1)^\ell}{K_3^2-s_\ell^2} T_{1\ell}$$

$$= \frac{h_3}{h_2} \frac{(1+i\phi_2)}{(1+i\phi_3)} \left\{ - k_3^{(0)} b \, e^{-i k_3^{(0)} a} + A_0 k_3^{(0)} \frac{1}{2K_3} e^{i k_3^{(0)} a} \left[e^{2K_3 b} - 1 \right] \right.$$

$$\left. + \sum A_\ell e^{i k_3^{(\ell)} a} k_3^{(\ell)} \frac{1}{K_3^2+(\frac{\ell\pi}{b})^2} \left[K_3 - \mu_\ell \frac{\ell\pi}{b} \right] \left[(-1)^\ell e^{K_3 b} - 1 \right] \right\}, \qquad 3.5.17$$

(Note that if $h_3 = h_2$, the term with coefficient E_0 is $-E_0 b k_2^{(0)} e^{-i k_2^{(0)} a + K_3 b}$), where

$$T_{1\ell} = K_3 (e^{K_3 b} - \cosh s_\ell b) - s_\ell \sinh s_\ell b, \quad \ell = 0,1,\ldots,N$$

$$T_{2\ell} = K_3 \sinh s_\ell b - s_\ell (e^{K_3 b} - \cosh s_\ell b), \quad \ell = 0,1,\ldots,N$$

and, defining

$$T_{3\ell} = s_\ell \sinh s_\ell b + \mu_m \frac{m\pi}{b} (\cosh s_\ell b - (-1)^m),$$

$$T_{4\ell} = s_\ell (\cosh s_\ell b - (-1)^m) + \mu_m \frac{m\pi}{b} \sinh s_\ell b, \qquad \ell = 0,1,\ldots,N$$

$$- E_0 k_2^{(0)} e^{-ik_2^{(0)}a} \frac{1}{K_2^2+(\frac{m\pi}{b})^2} \left[K_2 + \mu_m \frac{m\pi}{b}\right]\left[e^{K_2 b} - (-1)^m\right]$$

$$+ G_0 k_2^{(0)} e^{ik_2^{(0)}a} \frac{1}{K_2^2+(\frac{m\pi}{b})^2} \left[- K_2 + \mu_m \frac{m\pi}{b}\right]\left[e^{-K_2 b} - (-1)^m\right]$$

$$- E_m \frac{b}{2} e^{-ik_2^{(m)}a} k_2^{(m)} \left[1 - \nu_m \mu_m\right] + G_m \frac{b}{2} e^{ik_2^{(m)}a} k_2^{(m)} \left[1 + \nu_m \mu_m\right]$$

$$- \sum{}' E_\ell e^{-ik_2^{(\ell)}a} k_2^{(\ell)} \left[\mu_m \hat{I}_{\ell m} - \nu_\ell \hat{I}_{m\ell}\right]$$

$$+ \sum{}' G_\ell e^{ik_2^{(\ell)}a} k_2^{(\ell)} \left[\mu_m \hat{I}_{\ell m} + \nu_\ell \hat{I}_{m\ell}\right]$$

$$- D_0 \frac{1}{s_0^2+(\frac{m\pi}{b})^2} \left[iK_1 \sinh K_1 a\, T_{30} + \frac{\theta}{s_0} \frac{\omega^2}{gh_2} \cosh K_1 a\, T_{40}\right]$$

$$+ F_0 \frac{1}{s_0^2+(\frac{m\pi}{b})^2} \left[iK_1 \cosh K_1 a\, T_{30} + \frac{\theta}{s_0} \frac{\omega^2}{gh_2} \sinh K_1 a\, T_{40}\right]$$

$$- \sum D_\ell \frac{\theta}{s_\ell} \frac{\omega^2}{gh_2} \frac{(-1)^\ell}{s_\ell^2+(\frac{m\pi}{b})^2} T_{4\ell} + \sum F_\ell\, i \frac{\ell\pi}{a} \frac{(-1)^\ell}{s_\ell^2+(\frac{m\pi}{b})^2} T_{3\ell}$$

$$= \frac{h_3}{h_2} \frac{(1+i\phi_2)}{(1+i\phi_3)} \left\{- k_3^{(0)} e^{-ik_3^{(0)}a} \frac{1}{K_3^2+(\frac{m\pi}{b})^2} \left[K_3 + \mu_m \frac{m\pi}{b}\right]\left[1 - (-1)^m e^{-K_3 b}\right]\right.$$

$$+ A_0 k_3^{(0)} e^{ik_3^{(0)}a} \frac{1}{K_3^2+(\frac{m\pi}{b})^2} \left[K_3 - \mu_m \frac{m\pi}{b}\right]\left[(-1)^m e^{K_3 b} - 1\right]$$

$$+ A_m \frac{b}{2} e^{ik_3^{(m)}a} k_3^{(m)} \left[1 + \rho_m^2\right]$$

$$\left. + \sum{}' A_\ell e^{ik_3^{(\ell)}a} k_3^{(\ell)} \left[\mu_m \hat{I}_{\ell m} + \mu_\ell \hat{I}_{m\ell}\right]\right\}, \quad m = 1,\ldots,N. \qquad 3.5.18$$

(3) Continuity of Elevation at $y = 0$, $-a \leq x \leq 0$.

If expressions 3.3.5 and 3.4.15 are to be consistent with equation 3.5.3, the coefficients must satisfy the equation

$$B_0 \cos p_0 d\left[\cosh K_1 x + \gamma_0 \sinh K_1 x\right]$$

$$- C_0 i \cos p_0 d\left[\sinh K_1 x + \gamma_0 \cosh K_1 x\right]$$

$$+ \sum_{\ell=1}^{\infty} B_\ell \cos p_\ell d\left[\cos \frac{\ell\pi x}{a} + \gamma_\ell \sin \frac{\ell\pi x}{a}\right]$$

$$+ \sum_{\ell=1}^{\infty} C_\ell \sin p_\ell d\left[\cos \frac{\ell\pi x}{a} - \frac{\gamma_\ell}{\tan^2 p_\ell d} \sin \frac{\ell\pi x}{a}\right]$$

$$= E_0 e^{i k_2^{(0)} x + K_2 b} + \sum_{\ell=1}^{\infty} E_\ell \, e^{i k_2^{(\ell)} x}$$

$$+ G_0 \, e^{-i k_2^{(0)} x - K_2 b} + \sum_{\ell=1}^{\infty} G_\ell \, e^{-i k_2^{(\ell)} x}$$

$$+ D_0 \cosh s_0 b\left[\cosh K_1 x + \eta_0 \sinh K_1 x\right]$$

$$+ F_0 \cosh s_0 b\left[\sinh K_1 x + \eta_0 \cosh K_1 x\right]$$

$$+ \sum_{\ell=1}^{\infty} D_\ell \cosh s_\ell b\left[\cos \frac{\ell\pi x}{a} + \eta_\ell \sin \frac{\ell\pi x}{a}\right]$$

$$+ \sum_{\ell=1}^{\infty} F_\ell \cosh s_\ell b\left[\sin \frac{\ell\pi x}{a} - \eta_\ell \cos \frac{\ell\pi x}{a}\right] , \qquad 3.5.19$$

with

$$\gamma_0 = i \tan p_0 d \qquad 3.5.20$$

$$\gamma_\ell = \frac{i\theta}{(1+i\phi_1)} \frac{a}{\ell\pi} p_\ell \tan p_\ell d, \quad \ell \in \mathbb{Z}^+$$

$$\eta_0 = \frac{-i\theta K_1}{(1+i\phi_2) s_0} \tanh s_0 b \qquad 3.5.21$$

$$\eta_\ell = \frac{i\theta}{(1+i\phi_2)} \frac{\ell\pi}{a s_\ell} \tanh s_\ell b, \quad \ell \in \mathbb{Z}^+ .$$

If the weighting functions are chosen to be

$$w_0 = \cosh K_1 x + \eta_0 \sinh K_1 x$$

$$w_m = \cos \frac{m\pi x}{a} + \eta_m \sin \frac{m\pi x}{a} , \; m = 1, \ldots, N, \qquad 3.5.22$$

then the Galerkin equations, found from

$$\int_{-a}^{0} w_m \, \tilde{\zeta}_1(x,0)dx = \int_{-a}^{0} w_m \, \tilde{\zeta}_2(x,0)dx, \quad m = 0,1,\ldots,N,$$

are

$$B_0 \frac{\cos p_0 d}{4K_1}\left[(1 - \gamma_0\eta_0)2K_1a + (1 + \gamma_0\eta_0)\sinh 2K_1a + (\gamma_0+\eta_0)(1 - \cosh 2K_1a)\right]$$

$$- C_0\, i \frac{\cos p_0 d}{4K_1}\left[(\gamma_0-\eta_0)2K_1a + (\gamma_0+\eta_0)\sinh 2K_1a + (1+\gamma_0\eta_0)(1 - \cosh 2K_1a)\right]$$

$$+ \sum B_\ell \cos p_\ell d \frac{1}{K_1^2+(\frac{\ell\pi}{a})^2}\left[(K_1 - \gamma_\ell \frac{\ell\pi}{a}\eta_0)T_{5\ell} + (\gamma_0K_1 - \gamma_\ell \frac{\ell\pi}{a})T_{6\ell}\right]$$

$$+ \sum C_\ell \sin p_\ell d \frac{1}{K_1^2+(\frac{\ell\pi}{a})^2}\left[(K_1 + \frac{\eta_0}{\tan^2 p_\ell d}\ \gamma_\ell \frac{\ell\pi}{a})\ T_{5\ell} + (\gamma_0K_1 + \frac{1}{\tan^2 p_\ell d}\ \gamma_\ell \frac{\ell\pi}{a})\ T_{6\ell}\right]$$

$$= E_0\, e^{K_2 b}\frac{1}{(k_2^{(0)})^2+K_1^2}\left[(\eta_0K_1 - ik_2^{(0)})T_{10} + (K_1 - ik_2^{(0)}\eta_0)\ T_{20}\right]$$

$$+ G_0\, e^{-K_2 b}\ \frac{1}{(k_2^{(0)})^2+K_1^2}\left[(\eta_0K_1 + ik_2^{(0)})T_{30} + (K_1 + ik_2^{(0)}\eta_0)T_{40}\right]$$

$$+ \sum E_\ell \frac{1}{(k_2^{(\ell)})^2+K_1^2}\left[(\eta_0K_1 - ik_2^{(\ell)})T_{1\ell} + (K_1 - ik_2^{(\ell)}\eta_0)T_{2\ell}\right]$$

$$+ \sum G_\ell \frac{1}{(k_2^{(\ell)})^2+K_1^2}\left[(\eta_0K_1 + ik_2^{(\ell)})T_{3\ell} + (K_1 + ik_2^{(\ell)}\eta_0)T_{4\ell}\right]$$

$$+ D_0 \frac{\cosh s_0 b}{4K_1}\left[(1-\eta_0^2)2K_1a + (1+\eta_0^2)\sinh 2K_1a + 2\eta_0(1 - \cosh 2\,K_1a)\right]$$

$$+ F_0 \frac{\cosh s_0 b}{4K_1}\left[2\eta_0 \sinh 2K_1a + (1+\eta_0^2)(1 - \cosh 2K_1a)\right]$$

$$+ \sum D_\ell \frac{\cosh s_\ell b}{K_1^2+(\frac{\ell\pi}{a})^2}\left[(K_1 - \eta_0\eta_\ell \frac{\ell\pi}{a})T_{5\ell} + (\eta_0K_1 - \eta_\ell \frac{\ell\pi}{a})T_{6\ell}\right]$$

$$- \sum F_\ell \frac{\cosh s_\ell b}{K_1^2+(\frac{\ell\pi}{a})^2}\left[(\eta_0 \frac{\ell\pi}{a} + \eta_\ell K_1)T_{5\ell} + (\frac{\ell\pi}{a} + \eta_\ell\eta_0K_1)T_{6\ell}\right], \qquad 3.5.23$$

where

$$T_{1\ell} = 1 - e^{-ik_2^{(\ell)}a}\cosh K_1 a$$

$$T_{2\ell} = e^{-ik_2^{(\ell)}a}\sinh K_1 a$$

$$T_{3\ell} = 1 - e^{ik_2^{(\ell)}a}\cosh K_1 a$$

$$T_{4\ell} = e^{ik_2^{(\ell)}a}\sinh K_1 a,\ \ell = 0,1,\ldots,N$$

$$T_{5\ell} = (-1)^{\ell}\sinh K_1 a$$

and $$T_{6\ell} = 1 - (-1)^{\ell}\cosh K_1 a,\quad \ell = 1,\ldots,N;$$

and

$$B_0\frac{\cos p_0 d}{K_1^2+(\frac{m\pi}{a})^2}\left[(K_1 - \gamma_0\eta_m\frac{m\pi}{a})T_{5m} + (K_1\gamma_0 - \eta_m\frac{m\pi}{a})T_{6m}\right]$$

$$- i\,C_0\frac{\cos p_0 d}{K_1^2+(\frac{m\pi}{a})^2}\left[(K_1\gamma_0 - \eta_m\frac{m\pi}{a})T_{5m} + (K_1 - \gamma_0\eta_m\frac{m\pi}{a})T_{6m}\right]$$

$$+ B_m\frac{a}{2}\cos p_m d\left[1 + \gamma_m\eta_m\right] + \sum{}' B_\ell\cos p_\ell d\left[\eta_m I_{\ell m} + \gamma_\ell I_{m\ell}\right]$$

$$+ C_m\frac{a}{2}\sin p_m d\left[1 - \frac{\gamma_m\eta_m}{\tan^2 p_m d}\right] + \sum{}' C_\ell\sin p_\ell d\left[\eta_m I_{\ell m} - \frac{\gamma_\ell}{\tan^2 p_\ell d}I_{m\ell}\right]$$

$$= D_0\frac{\cosh s_0 b}{K_1^2+(\frac{m\pi}{a})^2}\left[(K_1 - \eta_0\eta_m\frac{m\pi}{a})T_{5m} + (K_1\eta_0 - \eta_m\frac{m\pi}{a})T_{6m}\right]$$

$$+ F_0\frac{\cosh s_0 b}{K_1^2+(\frac{m\pi}{a})^2}\left[(K_1\eta_0 - \eta_m\frac{m\pi}{a})T_{5m} + (K_1 - \eta_0\eta_m\frac{m\pi}{a})T_{6m}\right]$$

$$+ D_m\frac{a}{2}\cosh s_m b\left[1+\eta_m^2\right] + \sum{}' D_\ell\cosh s_\ell b\left[\eta_m I_{\ell m} + \eta_\ell I_{m\ell}\right]$$

$$+ \sum{}' F_\ell\cosh s_\ell b\left[I_{m\ell} - \eta_\ell\eta_m I_{\ell m}\right]$$

$$+ E_0 e^{K_2 b}\frac{1}{(k_2^{(0)})^2-(\frac{m\pi}{a})^2}\left[\eta_m\frac{m\pi}{a} - ik_2^{(0)}\right]\left[1 - (-1)^m e^{-ik_2^{(0)}a}\right]$$

$$+ \sum E_\ell\frac{1}{(k_2^{(\ell)})^2-(\frac{m\pi}{a})^2}\left[\eta_m\frac{m\pi}{a} - ik_2^{(\ell)}\right]\left[1 - (-1)^m e^{-ik_2^{(\ell)}a}\right]$$

$$+ G_0 e^{-K_2 b}\frac{1}{(k_2^{(0)})^2-(\frac{m\pi}{a})^2}\left[\eta_m\frac{m\pi}{a} + ik_2^{(0)}\right]\left[1 - (-1)^m e^{ik_2^{(0)}a}\right]$$

$$+ \sum G_\ell\frac{1}{(k_2^{(\ell)})^2-(\frac{m\pi}{a})^2}\left[\eta_m\frac{m\pi}{a} + ik_2^{(\ell)}\right]\left[1 - (-1)^m e^{ik_2^{(\ell)}a}\right],\ m = 1,\ldots,N \quad 3.5.24$$

where

$$I_{m\ell} = \frac{a}{\pi} \frac{\ell}{\ell^2-m^2} \left[(-1)^{\ell-m}-1\right] \quad , \ \ell \neq m. \tag{3.5.25}$$

(4) Zero Normal Velocity at the Boundary $x = 0,\ 0 \leq y \leq b$.

Expression 3.4.18, substituted into equation 3.5.4, yields

$$\sum_{\ell=0}^{\infty} D_\ell \frac{\theta}{s_\ell} \frac{\omega^2}{gh_2} \sinh s_\ell(y-b) + \sum_{\ell=0}^{\infty} F_\ell \alpha_\ell \cosh s_\ell(y-b)$$

$$- E_0 k_2^{(0)} e^{-K_2(y-b)} - \sum_{\ell=1}^{\infty} E_\ell k_2^{(\ell)} \left[\cos \frac{\ell\pi y}{b} - \nu_\ell \sin \frac{\ell\pi y}{b}\right]$$

$$+ G_0 k_2^{(0)} e^{K_2(y-b)} + \sum_{\ell=1}^{\infty} G_\ell k_2^{(\ell)} \left[\cos \frac{\ell\pi y}{b} + \nu_\ell \sin \frac{\ell\pi y}{b}\right] = 0, \tag{3.5.26}$$

with ν_ℓ as defined in 3.5.14a and

$$\alpha_0 = iK_1$$

$$\alpha_\ell = i \frac{\ell\pi}{a} \ , \ \ell \in \mathbb{Z}^+ \ . \tag{3.5.27}$$

Application of 3.5.26 to

$$\int_0^b w_m \tilde{u}_2(0,y)dy = 0, \quad m = 0,1,\ldots,N,$$

with

$$w_0 = e^{K_2(y-b)}$$

$$w_m = \cos \frac{m\pi y}{b} + \nu_m \sin \frac{m\pi y}{b} \ , \ m = 1,\ldots,N,$$

yields the Galerkin equations, which are

$$\sum_{\ell=0}^{N} D_\ell \frac{\theta}{s_\ell} \frac{\omega^2}{gh_2} \frac{1}{K_2^2-s_\ell^2} \left[s_\ell \{1 - e^{-K_2 b} \cosh s_\ell b\} - K_2 e^{-K_2 b} \sinh s_\ell b\right]$$

$$+ \sum_{\ell=0}^{N} F_\ell \alpha_\ell \frac{1}{K_2^2-s_\ell^2} \left[s_\ell e^{-K_2 b} \sinh s_\ell b - K_2\{1 - e^{-K_2 b} \cosh s_\ell b\}\right]$$

$$+ E_0 k_2^{(0)} b - G_0 k_2^{(0)} \frac{1}{2K_2}\left[1 - e^{-2K_2 b}\right] - \sum E_\ell k_2^{(\ell)} \frac{1}{K_2^2+(\frac{\ell\pi}{b})^2} \left[K_2 + \nu_\ell \frac{\ell\pi}{b}\right]\left[e^{-K_2 b} - (-1)^\ell\right]$$

$$+ \sum G_\ell k_2^{(\ell)} \frac{1}{K_2^2+(\frac{\ell\pi}{b})^2} \left[K_2 - \nu_\ell \frac{\ell\pi}{b}\right]\left[e^{-K_2 b} - (-1)^\ell\right] = 0; \tag{3.5.28}$$

and

$$- \sum_{\ell=0}^{N} D_\ell \frac{\theta}{s_\ell} \frac{\omega^2}{gh_2} \frac{1}{s_\ell^2+(\frac{m\pi}{b})^2} \left[s_\ell(\cosh s_\ell b - (-1)^m) + \nu_m \frac{m\pi}{b} \sinh s_\ell b \right]$$

$$+ \sum_{\ell=0}^{N} F_\ell \alpha_\ell \frac{1}{s_\ell^2+(\frac{m\pi}{b})^2} \left[s_\ell \sinh s_\ell b + \nu_m \frac{m\pi}{b} (\cosh s_\ell b - (-1)^m) \right]$$

$$- E_0 k_2^{(0)} \frac{1}{K_2^2+(\frac{m\pi}{b})^2} \left[K_2 + \nu_m \frac{m\pi}{b} \right] \left[e^{K_2 b} - (-1)^m \right] - E_m \frac{b}{2} k_2^{(m)} \left[1 - \nu_m^2 \right]$$

$$- G_0 k_2^{(0)} \frac{1}{K_2^2+(\frac{m\pi}{b})^2} \left[K_2 - \nu_m \frac{m\pi}{b} \right] \left[e^{-K_2 b} - (-1)^m \right] + G_m \frac{b}{2} k_2^{(m)} \left[1 + \nu_m^2 \right]$$

$$+ \sum{}' E_\ell k_2^{(\ell)} \left[\nu_m \hat{I}_{\ell m} - \nu_\ell \hat{I}_{m\ell} \right] + \sum{}' G_\ell k_2^{(\ell)} \left[\nu_m \hat{I}_{\ell m} + \nu_\ell \hat{I}_{m\ell} \right] = 0,$$

$$m = 1,\ldots,N. \qquad 3.5.29$$

(5) Zero Normal Velocity at the Boundary, $y = -d$, $-a \leq x \leq 0$.

Use of 3.3.9 in the equation 3.5.5 gives the relationship

$$- B_0 p_0 \sinh K_1 x + i C_0 p_0 \cosh K_1 x$$

$$- \sum_{\ell=1}^{\infty} B_\ell \, \theta \, \frac{\omega^2}{g h_1} \frac{a}{\ell\pi} \sin \frac{\ell\pi x}{a} + \sum_{\ell=1}^{\infty} C_\ell \, i p_\ell \cos \frac{\ell\pi x}{a} = 0. \qquad 3.5.30$$

The Galerkin equations are produced from the integration

$$\int_{-a}^{0} w_m \, \tilde{v}_1(x,-d)dx = 0, \quad m = 0,1,\ldots,N,$$

where the weighting functions are chosen to be

$$w_0 = \cosh K_1 x$$

$$w_m = \cos \frac{m\pi x}{a}, \quad m = 1,\ldots,N. \qquad 3.5.31$$

The resulting equations are

$$- B_0 \frac{p_0}{4K_1} \left[1 - \cosh 2K_1 a\right] - \sum B_\ell \, \theta \, \frac{\omega^2}{g h_1} \frac{1}{K_1^2 + (\frac{\ell\pi}{a})^2} \left[(-1)^\ell \cosh K_1 a - 1\right]$$

$$+ i C_0 \frac{p_0}{4K_1} \left[\sinh 2K_1 a + 2K_1 a\right] + \sum C_\ell \frac{i p_\ell K_1}{K_1^2 + (\frac{\ell\pi}{a})^2} (-1)^\ell \sinh K_1 a = 0; \qquad 3.5.32$$

and

$$B_0 \frac{p_0 K_1}{K_1^2 + (\frac{m\pi}{a})^2} \left[(-1)^m \cosh K_1 a - 1\right] - \sum{}' B_\ell \, \theta \, \frac{\omega^2}{g h_1} \frac{a}{\ell\pi} I_{m\ell}$$

$$+ C_0 \frac{i p_0 K_1}{K_1^2 + (\frac{m\pi}{a})^2} (-1)^m \sinh K_1 a + C_m \, i p_m \frac{a}{2} = 0, \quad m = 1,\ldots,N, \qquad 3.5.33$$

where $I_{m\ell}$ is as defined in 3.5.25.

(6) Continuity of Volume Flux at $y = 0$, $-a \leq x \leq 0$.

For completion, the equations 3.4.16, which ensure that the condition

$$h_1 v_1(x,0) = h_2 v_2(x,0), \quad -a \leq x \leq 0$$

is satisfied exactly, are presented again here:

$$D_0 = \frac{\Omega\, p_0 s_0 (1+i\phi_2)}{[\theta^2 K_1^2 + (1+i\phi_2)^2 s_0^2] \sinh s_0 b} [B_0 \sin p_0 d - C_0 \cos p_0 d] \qquad 3.5.34$$

$$D_\ell = -\frac{\Omega\, p_\ell s_\ell (1+i\phi_2)}{[(\frac{\ell\pi\theta}{a})^2 - (1+i\phi_2)^2 s_\ell^2] \sinh s_\ell b} [B_\ell \sin p_\ell d - C_\ell \cos p_\ell d], \quad \ell = 1,\ldots,N \qquad 3.5.35$$

$$F_0 = -\frac{\Omega\, i p_0 s_0 (1+i\phi_2)}{[\theta^2 K_1^2 + (1+i\phi_2)^2 s_0^2] \sinh s_0 b} [B_0 \cos p_0 d + C_0 \sin p_0 d] \qquad 3.5.36$$

$$F_\ell = \frac{\Omega\, i\, \theta\, s_\ell (1+i\phi_2)}{[(\frac{\ell\pi\theta}{a})^2 - (1+i\phi_2)^2 s_\ell^2] \sinh s_\ell b} \frac{\omega^2}{g h_1} \frac{a}{\ell\pi} [B_\ell \cos p_\ell d + C_\ell \sin p_\ell d], \quad \ell = 1,\ldots,N \qquad 3.5.37$$

where

$$\Omega = \frac{h_1}{h_2} \frac{[(1+i\phi_2)^2 - \theta^2]}{(1+i\phi_1)} .$$

The linear simultaneous equations described above may be solved for the unknowns A_ℓ, B_ℓ, C_ℓ, D_ℓ, E_ℓ, F_ℓ, G_ℓ, $(\ell = 0,1,\ldots,N)$ by inverting the $(7N+7)\times(7N+7)$ complex matrix whose elements are defined by the equations derived in this section. The convergence of the method is tested by checking that the residuals of each equation become smaller as N is increased, as shown in Chapter 6.

CHAPTER 4

AN EXTENSION TO THE MODEL: AN ADJOINING CHANNEL

4.1 The Equations

The model in the previous chapter can be extended to include the presence of tidal forcing in a second semi-infinite channel, adjoining the junction region and occupying the area $x \geq 0$, $w_2 \leq y \leq w_3$. Williams (1972) (and, subsequently, Buchwald and Williams (1975)) has considered the case $w_2 = 0$, $w_3 = b$ in his earlier analysis which neglected Coriolis as well as friction. Here, the two semi-infinite channels, not necessarily the same width, could be as depicted in Figure 4.1a, if $w_3 \leq b$, or in Figure 4.1b, if $w_3 \geq b$, with both cases allowing for $0 \leq w_2 < b$. The analysis which follows is carried out for the situation in Figure 4.1a, but that for the case of Figure 4.1b does not differ substantially from the presentation below.

The area is now divided into four regions with a depth discontinuity at the junction of two adjacent regions, indicated by broken lines in the figure. Once again, the solution is sought to the equations

$$\nabla^2\zeta_j + \chi_j^2\zeta_j = 0, \quad j = 1,2,3,4 \qquad 4.1.1$$

where

$$\chi_j^2 = \frac{\omega^2}{gh_j} \frac{\{(1+i\phi_j)^2-\theta^2\}}{(1+i\phi_j)} .$$

The solution must satisfy a radiation condition in each of the semi-infinite channels, as well as the following boundary conditions:

(a)

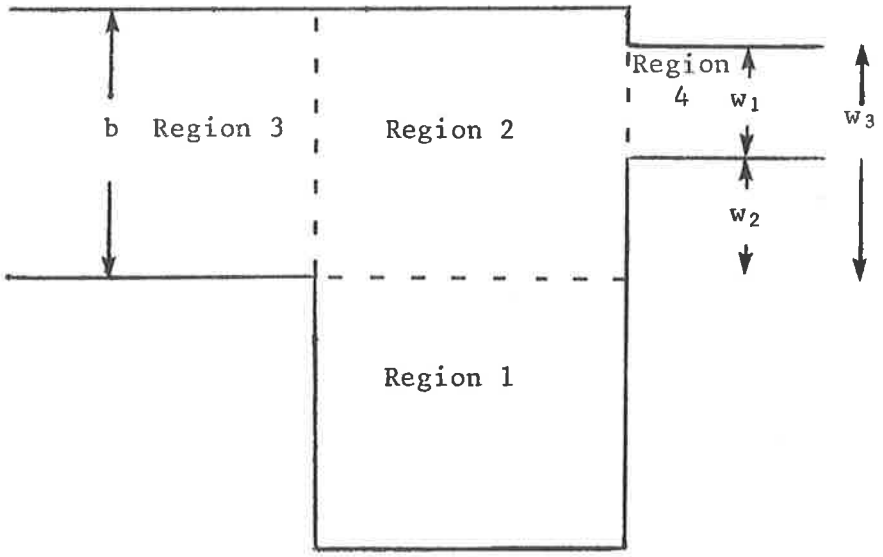

(b)

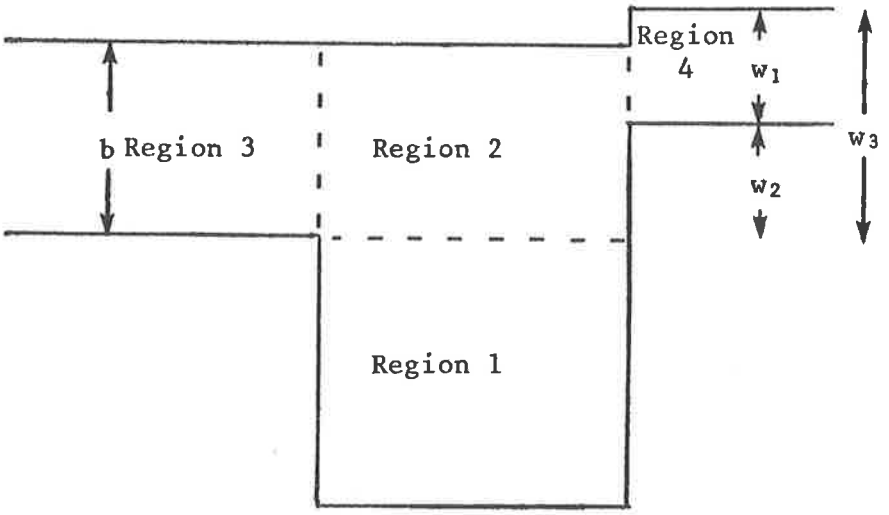

Figure 4.1 The rectangular resonator-channel system, with two connecting channels. The case of $w_3 \leqslant b$ is shown in (a), while $w_3 \geqslant b$ is depicted in (b).

$$u_1(0,y) = u_1(-a,y) = 0, \quad -d \leq y \leq 0$$

$$v_2(x,b) = 0, \quad -a \leq x \leq 0$$

$$v_3(x,0) = v_3(x,b) = 0, \quad x \leq -a$$

$$v_4(x,w_2) = v_4(x,w_3) = 0, \quad x \geq 0$$

$$v_1(x,-d) = 0, \quad -a \leq x \leq 0$$

and matching conditions

$$\zeta_2(-a,y) = \zeta_3(-a,y), \quad 0 \leq y \leq b$$

$$h_2u_2(-a,y) = h_3u_3(-a,y), \quad 0 \leq y \leq b$$

$$h_2u_2(0,y) = \begin{cases} 0, & w_3 < y \leq b \\ h_4u_4(0,y), & w_2 \leq y \leq w_3 \\ 0, & 0 \leq y < w_2 \end{cases}$$

$$\zeta_2(0,y) = \zeta_4(0,y), \quad w_2 \leq y \leq w_3$$

$$\zeta_1(x,0) = \zeta_2(x,0), \quad -a \leq x \leq 0$$

$$h_1v_1(x,0) = h_2v_2(x,0), \quad -a \leq x \leq 0.$$

The $u_j(x,y)$ and $v_j(x,y)$ may be found from the relations 2.3.4.

4.2 The Solutions

The expressions for $\zeta_j(x,y)$, $u_j(x,y)$, $v_j(x,y)$, $j = 1,2,3$, are exactly the same as those containing the unknown coefficients, found in Chapter 3. The solution in region 4 is found analogously to $\zeta_3(x,y)$ in Section 3.2, so that

$$\zeta_4(x,y) = \hat{\alpha}\, e^{-i k_4^{(0)} x + K_4 y} + \hat{A}_0\, e^{i k_4^{(0)} x - K_4 y}$$

$$+ \sum_{\ell=1}^{\infty} \hat{A}_\ell\, e^{i k_4^{(\ell)} x} \left[\cos \frac{\ell\pi}{w_1}(y-w_2) - \frac{\theta}{(1+i\phi_4)} \frac{w_1}{\ell\pi} k_4^{(\ell)} \sin \frac{\ell\pi}{w_1}(y-w_2) \right], \qquad 4.2.1$$

where

$$K_4 = \theta\left\{\frac{\omega^2}{gh_4}\,\frac{1}{(1+i\phi_4)}\right\}^{\frac{1}{2}} \qquad 4.2.2$$

$$k_4^{(0)} = \left\{\frac{\omega^2}{gh_4}\,(1+i\phi_4)\right\}^{\frac{1}{2}}$$

$$k_4^{(\ell)} = \left\{\chi_4^2 - \left(\frac{\ell\pi}{w_1}\right)^2\right\}^{\frac{1}{2}}, \quad \ell \in \mathbb{Z}^+ \qquad 4.2.3$$

and

$$w_1 = w_3 - w_2 \,. \qquad 4.2.4$$

The velocities may be written as

$$u_4(x,y) = \frac{-g}{\omega(1+i\phi_4)}\left\{\hat{\alpha}\;k_4^{(0)}\;e^{-i\,k_4^{(0)}x + K_4 y} - \hat{A}_0\;k_4^{(0)}\;e^{i\,k_4^{(0)}x - K_4 y}\right.$$

$$\left. + \sum_{\ell=1}^{\infty}\hat{A}_\ell\;e^{i\,k_4^{(\ell)}x}\left[-k_4^{(\ell)}\cos\frac{\ell\pi}{w_1}(y-w_2) + \theta\,\frac{w_1}{\ell\pi}\,\frac{\omega^2}{gh_4}\sin\frac{\ell\pi}{w_1}(y-w_2)\right]\right\}, \qquad 4.2.5$$

and

$$v_4(x,y) = \frac{ig}{\omega(1+i\phi_4)}\sum_{\ell=1}^{\infty}\hat{A}_\ell\;e^{i\,k_4^{(\ell)}x}\,\frac{w_1}{\ell\pi}\left[K_4^2 + \left(\frac{\ell\pi}{w_1}\right)^2\right]\sin\frac{\ell\pi}{w_1}(y-w_2). \qquad 4.2.6$$

As was the case in Chapter 3, some of the conditions listed in Section 4.1 still remain to be satisfied. These are

(i) $\zeta_2(-a,y) = \zeta_3(-a,y)$, $0 \leq y \leq b$

(ii) $h_2u_2(-a,y) = h_3u_3(-a,y)$, $0 \leq y \leq b$

(iii) $\zeta_1(x,0) = \zeta_2(x,0)$, $-a \leq x \leq 0$

(iv) $v_1(x,-d) = 0$, $-a \leq x \leq 0$

(v) $h_1v_1(x,0) = h_2v_2(x,0)$, $-a \leq x \leq 0$

(vi) $\zeta_2(0,y) = \zeta_4(0,y)$, $w_2 \leq y \leq w_3$ 4.2.7

(vii) $$h_2u_2(0,y) = \begin{cases} 0, & w_3 < y \leq b \\ h_4u_4(0,y), & w_2 \leq y \leq w_3 \\ 0, & 0 \leq y < w_2 \end{cases} \,. \qquad 4.2.8$$

As before, a Galerkin technique is used to find an approximate solution to satisfy these equations. The algebraic equations resulting from application of the Galerkin process to (i) - (v) are those found in the previous chapter, namely, 3.5.10 and .11, 3.5.17 and .18, 3.5.23 and .24, 3.5.32 and .33 and 3.5.34, .35, .36, .37. Conditions (vi) and (vii) are now considered.

Condition (vi). Continuity of Elevation at $x = 0$, $w_2 \leq y \leq w_3$.

Substitution of the expressions 3.4.15 and 4.2.1 into equation 4.2.7 yields

$$\sum_{\ell=0}^{\infty} D_\ell \cosh s_\ell(y-b) + \sum_{\ell=0}^{\infty} F_\ell \frac{\alpha_\ell}{s_\ell} \frac{\theta}{(1+i\phi_2)} \sinh s_\ell(y-b)$$

$$+ E_0 e^{-K_2(y-b)} + \sum_{\ell=1}^{\infty} E_\ell \left[\cos \frac{\ell\pi y}{b} - \beta_\ell \sin \frac{\ell\pi y}{b}\right]$$

$$+ G_0 e^{K_2(y-b)} + \sum_{\ell=1}^{\infty} G_\ell \left[\cos \frac{\ell\pi y}{b} + \beta_\ell \sin \frac{\ell\pi y}{b}\right]$$

$$= \hat{\alpha} e^{K_4 y} + \hat{A}_0 e^{-K_4 y} + \sum_{\ell=1}^{\infty} \hat{A}_\ell \left[\cos \frac{\ell\pi}{w_1}(y-w_2) - \xi_\ell \sin \frac{\ell\pi}{w_1}(y-w_2)\right] \quad 4.2.9$$

where

$$\beta_\ell = \frac{\theta}{(1+i\phi_2)} \frac{b}{\ell\pi} k_2^{(\ell)}$$

$$\ell \in \mathbb{Z}^+ \quad 4.2.10$$

$$\xi_\ell = \frac{\theta}{(1+i\phi_4)} \frac{w_1}{\ell\pi} k_4^{(\ell)}$$

and α_ℓ is as defined by 3.5.27.

The weighting functions which are chosen for the evaluation of

$$\int_{w_2}^{w_3} w_m \tilde{\zeta}_2(0,y)dy = \int_{w_2}^{w_3} w_m \tilde{\zeta}_4(0,y)dy, \quad m = 0,1,\ldots,N$$

are

$$w_0 = e^{K_2 y}$$

$$w_m = \cos \frac{m\pi y}{b} + \beta_m \sin \frac{m\pi y}{b}, \quad m = 1,\ldots,N.$$

The Galerkin equation for $m = 0$ produced from this integration is

$$\sum_{\ell=0}^{N} D_\ell \frac{1}{K_2^2-s_\ell^2}\left[K_2 T_{1\ell} - s_\ell T_{2\ell}\right] + \sum_{\ell=0}^{N} F_\ell \frac{\alpha_\ell}{s_\ell}\frac{\theta}{(1+i\phi_2)}\frac{1}{K_2^2-s_\ell^2}\left[K_2 T_{2\ell} - s_\ell T_{1\ell}\right]$$

$$+ E_0 w_1 e^{K_2 b} + G_0 \frac{1}{2K_2} e^{-K_2 b}\left[e^{2K_2 w_3} - e^{2K_2 w_2}\right]$$

$$+ \sum E_\ell \frac{1}{K_2^2+(\frac{\ell\pi}{b})^2}\left[\left\{K_2 + \beta_\ell \frac{\ell\pi}{b}\right\}T_{3\ell} + \left\{\frac{\ell\pi}{b} - \beta_\ell K_2\right\}T_{4\ell}\right]$$

$$+ \sum G_\ell \frac{1}{K_2^2+(\frac{\ell\pi}{b})^2}\left[\left\{K_2 - \beta_\ell \frac{\ell\pi}{b}\right\}T_{3\ell} + \left\{\frac{\ell\pi}{b} + \beta_\ell K_2\right\}T_{4\ell}\right]$$

$$= \hat{\alpha}\frac{1}{K_4+K_2}\left[e^{(K_4+K_2)w_3} - e^{(K_4+K_2)w_2}\right]$$

$$+ \hat{A}_0 \frac{1}{K_2-K_4}\left[e^{(K_2-K_4)w_3} - e^{(K_2-K_4)w_2}\right]$$

$$+ \sum \hat{A}_\ell \frac{1}{K_2^2+(\frac{\ell\pi}{w_1})^2}\left[K_2 + \xi_\ell \frac{\ell\pi}{w_1}\right]\left[(-1)^\ell e^{K_2 w_3} - e^{K_2 w_2}\right], \qquad 4.2.11$$

(Note that if $h_2 = h_4$, the term with coefficient $\hat{A}_0$ is $\hat{A}_0 w_1$),

where

$$T_{1\ell} = e^{K_2 w_3}\cosh s_\ell t_3 - e^{K_2 w_2}\cosh s_\ell t_2 \qquad \ell = 0,1,\ldots,N$$

$$T_{2\ell} = e^{K_2 w_3}\sinh s_\ell t_3 - e^{K_2 w_2}\sinh s_\ell t_2$$

$$T_{3\ell} = e^{K_2 w_3}\cos\frac{\ell\pi w_3}{b} - e^{K_2 w_2}\cos\frac{\ell\pi w_2}{b} \qquad \ell = 1,\ldots,N$$

$$T_{4\ell} = e^{K_2 w_3}\sin\frac{\ell\pi w_3}{b} - e^{K_2 w_2}\sin\frac{\ell\pi w_2}{b}$$

and $t_j = w_j - b, \quad j = 2,3.$

The Galerkin equations for $m = 1,\ldots,N$ are

$$\sum_{\ell=0}^{N} D_\ell \frac{1}{s_\ell^2+(\frac{m\pi}{b})^2}\left[\frac{m\pi}{b}T_{D1\ell} + s_\ell T_{D2\ell} - \beta_m \frac{m\pi}{b} T_{D3\ell} + \beta_m s_\ell T_{D4\ell}\right]$$

$$+ \sum_{\ell=0}^{N} F_\ell \frac{\alpha_\ell/s_\ell}{s_\ell^2+(\frac{m\pi}{b})^2}\left[s_\ell T_{D3\ell} + \frac{m\pi}{b}T_{D4\ell} - \beta_m \frac{m\pi}{b}T_{D2\ell} + \beta_m s_\ell T_{D1\ell}\right]\frac{\theta}{(1+i\phi_2)}$$

$$+ E_0\, e^{K_2 b}\frac{1}{K_2^2+(\frac{m\pi}{b})^2}\left[-\{K_2 + \beta_m\frac{m\pi}{b}\}\{e^{-K_2 w_3}\cos\frac{m\pi w_3}{b} - e^{-K_2 w_2}\cos\frac{m\pi w_2}{b}\}\right.$$

$$\left. + \{\frac{m\pi}{b} - \beta_m K_2\}\{e^{-K_2 w_3}\sin\frac{m\pi w_3}{b} - e^{-K_2 w_2}\sin\frac{m\pi w_2}{b}\}\right]$$

$$+ E_m\left[\{1-\beta_m^2\}\tfrac{1}{2}(w_3-w_2) + \frac{b}{4m\pi}\{1+\beta_m^2\}\{\sin\frac{2m\pi w_3}{b} - \sin\frac{2m\pi w_2}{b}\}\right]$$

$$+ \sum{}' E_\ell \frac{b}{\pi}\frac{1}{\ell^2-m^2}\left[\{\ell - m\beta_\ell\beta_m\}T_{E1\ell} - \{m - \ell\beta_\ell\beta_m\}T_{E2\ell} + \{m\beta_m + \ell\beta_\ell\}T_{E3\ell}\right.$$

$$\left. + \{\ell\beta_m + m\beta_\ell\}T_{E4\ell}\right]$$

$$+ G_0\, e^{-K_2 b}\frac{1}{K_2^2+(\frac{m\pi}{b})^2}\left[\{K_2 - \beta_m\frac{m\pi}{b}\}\{e^{K_2 w_3}\cos\frac{m\pi w_3}{b} - e^{K_2 w_2}\cos\frac{m\pi w_2}{b}\}\right.$$

$$\left. + \{\frac{m\pi}{b} + \beta_m K_2\}\{e^{K_2 w_3}\sin\frac{m\pi w_3}{b} - e^{K_2 w_2}\sin\frac{m\pi w_2}{b}\}\right]$$

$$+ G_m\left[\{1+\beta_m^2\}\tfrac{1}{2}(w_3-w_2) + \frac{b}{4m\pi}\{1-\beta_m^2\}\{\sin\frac{2m\pi w_3}{b} - \sin\frac{2m\pi w_2}{b}\}\right.$$

$$\left. - \beta_m\frac{b}{2m\pi}\{\cos\frac{2m\pi w_3}{b} - \cos\frac{2m\pi w_2}{b}\}\right]$$

$$+ \sum{}' G_\ell \frac{b}{\pi}\frac{1}{\ell^2-m^2}\left[\{\ell + m\beta_\ell\beta_m\}T_{E1\ell} - \{m + \ell\beta_\ell\beta_m\}T_{E2\ell} + \{m\beta_m - \ell\beta_\ell\}T_{E3\ell}\right.$$

$$\left. + \{\ell\beta_m - m\beta_\ell\}T_{E4\ell}\right]$$

$$= \hat{\alpha}\ \frac{1}{K_4^2+(\frac{m\pi}{b})^2}\left[\{K_4 - \beta_m \frac{m\pi}{b}\}\{e^{K_4 w_3}\cos\frac{m\pi w_3}{b} - e^{K_4 w_2}\cos\frac{m\pi w_2}{b}\}\right.$$

$$\left. + \{\frac{m\pi}{b} + \beta_m K_4\}\{e^{K_4 w_3}\sin\frac{m\pi w_3}{b} - e^{K_4 w_2}\sin\frac{m\pi w_2}{b}\}\right]$$

$$+ \hat{A}_0\ \frac{1}{K_4^2+(\frac{m\pi}{b})^2}\left[-\{K_4 + \beta_m \frac{m\pi}{b}\}\{e^{-K_4 w_3}\cos\frac{m\pi w_3}{b} - e^{-K_4 w_2}\cos\frac{m\pi w_2}{b}\}\right.$$

$$\left. + \{\frac{m\pi}{b} - \beta_m K_4\}\{e^{-K_4 w_3}\sin\frac{m\pi w_3}{b} - e^{-K_4 w_2}\sin\frac{m\pi w_2}{b}\}\right]$$

$$+ \sum{}'' \hat{A}_\ell\ \frac{1}{(\frac{m\pi}{b})^2-(\frac{\ell\pi}{w_1})^2}\left[\{\frac{m\pi}{b} - \beta_m \xi_\ell \frac{\ell\pi}{w_1}\}\{(-1)^\ell \sin\frac{m\pi w_3}{b} - \sin\frac{m\pi w_2}{b}\}\right.$$

$$\left. - \{\xi_\ell \frac{\ell\pi}{w_1} + \beta_m \frac{m\pi}{b}\}\{(-1)^\ell \cos\frac{m\pi w_3}{b} - \cos\frac{m\pi w_2}{b}\}\right]$$

$$+ \hat{A}_L \tfrac{1}{2} w_1\left[\{1-\beta_m \xi_L\}\cos\frac{m\pi w_2}{b} + \{\beta_m + \xi_L\}\sin\frac{m\pi w_2}{b}\right] \quad , \ m = 1,\ldots,N, \qquad 4.2.12$$

where

$$T_{D1\ell} = \cosh s_\ell t_3 \sin\frac{m\pi w_3}{b} - \cosh s_\ell t_2 \sin\frac{m\pi w_2}{b}$$

$$T_{D2\ell} = \sinh s_\ell t_3 \cos\frac{m\pi w_3}{b} - \sinh s_\ell t_2 \cos\frac{m\pi w_2}{b}$$

$$T_{D3\ell} = \cosh s_\ell t_3 \cos\frac{m\pi w_3}{b} - \cosh s_\ell t_2 \cos\frac{m\pi w_2}{b}$$

$$T_{D4\ell} = \sinh s_\ell t_3 \sin\frac{m\pi w_3}{b} - \sinh s_\ell t_2 \sin\frac{m\pi w_2}{b} \quad , \ \ell = 0,1,\ldots,N$$

$$T_{E1\ell} = \sin\frac{\ell\pi w_3}{b}\cos\frac{m\pi w_3}{b} - \sin\frac{\ell\pi w_2}{b}\cos\frac{m\pi w_2}{b}$$

$$T_{E2\ell} = \sin\frac{m\pi w_3}{b}\cos\frac{\ell\pi w_3}{b} - \sin\frac{m\pi w_2}{b}\cos\frac{\ell\pi w_2}{b}$$

$$T_{E3\ell} = \cos\frac{\ell\pi w_3}{b}\cos\frac{m\pi w_3}{b} - \cos\frac{\ell\pi w_2}{b}\cos\frac{m\pi w_2}{b}$$

$$T_{E4\ell} = \sin\frac{\ell\pi w_3}{b}\sin\frac{m\pi w_3}{b} - \sin\frac{\ell\pi w_2}{b}\sin\frac{m\pi w_2}{b} \quad , \quad \ell = 1,\ldots,N;$$

L is such that $\frac{m}{b} = \frac{L}{w_1}$ 4.2.13

and $\sum{}''$ denotes $\sum_{\substack{\ell=1 \\ \ell\neq L}}^{N}$

Condition (vii). Continuity of Volume Flux at $x = 0$, $w_2 \leq y \leq w_3$.

Using 3.4.18 and 4.2.5 in equation 4.2.8 gives

$$\sum_{\ell=0}^{\infty} D_\ell \frac{\theta}{s_\ell} \frac{\omega^2}{gh_2} \sinh s_\ell(y-b) + \sum_{\ell=0}^{\infty} F_\ell \alpha_\ell \cosh s_\ell(y-b)$$

$$- E_0 k_2^{(0)} e^{-K_2(y-b)} - \sum_{\ell=1}^{\infty} E_\ell k_2^{(\ell)} \left[\cos \frac{\ell\pi y}{b} - \nu_\ell \sin \frac{\ell\pi y}{b}\right]$$

$$+ G_0 k_2^{(0)} e^{K_2(y-b)} + \sum_{\ell=1}^{\infty} G_\ell k_2^{(\ell)} \left[\cos \frac{\ell\pi y}{b} + \nu_\ell \sin \frac{\ell\pi y}{b}\right]$$

$$= \begin{cases} 0, \quad 0 \leq y < w_2 \quad \text{and} \quad w_3 < y \leq b \\ \\ -\frac{h_4}{h_2} \frac{(1+i\phi_2)}{(1+i\phi_4)} \left\{ -\hat{\alpha}\, k_4^{(0)} e^{K_4 y} + \hat{A}_0 k_4^{(0)} e^{-K_4 y} \right. \\ \qquad \left. + \sum_{\ell=1}^{\infty} \hat{A}_\ell k_4^{(\ell)} \left[\cos \frac{\ell\pi}{w_1}(y-w_2) - \kappa_\ell \sin \frac{\ell\pi}{w_1}(y-w_2)\right]\right\}, \\ \qquad\qquad w_2 \leq y \leq w_3 , \end{cases} \qquad 4.2.14$$

with ν_ℓ as defined in 3.5.14a

α_ℓ as defined in 3.5.27

and $\kappa_\ell = \theta \frac{\omega^2}{gh_4} \frac{w_1}{\ell\pi} \frac{1}{k_4^{(\ell)}}$, $\ell \in \mathbb{Z}^+$. 4.2.15

With the weighting functions

$$w_0 = e^{K_2(y-b)}$$

$$w_m = \cos \frac{m\pi y}{b} + \nu_m \sin \frac{m\pi y}{b} , \quad m = 1,\ldots,N,$$

the Galerkin equations, which are produced from

$$\int_0^b w_m h_2 \tilde{u}_2(0,y)dy = \int_{w_2}^{w_3} w_m h_4 \tilde{u}_4(0,y)dy, \quad m = 0,1,\ldots,N,$$

are

$$\sum_{\ell=0}^{N} D_\ell \frac{\theta}{s_\ell} \frac{\omega^2}{gh_2} \frac{1}{K_2^2-s_\ell^2} \left[s_\ell \{1 - e^{-K_2 b} \cosh s_\ell b\} - K_2 e^{-K_2 b} \sinh s_\ell b \} \right]$$

$$+ \sum_{\ell=0}^{N} F_\ell \alpha_\ell \frac{1}{K_2^2-s_\ell^2} \left[s_\ell e^{-K_2 b} \sinh s_\ell b - K_2 \{1 - e^{-K_2 b} \cosh s_\ell b\} \right]$$

$$+ E_0 k_2^{(0)} b - \sum E_\ell k_2^{(\ell)} \frac{1}{K_2^2+(\frac{\ell\pi}{b})^2} \left[K_2 + \nu_\ell \frac{\ell\pi}{b} \right] \left[e^{-K_2 b} - (-1)^\ell \right]$$

$$- G_0 k_2^{(0)} \frac{1}{2K_2} \left[1 - e^{-2K_2 b} \right] + \sum G_\ell k_2^{(\ell)} \frac{1}{K_2^2+(\frac{\ell\pi}{b})^2} \left[K_2 - \nu_\ell \frac{\ell\pi}{b} \right] \left[e^{-K_2 b} - (-1)^\ell \right]$$

$$= \frac{h_4}{h_2} \frac{(1+i\phi_2)}{(1+i\phi_4)} e^{-K_2 b} \left\{ - \hat{\alpha} k_4^{(0)} \frac{1}{K_4+K_2} \left[e^{(K_4+K_2)w_3} - e^{(K_4+K_2)w_2} \right] \right.$$

$$+ \hat{A}_0 k_4^{(0)} \frac{1}{K_2-K_4} \left[e^{(K_2-K_4)w_3} - e^{(K_2-K_4)w_2} \right]$$

$$\left. + \sum \hat{A}_\ell k_4^{(\ell)} \frac{1}{K_2^2+(\frac{\ell\pi}{w_1})^2} \left[K_2 + \kappa_\ell \frac{\ell\pi}{w_1} \right] \left[(-1)^\ell e^{K_2 w_3} - e^{K_2 w_2} \right] \right\} \quad 4.2.16$$

(Note that if $h_2 = h_4$, the term with coefficient $\hat{A}_0$ is $\hat{A}_0 w_1$);

and

$$\sum_{\ell=0}^{N} D_\ell \frac{\theta}{s_\ell} \frac{\omega^2}{gh_2} \frac{1}{s_\ell^2+(\frac{m\pi}{b})^2} \left[s_\ell \{\cosh s_\ell b - (-1)^m\} + \nu_m \frac{m\pi}{b} \sinh s_\ell b \right]$$

$$- \sum_{\ell=0}^{N} F_\ell \alpha_\ell \frac{1}{s_\ell^2+(\frac{m\pi}{b})^2} \left[s_\ell \sinh s_\ell b + \nu_m \frac{m\pi}{b} \{\cosh s_\ell b - (-1)^m\} \right]$$

$$+ E_0 k_2^{(0)} \frac{1}{K_2^2+(\frac{m\pi}{b})^2} \left[K_2 + \nu_m \frac{m\pi}{b} \right] \left[e^{K_2 b} - (-1)^m \right] + E_m \frac{b}{2} k_2^{(m)} \left[1 - \nu_m^2 \right]$$

$$+ G_0 k_2^{(0)} \frac{1}{K_2^2+(\frac{m\pi}{b})^2} \left[K_2 - \nu_m \frac{m\pi}{b} \right] \left[e^{-K_2 b} - (-1)^m \right] - G_m \frac{b}{2} k_2^{(m)} \left[1 + \nu_m^2 \right]$$

$$+ \sum{}' E_\ell k_2^{(\ell)} \left[\nu_m \hat{I}_{\ell m} - \nu_\ell \hat{I}_{m\ell} \right] - \sum{}' G_\ell k_2^{(\ell)} \left[\nu_m \hat{I}_{\ell m} + \nu_\ell \hat{I}_{m\ell} \right]$$

$$= \frac{h_4}{h_2} \frac{(1+i\phi_2)}{(1+i\phi_4)} \left\{ -\hat{\alpha} \frac{k_4^{(0)}}{K_4^2+(\frac{m\pi}{b})^2} \left[\{K_4 - \nu_m \frac{m\pi}{b}\} \{e^{K_4 w_3} \cos \frac{m\pi w_3}{b} - e^{K_4 w_2} \cos \frac{m\pi w_2}{b}\} \right.\right.$$

$$\left. + \{\frac{m\pi}{b} + \nu_m K_4\} \{e^{K_4 w_3} \sin \frac{m\pi w_3}{b} - e^{K_4 w_2} \sin \frac{m\pi w_2}{b}\} \right]$$

$$- \hat{A}_0 k_4^{(0)} \frac{1}{K_4^2+(\frac{m\pi}{b})^2} \left[\{K_4 + \nu_m \frac{m\pi}{b}\} \{e^{-K_4 w_3} \cos \frac{m\pi w_3}{b} - e^{-K_4 w_2} \cos \frac{m\pi w_2}{b}\} \right.$$

$$\left. + \{\nu_m K_4 - \frac{m\pi}{b}\} \{e^{-K_4 w_3} \sin \frac{m\pi w_3}{b} - e^{-K_4 w_2} \sin \frac{m\pi w_2}{b}\} \right]$$

$$+ \hat{A}_L k_4^{(L)} \tfrac{1}{2} w_1 \left[\{1 - \nu_m \kappa_L\} \cos \frac{m\pi w_2}{b} + \{\nu_m + \kappa_L\} \sin \frac{m\pi w_2}{b} \right]$$

$$+ \sum{}'' \hat{A}_\ell k_4^{(\ell)} \frac{1}{(\frac{m\pi}{b})^2-(\frac{\ell\pi}{w_1})^2} \left[\{\frac{m\pi}{b} - \nu_m \kappa_\ell \frac{\ell\pi}{w_1}\} \{(-1)^\ell \sin \frac{m\pi w_3}{b} - \sin \frac{m\pi w_2}{b}\} \right.$$

$$\left.\left. - \{\nu_m \frac{m\pi}{b} + \kappa_\ell \frac{\ell\pi}{w_1}\} \{(-1)^\ell \cos \frac{m\pi w_3}{b} - \cos \frac{m\pi w_2}{b}\} \right] \right\} ,$$

$$m = 1,\ldots,N, \qquad 4.2.17$$

where L is as defined in 4.2.13

and $\hat{I}_{\ell m}$ is as defined in 3.5.12.

4.3 Determination of $\hat{\alpha}$

The equations in the previous section contain the factor $\hat{\alpha}$ which represents the amplitude and phase of the input wave in region 4 relative to the input in region 3. Since, in collecting data, one cannot distinguish between input and output waves, the value of $\hat{\alpha}$ cannot be specified but must be included as an unknown and determined as a solution to the system as a whole. This can be achieved if data is available in the two regions.

The elevations at two positions (X_3,Y_3) and (X_4,Y_4), in regions 3 and 4 respectively, are related by the equation

$$\zeta_3(X_3,Y_3) = \delta\, e^{-i\Phi}\, \zeta_4(X_4,Y_4)$$

where δ and Φ may be determined from measured tidal data. Using expressions 3.2.9 and 4.2.1, this equation may be replaced by the approximation

$$\begin{aligned} & e^{i k_3^{(0)} X_3 - K_3 Y_3} + A_0\, e^{-i k_3^{(0)} X_3 + K_3 Y_3} \\ & + \sum A_\ell\, e^{-i k_3^{(\ell)} X_3} \left[\cos \frac{\ell\pi Y_3}{b} + \rho_\ell \sin \frac{\ell\pi Y_3}{b} \right] \\ = \; & \delta\, e^{-i\Phi} \Big\{ \hat{\alpha}\, e^{-i k_4^{(0)} X_4 + K_4 Y_4} + \hat{A}_0\, e^{i k_4^{(0)} X_4 - K_4 Y_4} \\ & + \sum \hat{A}_\ell\, e^{i k_4^{(\ell)} X_4} \left[\cos \frac{\ell\pi}{w_1} (Y_4 - w_2) - \xi_\ell \sin \frac{\ell\pi}{w_1} (Y_4 - w_2) \right] \Big\} \qquad .4.3.1 \end{aligned}$$

This equation, with the $8(N+1)$ equations 3.5.10, .11; 3.5.17, .18; 3.5.23, .24; 3.5.32, .33; 3.5.34 - .37; 4.2.11, .12; 4.2.16, .17 are solved for the $8N+9$ unknowns $\hat{\alpha}$, A_ℓ, B_ℓ, C_ℓ, D_ℓ, E_ℓ, F_ℓ, G_ℓ, $\hat{A}_\ell$, $\ell = 0,1,\ldots,N$, by using a complex matrix inversion routine. The results are presented in Chapter 6.

CHAPTER 5

TWO NUMERICAL MODELS

Analytic models have a number of important attributes which make their development worthwhile. Although they simplify the features of the region of study to enable a solution to be found, they can throw a great deal of light on the important factors governing the fluid motion in the region. They also provide a guideline against which to compare numerical models. These latter must be developed for more realistic quantitative analyses, since, except in cases where perturbation techniques may be applicable, analytic solutions can only be found for systems which are aptly described by linear equations and have simple geometrical boundaries and depth profiles.

The restriction of linearization is not as serious as the other two; many models, including those of Platzman (1958) and Heaps (1969) have used the linear equations to good effect. Sometimes, as, for example, for residual circulation studies (see Nihoul and Ronday (1976)) or for areas which are quite shallow so that the surface elevation is comparable with the mean depth (see Flather and Heaps (1975)), the inclusion of the non-linear terms in a numerical model is essential. However, if the water is deep enough to justify the omission of these terms, and yet, to gain a realistic view of the behaviour of the system, complicated boundaries and depth contours need to be taken into account, a linear numerical model can be quite useful.

5.1 A Linear Finite-Difference Numerical Model

Assuming the time dependence factor $e^{-i\omega t}$, the linear equations governing tidal motion are those given by 2.2.1, that is,

$$(-i\omega + r/h)u - fv = -g\frac{\partial \zeta}{\partial x} \qquad 5.1.1a$$

$$(-i\omega + r/h)v + fu = -g\frac{\partial \zeta}{\partial y} \qquad 5.1.1b$$

$$\frac{\partial}{\partial x}(hu) + \frac{\partial}{\partial y}(hv) = i\omega\zeta \ . \qquad 5.1.1c$$

The numerical model uses finite-difference approximations to these equations. To determine the appropriate finite-difference forms, a two-dimensional rectangular grid is superimposed on the region of study, the boundaries thus being approximated by horizontal and vertical straight line segments. The grid points lie at the intersection of the lines drawn parallel to the x- and y-axes; the grid spacing in the x-direction is Δx and that in the y-direction is Δy.

The grid is composed of elements; within each element are a ζ-, a u- and a v-point arranged in a staggered fashion, as shown in Figure 5.1. This configuration has been used by many authors, including Platzman (1958), Leendertse (1967) and Ronday (1976), because of the simple form the coastal boundary conditions take. If ζ is evaluated at a grid-point with coordinates (x,y), u is evaluated at $(x-\Delta x,y)$ and v at $(x,y-\Delta y)$; the depth, h, is specified at the position (x,y). Each element is identified by an ordered pair, (ℓ,j), with $1 \leq \ell \leq m$ and $1 \leq j \leq n$, ℓ increasing in the positive x-direction, j increasing in the positive y-direction. The corresponding values of ζ, u, v, h are denoted by $\zeta_{\ell,j}$, $u_{\ell,j}$, $v_{\ell,j}$ and $h_{\ell,j}$. Figure 5.1 shows the (ℓ,j)th element and surrounding grid-points. Each element is further labelled according to which one of 12 classes it belongs. These classes identify

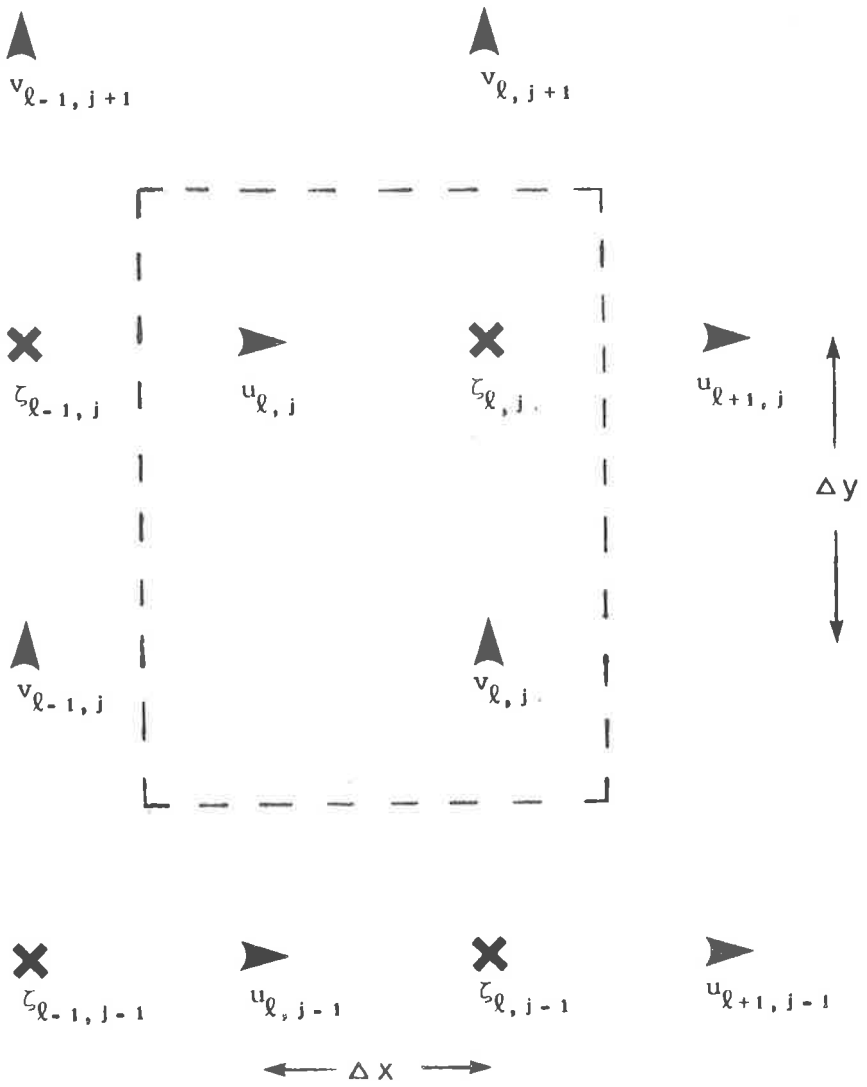

Figure 5.1 The (ℓ,j)th element and surrounding grid-points.

the manner of allocation of values to ζ, u and v and are set out in Table 5.1. From this table it can be seen that the coastal boundaries are always approximated in such a manner as to ensure that, if a land boundary is parallel to the y-direction, it passes through a u-point, and, if parallel to the x-direction, it passes through a v-point.

As far as is practicable, centred finite-difference approximations to 5.1.1 are used. Consider, for example, equation 5.1.1a which may be written

$$\{-i\omega + r(x-\Delta x,y)h^{-1}(x-\Delta x,y)\}u(x-\Delta x,y) - f\,v(x-\Delta x,y)$$

$$= - g \frac{\partial \zeta}{\partial x}(x-\Delta x,y) \quad . \qquad 5.1.2$$

Now, using Taylor series expansions

$$\zeta(x,y) = \zeta(x-\Delta x,y) + \Delta x \frac{\partial \zeta}{\partial x}(x-\Delta x,y) + \frac{(\Delta x)^2}{2}\frac{\partial^2 \zeta}{\partial x^2}(x-\Delta x,y) + O(\Delta x^3)$$

and

$$\zeta(x-2\Delta x,y) = \zeta(x-\Delta x,y) - \Delta x \frac{\partial \zeta}{\partial x}(x-\Delta x,y)$$

$$+ \frac{(\Delta x)^2}{2}\frac{\partial^2 \zeta}{\partial x^2}(x-\Delta x,y) + O(\Delta x^3),$$

so that

$$\zeta(x,y) - \zeta(x-2\Delta x,y) = 2\Delta x \frac{\partial \zeta}{\partial x}(x-\Delta x,y) + O(\Delta x^3),$$

that is, if the (ℓ,j)th element is being considered,

$$\frac{\partial \zeta}{\partial x}(x-\Delta x,y) = \frac{1}{2\Delta x}(\zeta_{\ell,j} - \zeta_{\ell-1,j}) + O(\Delta x^2).$$

In the same manner, the best approximation to $v(x-\Delta x,y)$ is

$$\tfrac{1}{4}(v_{\ell,j} + v_{\ell,j+1} + v_{\ell-1,j+1} + v_{\ell-1,j}) + O(\Delta x^2,\Delta y^2),$$

but, to avoid the inversion of a large $3mn \times 3mn$ complex matrix, an explicit system is developed, so that the approximation used is

$$v(x-\Delta x,y) = \tfrac{1}{2}(v_{\ell-1,j} + v_{\ell-1,j+1}) + O(\Delta x,\Delta y^2).$$

Hence, 5.1.2 may be written as

$$\{-i\omega + r_{u_{\ell,j}} h^{-1}_{u_{\ell,j}}\}u_{\ell,j} - \tfrac{1}{2}f(v_{\ell-1,j} + v_{\ell-1,j+1})$$

$$= -\frac{g}{2\Delta x}(\zeta_{\ell,j} - \zeta_{\ell-1,j}) + O(\Delta x,\Delta y^2), \qquad 5.1.3a$$

where $r_{u_{\ell,j}}$ is the friction parameter value at the grid point associated with $u_{\ell,j}$ (this parameter is discussed in Section 5.4) and

$$h_{u_{\ell,j}} = \begin{cases} \tfrac{1}{2}(h_{\ell,j} + h_{\ell-1,j}), & \ell \neq 1 \\ h_{1,j}, & \ell = 1. \end{cases}$$

In the same manner, the finite-difference approximations to equations 5.1.1b and c are found to be

$$\{-i\omega + r_{v_{\ell,j}} h^{-1}_{v_{\ell,j}}\}v_{\ell,j} + \tfrac{1}{2}f(u_{\ell,j} + u_{\ell,j-1})$$

$$= \frac{-g}{2\Delta y}(\zeta_{\ell,j} - \zeta_{\ell,j-1}) + O(\Delta y,\Delta x^2) \qquad 5.1.3b$$

and $$\frac{1}{2\Delta x}\{h_{u_{\ell+1,j}} u_{\ell+1,j} - h_{u_{\ell,j}} u_{\ell,j}\} + \frac{1}{2\Delta y}\{h_{v_{\ell,j+1}} v_{\ell,j+1} - h_{v_{\ell,j}} v_{\ell,j}\}$$

$$= i\omega\,\zeta_{\ell,j} + O(\Delta x^2,\Delta y^2), \qquad 5.1.3c$$

where

$$h_{v_{\ell,j}} = \begin{cases} \tfrac{1}{2}(h_{\ell,j} + h_{\ell,j-1}), & j \neq 1 \\ h_{\ell,1}, & j = 1 \end{cases}.$$

These equations are rearranged to give, in explicit form, the equations for the evaluation of $u_{\ell,j}$, $v_{\ell,j}$ and $\zeta_{\ell,j}$ at all interior points:-

$$u_{\ell,j} = h^{-1}_{u_{\ell,j}} \{h_{u_{\ell-1,j}} u_{\ell-1,j} - \frac{\Delta x}{\Delta y}(h_{v_{\ell-1,j+1}} v_{\ell-1,j+1} - h_{v_{\ell-1,j}} v_{\ell-1,j})$$

$$+ 2i\omega\Delta x\, \zeta_{\ell-1,j}\} \qquad 5.1.4a$$

$$\zeta_{\ell,j} = \zeta_{\ell-1,j} - \frac{2\Delta x}{g}\{(-i\omega + r_{u_{\ell,j}} h^{-1}_{u_{\ell,j}})u_{\ell,j}$$

$$- \tfrac{1}{2}f(v_{\ell-1,j} + v_{\ell-1,j+1})\} \qquad 5.1.4b$$

$$v_{\ell,j} = -\{-i\omega + r_{v_{\ell,j}} h^{-1}_{v_{\ell,j}}\}^{-1}\{\tfrac{1}{2}f(u_{\ell,j} + u_{\ell,j-1})$$

$$+ \frac{g}{2\Delta y}(\zeta_{\ell,j} - \zeta_{\ell,j-1})\}\,. \qquad 5.1.4c$$

The first equation is obtained by rearranging 5.1.3c after replacing ℓ by $\ell-1$, the second by rearranging 5.1.3a and the third by rearrangement of 5.1.3b. These equations are explicit since, on calculation of any of the unknowns on the left-hand side, all the quantities on the right-hand side are known provided that the sweep through the grid follows increasing values of ℓ and, for each ℓ, increasing values of j. The equations 5.1.4 must also be evaluated in the order given above.

The appropriate forms of these equations for non-interior points are given in Table 5.1.

5.2 The EVP Method

The solution, using the equations 5.1.4, is found by the EVP method described by Roache (1972, p.124). From Table 5.1, it can be seen that, for elements labelled 3 and 7, the value of $u_{\ell,j}$ is calculated according to equation 5.1.4a; the desired result of such a calculation is, naturally, zero, since the associated grid-point lies on a land boundary. Also, for elements labelled 11 and 12, $\zeta_{\ell,j}$ is calculated according to 5.1.4b, the desired result being some known input value along an open

1. 

$u_{\ell,j} = 0$

$\zeta_{\ell,j}$ provisionally assigned

$v_{\ell,j} = 0$

2. 

$u_{\ell,j}$, $\zeta_{\ell,j}$ } as in 5.1.4

$v_{\ell,j} = 0$

3. 

$u_{\ell,j}$ as in 5.1.4a

$\zeta_{\ell,j}$, $v_{\ell,j}$ } not calculated

4. 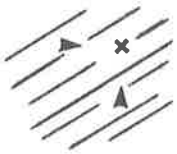

$u_{\ell,j}$, $\zeta_{\ell,j}$, $v_{\ell,j}$ } not calculated

5. 

$u_{\ell,j} = 0$

$\zeta_{\ell,j}$ provisionally assigned

$v_{\ell,j}$ as in 5.1.4c

6. 

$u_{\ell,j}$, $\zeta_{\ell,j}$, $v_{\ell,j}$ } as in 5.1.4

7. 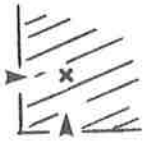

$u_{\ell,j}$ as in 5.1.4a

$\zeta_{\ell,j}$ not calculated

$v_{\ell,j} = 0$

8. 

$u_{\ell,j}$, $\zeta_{\ell,j}$ } not calculated

$v_{\ell,j} = 0$

9. (Western open boundary)

$u_{\ell,j}$ provisionally assigned

$\zeta_{\ell,j}$ is given

$v_{\ell,j}$ as in 5.1.4c

10. (Western open boundary)

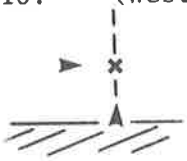

$u_{\ell,j}$ provisionally assigned

$\zeta_{\ell,j}$ is given

$v_{\ell,j} = 0$

11. (Eastern open boundary)

$u_{\ell,j}$, $\zeta_{\ell,j}$, $v_{\ell,j}$ } as in 5.1.4

12. (Eastern open boundary)

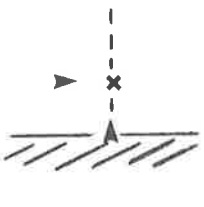

$u_{\ell,j}$, $\zeta_{\ell,j}$ } as in 5.1.4

$v_{\ell,j} = 0$

TABLE 5.1: The classes of elements for the linear numerical model and their associated methods of allocation of values to ζ, u and v . ////// indicates land, —— indicates a solid boundary and - - - an open boundary, while ► depicts a u-point, × a ζ-point and ▲ a v-point.

boundary at the Eastern extremity of the region of interest. Hence, it is necessary that those values (called starting-values) designated as "provisionally assigned", namely, $\zeta_{\ell,j}$ in elements labelled 1 and 5 and $u_{\ell,j}$ in elements labelled 9 and 10, should be such that a sweep through the grid produces the correct end-values for elements labelled 3, 7,11 or 12 on calculation of 5.1.4. The correct starting values are determined by finding the end-values produced by specific provisional starting-values.

For a consistent scheme with a unique solution the number of starting values, say K, is the same as the number of end-values. The two sets of values are numbered in increasing order as they are encountered in the scheme. For any set of starting-values $\{s_\alpha, \alpha = 1,\ldots,K\}$, the sweep through the grid produces a corresponding set of end-values, $\{\in_\alpha, \alpha = 1,\ldots,K\}$. Since the equations 5.1.4 are linear, there is a simple linear relation between the s_α and the $\in_\alpha$, namely

$$\underset{\sim}{\in} = A\underset{\sim}{s} + \underset{\sim}{\in}_0$$

where $\underset{\sim}{s} = (s_1,\ldots,s_K)^T$

$\underset{\sim}{\in} = (\in_1,\ldots,\in_K)^T$

$\underset{\sim}{\in}_0$ is the end-vector produced by $\underset{\sim}{s} = \underset{\sim}{0}$.

A is a K×K complex matrix whose columns are generated by starting-vectors of the form $\underset{\sim}{s}_\ell = (\delta_{k\ell})$ where $\delta_{k\ell}$ is the Kronecker delta. Thus, if $\underset{\sim}{\in}_\ell = A\underset{\sim}{s}_\ell + \underset{\sim}{\in}_0$, then $\underset{\sim}{a}_\ell = \underset{\sim}{\in}_\ell - \underset{\sim}{\in}_0$, where $\underset{\sim}{a}_\ell$ is the ℓth column of A.

Once these quantities have been determined, the correct starting-vector, $\underset{\sim}{s}^*$, is determined by

$$\underset{\sim}{s}^* = A^{-1}(\underset{\sim}{\in}^* - \underset{\sim}{\in}_0)$$

where $\underset{\sim}{\in}^*$ is the desired end-vector. Hence, (K+1) sweeps through the grid produce the correct starting-values which are then used in a final run to determine the values of ζ, u and v throughout the whole system.

5.3 Stability, Consistency and Convergence

The concepts of stability, consistency and convergence are discussed in all books which deal with the numerical analysis of finite-difference methods. Roache (1972, p.7 and p.50) gives an informative discussion of these features yet keeps them in their proper perspective with regard to an analysis of a finite-difference approximation (FDA) to a set of partial differential equations (PDE).

Consistency is simply the requirement that, as $\Delta x, \Delta y \to 0$, the truncation errors (as evident in equations 5.1.3) must approach zero, so that the FDA approaches the PDE.

As $\Delta x, \Delta y \to 0$, the discrete solution must approach the continuum solution, that is, the solution to the FDA must converge to the solution of the PDE. This is usually hard to prove as the FDA is used solely because the solution to the PDE is not known. Linear initial-value problems may use Lax's Equivalence Theorem to relate consistency and stability to convergence. However, no analogous theorem exists for schemes such as the EVP method, which have no explicit time dependence and so cannot be classed as initial-value problems, nor for non-linear schemes. However, the FDA can be used to solve a similar, but more simple, problem for which there is an analytic solution, and a comparison between the two can be used as a guideline as to the likely convergence of the FDA in more general problems. Probably the best test of convergence of the FDA is a comparison with field data, if adequate information is available.

An FDA is stable if the difference between its theoretical solution and its actual numerical solution remains bounded. This difference arises because of round-off errors.

5.3.1 Stability

To determine the usefulness of the finite-difference model set up in Section 5.1, the error amplification properties of the scheme need to be analyzed. This examination can be carried out by means of a discrete perturbation analysis (Roache (1972), Noye (1978))which, although lacking the methodical formulation of the commonly used von Neumann stability analysis, has the advantage of providing a round-off error bound, rather than just the reassuring information that (for a time-stepping scheme) repeated progressions through the grid will not increase the error without bound.

In the analysis which follows, it is assumed that both the depth, h, and the friction parameter, r, are constant. The simplified finite-difference equations are

$$u_{\ell,j} = u_{\ell-1,j} - \alpha\{v_{\ell-1,j+1} - v_{\ell-1,j}\} + \delta_3 \zeta_{\ell-1,j} \qquad 5.3.1a$$

$$\zeta_{\ell,j} = \zeta_{\ell-1,j} - \delta_1\{\beta\, u_{\ell,j} - \tfrac{1}{2} f(v_{\ell-1,j} + v_{\ell-1,j+1})\} \qquad 5.3.1b$$

$$v_{\ell,j} = -\beta^{-1}\{\tfrac{1}{2} f(u_{\ell,j} + u_{\ell,j-1}) + \delta_2^{-1}(\zeta_{\ell,j} - \zeta_{\ell,j-1})\} \qquad 5.3.1c$$

where

$$\alpha = \Delta x/\Delta y$$

$$\beta = -i\omega + r/h$$

$$\delta_1 = 2\Delta x/g$$

$$\delta_2 = 2\Delta y/g$$

$$\delta_3 = 2i\omega\Delta x/h.$$

If the magnitude of any error in $\zeta_{\ell,j}$ is $|\Delta\zeta_{\ell,j}|$, then, from 5.3.1c, it can be seen that

$$|\Delta v_{\ell,j}| = |\Delta v_{\ell,j+1}| = |\beta^{-1}\,\delta_2^{-1}\,\Delta\zeta_{\ell,j}|$$

and so, from 5.3.1a,

$$|\Delta u_{\ell+1,j}| \leq 2\alpha|\beta^{-1}\delta_2^{-1}\,\Delta\,\zeta_{\ell,j}| + |\delta_3\,\Delta\,\zeta_{\ell,j}| \ .$$

Finally, using these error bounds and 5.3.1b, the upper estimate of the error in $\zeta_{\ell+1,j}$ is

$$|\Delta\,\zeta_{\ell+1,j}| \leq \{1 + 2\alpha\delta_1\delta_2^{-1} + \delta_1|\delta_3\beta| + |f\beta^{-1}|\delta_1\delta_2^{-1}\}|\Delta\,\zeta_{\ell,j}|$$

or

$$|\Delta\,\zeta_{\ell+1,j}| \leq \{1 + |\theta|[1+\phi^2]^{-\frac{1}{2}}\alpha + 2\alpha^2 + \frac{4\omega^2}{gh}(\Delta x)^2[1+\phi^2]^{\frac{1}{2}}\}|\Delta\,\zeta_{\ell,j}| \ , \qquad 5.3.2$$

where the notation of the analytic model is used, namely,

$$\theta = f/\omega$$

$$\phi = r/\omega h \ .$$

The expression 5.3.2 indicates that the scheme is unstable from the point of view that an error introduced at any point is increased at each stage of the progression through the grid. However, the largest error occurs at the end-boundary in the x-direction ($\ell = m$), and the error at any interior point is smaller than this end-error. Hence, by limiting m, the number of grid-steps in the x-direction, the round-off error at $\ell = m$ (and so for $\ell < m$) can be kept within a desirable range.

However, 5.3.2 also shows that the error is smaller for smaller values of Δx and α so that some compromise must be made between having a small value for Δx and a small number of grid-steps in the x-direction. Smaller values of α can be achieved with larger values of Δy, but this must increase the truncation error (as evident by 5.1.3) and, once

again, some compromise must be made between having small round-off error propagation characteristics and having an acceptable truncation error.

If an acceptable value of Δx results in a grid which does not cover the region of interest, double precision can be used so that a useful number of significant figures can be retained at the end boundary of a larger grid; however, this increases the computer memory and time required for calculations and so limits the usefulness of the model. Nevertheless, it has been found that, for regions which are not too extensive, the amplification of round-off errors does not limit the use of equations 5.1.4 in describing tidal propagation.

The results of the application of these equations to the Gulf of Carpentaria, Australia, are given in Chapter 6. The model values used are

$$\Delta x = 13 \text{ km}$$

$$\alpha = \frac{1}{3}$$

$$h \geq 5 \text{ m}$$

$$|\theta| \leq .5 \text{ (using a latitude of } 12\tfrac{1}{2}^{\circ}\text{S)},$$

so that the error amplification, given by

$$|\Delta \zeta_{\ell+1,j}| \leq 1.53 |\Delta \zeta_{\ell,j}| ,$$

is not too restrictive, and the maximum error in the end-condition, using $m = 25$, is $\sim 10^{-5}$, which is acceptably small.

5.3.2 Consistency

The Taylor expansion approach used to obtain the finite-difference equations may be reversed for an analysis of the scheme's consistency. Thus, for example, each variable in equation 5.1.4a may be expanded about the point (x,y), corresponding to the position where $\zeta_{\ell-1,j}$ is calculated, to yield

$$\frac{\partial}{\partial x}(hu) + \frac{\partial}{\partial y}(hv) = i\omega\zeta - (\Delta x)^2\left[\frac{2}{3}u\frac{\partial^3 h}{\partial x^3} + \frac{h}{6}\frac{\partial^3 u}{\partial x^3} + \frac{\partial u}{\partial x}\frac{\partial^2 h}{\partial x^2} + \tfrac{1}{2}\frac{\partial h}{\partial x}\frac{\partial^2 u}{\partial x^2}\right]$$

$$- (\Delta y)^2\left[\frac{\partial v}{\partial y}\frac{\partial^2 h}{\partial y^2} + \tfrac{1}{2}\frac{\partial h}{\partial y}\frac{\partial^2 v}{\partial y^2} + \frac{2}{3}v\frac{\partial^3 h}{\partial y^3} + \frac{h}{6}\frac{\partial^3 v}{\partial y^3}\right] + O(\Delta x^3, \Delta y^3).$$

Hence, it can be seen that, as Δx , $\Delta y \to 0$, 5.1.4a approaches equation 5.1.1c. Similar results are obtained when the process is applied to the other two equations, indicating that the FDA given by 5.1.4 is indeed consistent with the PDE 5.1.1.

5.3.3 Convergence

The convergence of the system is tested by using the equations 5.1.4 to find the solution for the exact situation as is modelled analytically in Chapter 3. The results, indicating satisfactory convergence, are presented in Chapter 6.

5.4 The Friction Parameter

The form chosen for the friction parameter is that given as A1.5 in Appendix 1, that is

$$r = \frac{8}{3\pi}\frac{g}{C^2}v_m ,$$

with C, the Chèzy coefficient and v_m some estimate of the maximum magnitude of the velocities. Using a value of .030 for Manning's n,

$$r = \frac{.00744}{h^{1/3}}v_m . \qquad 5.4.1$$

The value of v_m has been modelled in two ways:-

(i) v_m is constant over the whole region and is chosen as an estimate of the mean value of the maximum magnitude of the velocities as given by the analytic model for the dominant component (if it exists)

and (ii) v_m varies with the grid point according to

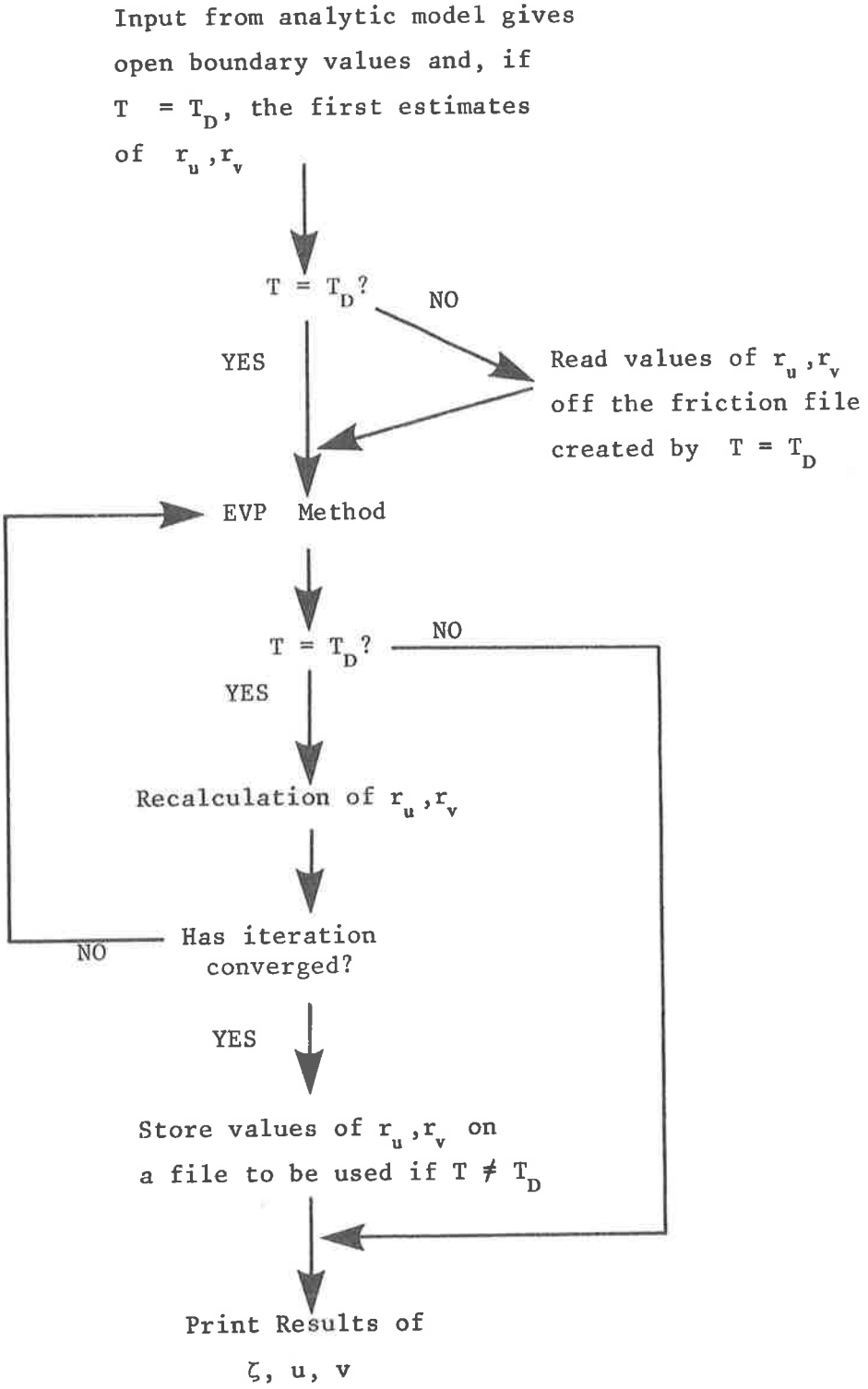

FIGURE 5.2: Flow chart for the linear numerical model, indicating iterative calculation of the friction parameter. T_D is the dominant tidal period.

$$\nu_{mu_{\ell,j}} = \{(u^*_{\ell,j})^2 + (\overline{\overline{v^*}}_{\ell,j})^2\}^{\frac{1}{2}}$$

$$\nu_{mv_{\ell,j}} = \{(\overline{\overline{u^*}}_{\ell,j})^2 + (v^*_{\ell,j})^2\}^{\frac{1}{2}} \quad , \qquad 5.4.2$$

where

$$\overline{\overline{v^*}}_{\ell,j} = \tfrac{1}{4}\{v^*_{\ell,j} + v^*_{\ell,j+1} + v^*_{\ell-1,j+1} + v^*_{\ell-1,j}\}$$

$$\overline{\overline{u^*}}_{\ell,j} = \tfrac{1}{4}\{u^*_{\ell,j} + u^*_{\ell+1,j} + u^*_{\ell+1,j-1} + u^*_{\ell,j-1}\} \quad ,$$

the *'s indicating that the values used are those obtained as a previous EVP solution. The values $\nu_{mu_{\ell,j}}$, $\nu_{mv_{\ell,j}}$ are thus found by iteration as shown in Figure 5.2. If a dominant tidal component exists, the iteration of the friction parameter is carried out only for this component. The values are then stored on a file to be used for any other component in accord with A1.6.

Hence, in general

$$r_{u_{\ell,j}} h^{-1}_{u_{\ell,j}} = \mu \ .00744 \ h^{-4/3}_{u_{\ell,j}} \nu_{mu_{\ell,j}}$$

$$r_{v_{\ell,j}} h^{-1}_{v_{\ell,j}} = \mu \ .00744 \ h^{-4/3}_{v_{\ell,j}} \nu_{mv_{\ell,j}}$$

where $\nu_{mu_{\ell,j}}$,$\nu_{mv_{\ell,j}}$ are either constant or as given by 5.4.2, and

$$\mu = \begin{cases} 1 & \text{, if the component is a dominant tidal component} \\ 1.5 & \text{, if the component is not dominant.} \end{cases}$$

5.5 A Non-linear Model

A non-linear model has been developed to provide a comparison with the linear model. The relevant equations of motion and continuity are those given as 2.1.1 in Chapter 2, omitting all the external influences

accumulated in the term $\underset{\sim}{\xi}$. These equations, written in component form with the notation of Chapter 2 are

$$\frac{\partial}{\partial t}(h+Z) + \frac{\partial}{\partial x}[(h+Z)U] + \frac{\partial}{\partial y}[(h+Z)V] = 0 \qquad 5.5.1a$$

$$\frac{\partial U}{\partial t} + U\frac{\partial U}{\partial x} + V\frac{\partial U}{\partial y} - fV = -g\frac{\partial Z}{\partial x} - \frac{\lambda}{(h+Z)^{4/3}} U(U^2+V^2)^{1/2} \qquad 5.5.1b$$

$$\frac{\partial V}{\partial t} + U\frac{\partial V}{\partial x} + V\frac{\partial V}{\partial y} + fU = -g\frac{\partial Z}{\partial y} - \frac{\lambda}{(h+Z)^{4/3}} V(U^2+V^2)^{1/2} , \qquad 5.5.1c$$

where the form A1.3, as discussed in Appendix 1, has been chosen for γ, that is

$$\gamma = \lambda/(h+Z)^{1/3} ,$$

with λ a constant, associated with a constant value of Manning's n.

The grid is composed of elements, exactly as described in Section 5.1. An explicit, forward-time, centred-space finite-difference approximation to the equations 5.5.1 is used, following along much the same lines as that used by Flather (1972). The approximations are found in the same manner as that given for equation 5.1.2 in Section 5.1. The notation is the same as used in that section with the addition of a superscript to designate the time level at which different quantities are used in the calculations. Thus $Z^{(n)}_{\ell,j}$ denotes Z evaluated in the (ℓ,j)th element at time $t = n\Delta t$, Δt being the time increment.

The approximations to equations 5.5.1 may be written

$$Z^{(n+1)}_{\ell,j} = Z^{(n)}_{\ell,j} - \frac{\Delta t}{2\Delta x}\left\{\overline{(h+Z^{(n)})}^{x}_{\ell+1,j}\, U^{(n)}_{\ell+1,j} - \overline{(h+Z^{(n)})}^{x}_{\ell,j}\, U^{(n)}_{\ell,j}\right\}$$

$$- \frac{\Delta t}{2\Delta y}\left\{\overline{(h+Z^{(n)})}^{y}_{\ell,j+1}\, V^{(n)}_{\ell,j+1} - \overline{(h+Z^{(n)})}^{y}_{\ell,j}\, V^{(n)}_{\ell,j}\right\} \qquad 5.5.2a$$

$$U_{\ell,j}^{(n+1)} = U_{\ell,j}^{(n)} - \frac{\Delta t}{4\Delta x} U_{\ell,j}^{(n)} \left\{ U_{\ell+1,j}^{(n)} - U_{\ell-1,j}^{(n)} \right\}$$

$$- \frac{\Delta t}{4\Delta y} \bar{\bar{V}}_{\ell,j}^{(n)} \left\{ U_{\ell,j+1}^{(n)} - U_{\ell,j-1}^{(n)} \right\} - \Delta t \, R_{u_{\ell,j}}^{(n)} U_{\ell,j}^{(n)}$$

$$+ \Delta t \, f \bar{\bar{V}}_{\ell,j}^{(n)} - \frac{\Delta t}{2\Delta x} g \left\{ Z_{\ell,j}^{(n+1)} - Z_{\ell-1,j}^{(n+1)} \right\} \qquad 5.5.2b$$

$$V_{\ell,j}^{(n+1)} = V_{\ell,j}^{(n)} - \frac{\Delta t}{4\Delta x} \bar{\bar{U}}_{\ell,j}^{(n+1)} \left\{ V_{\ell+1,j}^{(n)} - V_{\ell-1,j}^{(n)} \right\}$$

$$- \frac{\Delta t}{4\Delta y} V_{\ell,j}^{(n)} \left\{ V_{\ell,j+1}^{(n)} - V_{\ell,j-1}^{(n)} \right\} - \Delta t \, R_{v_{\ell,j}}^{(n)} V_{\ell,j}^{(n)}$$

$$- \Delta t \, f \bar{\bar{U}}_{\ell,j}^{(n+1)} - \frac{\Delta t}{2\Delta y} g \left\{ Z_{\ell,j}^{(n+1)} - Z_{\ell,j-1}^{(n+1)} \right\} , \qquad 5.5.2c$$

where

$$\overline{(h+Z^{(n)})}_{\ell,j}^{x} = \tfrac{1}{2}\{h_{\ell,j} + Z_{\ell,j}^{(n)} + h_{\ell-1,j} + Z_{\ell-1,j}^{(n)}\}$$

$$\overline{(h+Z^{(n)})}_{\ell,j}^{y} = \tfrac{1}{2}\{h_{\ell,j} + Z_{\ell,j}^{(n)} + h_{\ell,j-1} + Z_{\ell,j-1}^{(n)}\}$$

$$\bar{\bar{U}}_{\ell,j}^{(n)} = \tfrac{1}{4}\{U_{\ell,j}^{(n)} + U_{\ell+1,j}^{(n)} + U_{\ell+1,j-1}^{(n)} + U_{\ell,j-1}^{(n)}\}$$

$$\bar{\bar{V}}_{\ell,j}^{(n)} = \tfrac{1}{4}\{V_{\ell,j}^{(n)} + V_{\ell,j+1}^{(n)} + V_{\ell-1,j+1}^{(n)} + V_{\ell-1,j}^{(n)}\}$$

$$R_{u_{\ell,j}}^{(n)} = \lambda \{ \overline{(h+Z^{(n)})}_{\ell,j}^{x} \}^{-4/3} \{ (U_{\ell,j}^{(n)})^2 + (\bar{\bar{V}}_{\ell,j}^{(n)})^2 \}^{1/2} \qquad 5.5.3a$$

$$R_{v_{\ell,j}}^{(n)} = \lambda \{ \overline{(h+Z^{(n)})}_{\ell,j}^{y} \}^{-4/3} \{ (\bar{\bar{U}}_{\ell,j}^{(n)})^2 + (V_{\ell,j}^{(n)})^2 \}^{\frac{1}{2}} . \qquad 5.5.3b$$

Modified forms of these equations are required if the element is adjacent to a boundary. The classes of elements are the same as those for the linear model and are given, with the appropriate finite difference forms associated with them, in Appendix 4.

5.6 Consistency, Convergence and Stability

The analysis of the consistency of the non-linear FDA is carried out in the same manner as for the linear scheme. By expanding each variable in the equations 5.5.2 as a Taylor series about the position and time at which the first quantity on the right-hand-side of each equation is evaluated, it can be shown that the FDA differs from the PDE, 5.5.1, only by a truncation error of $O(\Delta x^2, \Delta y^2, \Delta x\Delta y, \Delta t)$. As Δx, Δy, $\Delta t \to 0$, it can be seen that the FDA approaches the PDE and so is consistent.

For the area in which the models were applied, it was considered unlikely that the non-linear advection terms would greatly influence the elevation of any fundamental frequency (though they would probably have a greater effect on the velocities and on any harmonics, as shown by, for example, Flather (1972), and Flather and Heaps (1975)). The friction parameter in the linear model was an adapted form of the frictional term in the non-linear model. Hence, the convergence of the non-linear FDA has been determined by a comparison of the results of the linear and non-linear models as shown in the next chapter.

The likely stability of a non-linear system is assessed by an investigation of the appropriate linearized problem:

$$Z_{\ell,j}^{(n+1)} = Z_{\ell,j}^{(n)} - \frac{h\Delta t}{2\Delta x}\{U_{\ell+1,j}^{(n)} - U_{\ell,j}^{(n)}\} - \frac{h\Delta t}{2\Delta y}\{V_{\ell,j+1}^{(n)} - V_{\ell,j}^{(n)}\} \qquad 5.6.1a$$

$$U_{\ell,j}^{(n+1)} = U_{\ell,j}^{(n)} - R\Delta t\, U_{\ell,j}^{(n)} - \frac{\Delta t}{2\Delta x} g\{Z_{\ell,j}^{(n+1)} - Z_{\ell-1,j}^{(n+1)}\}$$
$$+ f\frac{\Delta t}{4}\{V_{\ell,j}^{(n)} + V_{\ell,j+1}^{(n)} + V_{\ell-1,j+1}^{(n)} + V_{\ell-1,j}^{(n)}\} \qquad 5.6.1b$$

$$V_{\ell,j}^{(n+1)} = V_{\ell,j}^{(n)} - R\Delta t\, V_{\ell,j}^{(n)} - \frac{\Delta t}{2\Delta y} g\{Z_{\ell,j}^{(n+1)} - Z_{\ell,j-1}^{(n+1)}\}$$
$$- f\frac{\Delta t}{4}\{U_{\ell,j}^{(n+1)} + U_{\ell+1,j}^{(n+1)} + U_{\ell+1,j-1}^{(n+1)} + U_{\ell,j-1}^{(n+1)}\}\,, \qquad 5.6.1c$$

with R and h constants.

Using a von Neumann analysis (see, for example, Roache (1972)), the Fourier components of the solution for each Z, U, V may be written

$$(Z^{(n)}_{\ell,j}, U^{(n)}_{\ell,j}, V^{(n)}_{\ell,j}) = (A^n, B^n\, e^{-i k_x \Delta x}, C^n\, e^{-i k_y \Delta y}) e^{i 2(\ell k_x \Delta x + j k_y \Delta y)} \qquad 5.6.2$$

where A^n, B^n, C^n are the amplitude functions at time $t = n\Delta t$, k_x is the wave number in the x-direction, for any component, k_y the wave number in the y-direction and $i = \sqrt{-1}$.

Defining

$$\theta_x = k_x \Delta x$$

$$\theta_y = k_y \Delta y$$

$$\alpha = \frac{\Delta t}{\Delta x} \sin \theta_x$$

$$\beta = \frac{\Delta t}{\Delta y} \sin \theta_y$$

$$\in = R\Delta t$$

$$\delta = f\, \Delta t \cos \theta_x \cos \theta_y,$$

and using 5.6.2, the equations 5.6.1 may be rewritten as

$$A^{n+1} = A^n - ih\alpha\, B^n - ih\beta\, C^n$$

$$B^{n+1} = (1-\in)B^n - ig\alpha\, A^{n+1} + \delta\, C^n$$

$$C^{n+1} = (1-\in)C^n - gi\beta\, A^{n+1} - \delta\, B^{n+1}$$

which can be rearranged into the form,

$$\begin{bmatrix} A^{n+1} \\ B^{n+1} \\ C^{n+1} \end{bmatrix} = \underset{\approx}{G} \begin{bmatrix} A^n \\ B^n \\ C^n \end{bmatrix},$$

where

$$\underset{\approx}{G} = \begin{bmatrix} 1 & -ih\alpha & -ih\beta \\ -ig\alpha & 1-\epsilon-gh\alpha^2 & -gh\alpha\beta+\delta \\ \{ig\alpha\delta & \{-gh\alpha\beta & \{1-\epsilon-gh\beta^2 \\ -ig\beta\} & -\delta(1-\epsilon-gh\alpha^2)\} & +gh\alpha\beta\delta-\delta^2\} \end{bmatrix} .$$

The characteristic equation of this matrix is

$$-\lambda^3 + a_1\lambda^2 + a_2\lambda + a_3 = 0, \qquad 5.6.3$$

where

$$a_1 = 3 - 2\epsilon - \delta^2 - gh(\alpha^2+\beta^2) + gh\alpha\beta\delta$$

$$a_2 = -3 + 4\epsilon - \epsilon^2 + \delta^2 + (1-\epsilon)gh(\alpha^2+\beta^2) - gh\alpha\beta\delta$$

$$a_3 = (1-\epsilon)^2 \quad .$$

For a strongly stable scheme, $|\lambda| < 1$ for all θ_x, θ_y. For the case of $f = 0$, 5.6.3 may be factorized as

$$(1-\epsilon-\lambda)\{\lambda^2 + \lambda[-2+\epsilon+gh(\alpha^2+\beta^2)] + (1-\epsilon)\} = 0,$$

so that the eigenvalues are

$$\lambda_1 = 1 - \epsilon$$

$$\lambda_{2,3} = D \pm \{D^2 - (1-\epsilon)\}^{\frac{1}{2}}$$

where

$$D = 1 - \frac{\epsilon}{2} - \frac{gh}{2}(\alpha^2+\beta^2).$$

From these values, it is found that $|\lambda| < 1$ if

$$\epsilon < 2$$

and

$$\frac{\epsilon}{2} + \frac{gh}{4}(\alpha^2+\beta^2) < 1$$

or $$\frac{R\Delta t}{2} < 1$$

and $$\frac{R\Delta t}{2} + \frac{gh}{4}(\Delta t)^2\left\{\frac{1}{(\Delta x)^2} + \frac{1}{(\Delta y)^2}\right\} < 1.$$

(This second condition may be slightly over-restrictive depending on whether or not $(\theta_x = \pm\pi/2,\ \theta_y = \pm\pi/2)$ satisfies the condition

$$\left[\frac{\epsilon}{2} + \frac{gh}{2}(\alpha^2+\beta^2)\right]^2 > gh(\alpha^2+\beta^2). \quad)$$

This is a subcase of the conditions determined by Flather (1972). An explicit expression for the eigenvalues, λ, cannot be found when $R \neq 0, f \neq 0$ but an analysis is possible using the Routh-Hurwitz criteria set out in Appendix B in Leendertse's (1967) paper. The analysis is given in detail by Flather and the resulting conditions which ensure stability are

$$(R + |f|)\Delta t < 2$$

5.6.4

and

$$\frac{\Delta t}{2}(R + |f|) + \frac{gh}{4}(\Delta t)^2\left\{\frac{1}{(\Delta x)^2} + \frac{1}{(\Delta y)^2}\right\} < 1 .$$

CHAPTER 6

APPLICATIONS TO THE GULF OF CARPENTARIA

6.1 The Gulf of Carpentaria

The models developed in the previous chapters have been applied to the Gulf of Carpentaria and the adjacent waters. This Gulf is located in the North-Eastern part of Australia, between latitudes 10°S and 17°S and longitudes 135°E and 142°E. It has a roughly rectangular geometry, a surface area of about 193,000 km^2 and a relatively smooth bathymetry. It is a shallow area, the greatest depths being about 70 m, the nearest deeper water occurring either East of Torres Strait or in the Timor Trench. Figure 6.1 shows the overall geography of the area and the depth contours in metres (after Rochford (1966)).

6.1.1 Tidal Measurements

The amplitudes and phases of the four main tidal components at various places are given in the Australian National Tide Tables, 1978. These components are

Solar Diurnal (K_1) with period 23.9 hours

Lunar Diurnal (O_1) with period 25.8 hours

Solar Semi-diurnal (S_2) with period 12.0 hours

and Lunar Semi-diurnal (M_2) with period 12.4 hours.

However, all measurements are taken either very close to the mainland or on islands. The value of such measurements in providing a comparison for tidal models is questionable, since the data is collected"in the midst of the very coastal features most likely to exert anomalous effects on the phase and amplitude of the tide" (Hendershott and Munk (1970)).

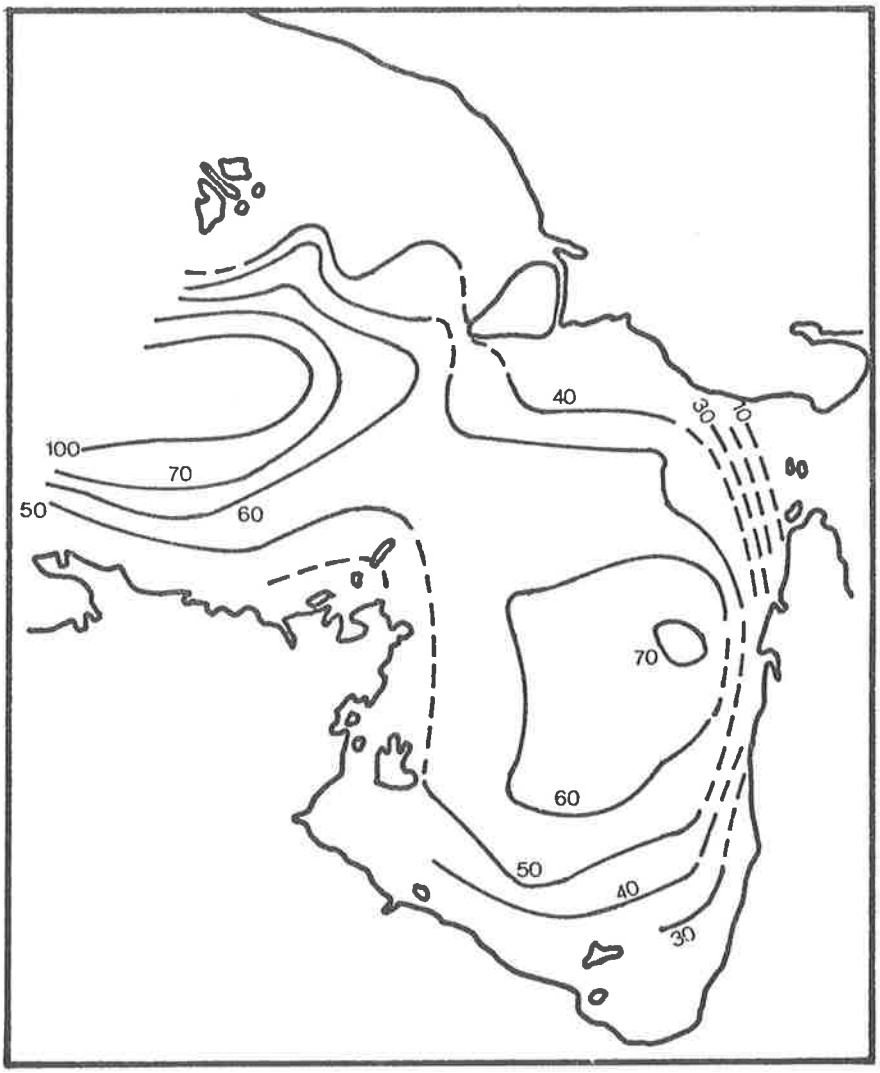

FIGURE 6.1: The Gulf of Carpentaria and adjacent waters. The depth contours are shown in metres (after Rochford (1966)).

6.1.2 Tidal Studies

An outline of the tidal features of the Gulf is given by Easton (1970), though his co-range lines are not very informative. He states that "the presence of a central amphidromic point is suggested by the diurnal amd semi-diurnal components; further nodal points occur probably near Karumba and Groote Eylandt." Cresswell's (1971) study supports the suggestion that "the diurnal wave travels clockwise around the perimeter of the Gulf, pivoting on some as-yet-unknown amphidromic point within the Gulf."

Williams (1972) has studied the response of the Gulf to tidal forcing by means of two analytic models, one without the effect of the Coriolis force (also published in Buchwald and Williams (1975)) and the other including rotation. Both of these studies neglected the effect of dissipation of energy by bottom friction and the presence of tidal forcing through Torres Strait.

Calculations by Miller (1966) indicate that approximately 10% of the total lunar tidal flux out of the deep oceans enters the Arafura sea and is dissipated in the vicinity of the Gulf of Carpentaria, so that the inclusion of some energy dissipation mechanism would appear to be almost mandatory. According to Teleki et al (1973), "the bottom friction should be of considerable amplitude for the entrainment of the fine grain size sediments found in the Southern part of the basin." Bottom friction is the mechanism chosen to model dissipation of energy in this thesis.

Torres Strait, complicated by its array of islands, shoals and atolls, is very shallow in comparison with the Gulf and, for this reason, Williams (1972) considers the Strait as a land barrier. However, during certain periods of the year, there is substantial water movement through the Strait into the Gulf (see Newell (1973)) and so its effect on the tides in the Gulf is considered in the model developed in Chapter 4.

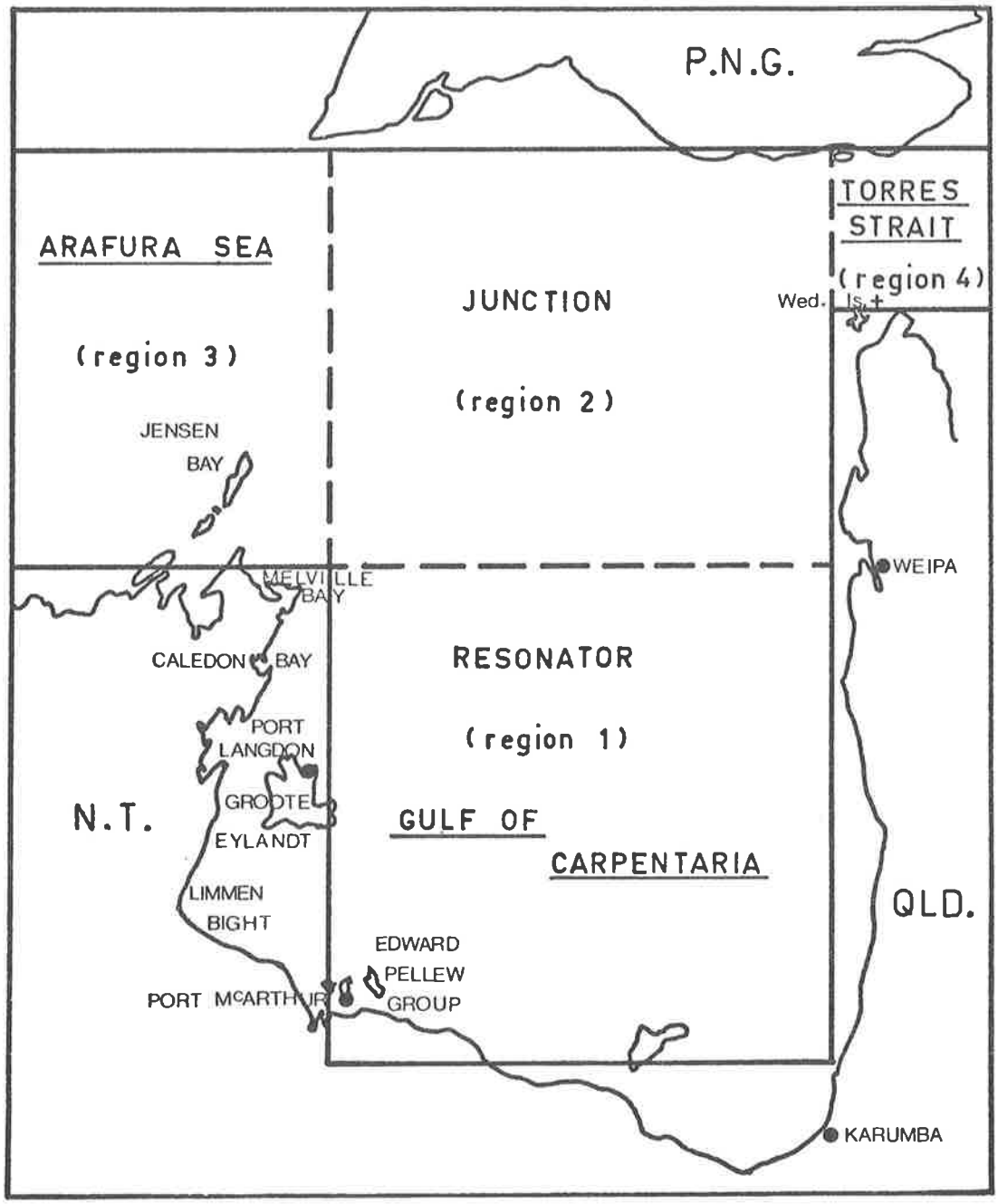

FIGURE 6.2: The boundary approximation for the analytic models, showing the regions into which the area is divided.

Williams (1972) includes a depth discontinuity between the junction and the resonator but uses a constant depth of 91.5 m in the channel (region 3) and junction. From Figure 6.1, it can be seen that a better approximation would be a depth discontinuity between the channel and the junction.

Figure 6.2 shows the rectangular resonator-channel system which has been used in this analytic study of the tidal propagation in the Gulf of Carpentaria. The dashed lines indicate the common boundaries of the regions into which the area has been divided and also the discontinuity in depths as modelled in Chapters 3 and 4.

6.2 The Analytic Model of Chapter 3

The values of the various constants used in Chapter 3 are

$a = 468$ km

$b = 390$ km

$d = 468$ km

$h_1 = 55$ m

$h_2 = 60$ m

$h_3 = 91.5$ m

$f = -3.1 \times 10^{-5} s^{-1}$ (corresponding to latitude $12\frac{1}{2}°S$).

The friction parameter used is that given as A1.5 in Appendix 1, that is

$$r = \frac{8}{3\pi} \frac{g}{C^2} \nu_m .$$

Using $n = .030$, this may be written as

$$r_j = .00744\, h_j^{-1/3}\, \nu_{m_j}, \quad j = 1,2,3, \qquad 6.2.1$$

where the value of ν_{m_j} is found, by trial and error from the M_2 tide, to be

$$\nu_{m_j} = .35 \text{ ms}^{-1}, \quad j = 1,2,3. \qquad 6.2.2$$

With these parameter values, the assumption that the input wave may be approximated by the form 3.2.8 which neglects all modes other than the Kelvin wave, must be justified.

Consider any component

$$\zeta_\ell(x,y) = \alpha_\ell \, e^{-\beta_\ell x + i\mu_\ell x} \, Y(y)$$

where $Y(y)$ is a sinusoidal function of Y,

α_ℓ is a constant,

$k_3^{(\ell)} = \mu_\ell + i\beta_\ell$ with $\beta_\ell > 0$, $\mu_\ell > 0$.

All such components decay exponentially as x becomes less negative. To neglect the components with $\ell \geq 1$, it is required that

$$\left|\frac{\zeta_\ell(-a,y)}{\zeta_\ell(-L,y)}\right| \ll 1 \text{ and } \left|\frac{\zeta_\ell(-a,y)}{\zeta_0(-a,y)}\right| \ll 1, \qquad 6.2.3$$

where $(L-a)$ is the effective length of the input channel $(L > a)$. Now, $\beta_\ell(a-L) < 0$ and if $|\beta_\ell(a-L)| \gg 1$, then 6.2.3 follows. Since, for the above parameter values, it is found that

$$\beta_0 \ll \beta_1 < \beta_2 < \ldots,$$

it is sufficient that $L-a \gg 1/\beta_1$ for it to be possible to neglect the Poincaré waves. In fact, $1/\beta_1 \approx 151$ km for the M_2 tide (this being the dominant tide in the area) and the effective length of the input channel is greater than 500 km. Hence, it may be considered that the form 3.2.8,

that is

$$\zeta_0(x,y) = e^{i k_3^{(0)} x - K_3 y} ,$$

is a good approximation to the tidal input for the Gulf of Carpentaria. It would not be expected, though, that the results present an accurate picture of tidal propagation farther up-channel, away from the channel/junction boundary.

The tide at Jensen Bay (see Figure 6.2) is used as the reference point for the scaling of the response as described in Section 3.2.

6.2.1 Convergence of the Galerkin Method

Using the above parameter values and the M_2 tide, the convergence of the Galerkin method is tested by checking that the residuals of each of the conditions in Section 3.5 become smaller as the value of N is increased (see Appendix 2).

(1) The errors in Condition 3.5.1, $\zeta_2(-a,y) = \zeta_3(-a,y)$, $0 \leq y \leq b$ are presented in Tables 6.1a and 6.1b. The percentage error is calculated according to the ratio $\Delta/|\zeta_2|$, when $\Delta = ||\zeta_3| - |\zeta_2||$, or $\Delta/\text{Arg}(\zeta_2)$ when $\Delta = |\text{Arg}(\zeta_3) - \text{Arg}(\zeta_2)|$. The errors in both the amplitude and the phase can be seen to become acceptably small as N is increased. The largest errors occur at the two ends, $y = 0$ and $y = b$, though the error at $y = b$ is less than 1% for $N = 6$. The larger error at $(-a,0)$ could be accounted for by the erroneous nature of the condition on the velocities at this corner (see Section 3.1).

(2) The convergence for the condition 3.5.2, $h_2u_2(-a,y) = h_3u_3(-a,y)$, $0 \leq y \leq b$, is much faster than for the previous condition, as can be seen by Table 6.2. The percentage error is calculated according to the ratio $\Delta/|h_2u_2|$, where $\Delta = |h_3|u_3| - h_2|u_2||$; a zero is entered in the table if $\Delta < .005$ and the percentage error is less than .05%.

y/b	N = 2		N = 4		N = 6		N = 8	
	Δ	%	Δ	%	Δ	%	Δ	%
0	.075	11.47	.056	8.75	.046	7.20	.040	6.20
1/10	.003	.47	.016	2.17	.016	2.16	.009	1.28
2/10	.024	3.17	.011	1.44	.005	.71	.006	.85
3/10	.023	2.93	.008	1.03	.003	.38	.005	.61
4/10	.008	1.01	.007	.94	.006	.69	.003	.41
5/10	.008	.94	.004	.52	.003	.33	.002	.23
6/10	.015	1.88	.006	.80	.002	.23	0	0
7/10	.013	1.56	.002	.21	.004	.46	0	0
8/10	.003	.35	.007	.75	.002	.18	.001	.21
9/10	.009	1.04	.001	.03	.002	.28	.002	.28
1	.019	2.08	.009	1.00	.005	.62	.004	.44

TABLE 6.1a: The error in the amplitude in condition 3.5.1, $\zeta_2(-a,y) = \zeta_3(-a,y)$, $0 \leq y \leq b$, using the Galerkin technique, for increasing values of N.

$\Delta = \big|\, |\zeta_2| - |\zeta_3| \,\big|$

y/b	N = 2		N = 4		N = 6		N = 8	
	Δ	%	Δ	%	Δ	%	Δ	%
0	.028	.37	.015	.20	.01	.13	.007	.09
1/10	.005	.06	0	0	0	0	0	0
2/10	.007	.09	.004	.06	0	0	0	0
3/10	.008	.11	0	0	0	0	0	0
4/10	.004	.06	0	0	0	0	0	0
5/10	0	0	0	0	0	0	0	0
6/10	0	0	0	0	0	0	0	0
7/10	0	0	0	0	0	0	0	0
8/10	.004	.05	0	0	0	0	0	0
9/10	0	0	0	0	0	0	0	0
1	.013	.17	.010	.12	.008	.09	.006	.07

TABLE 6.1b: The error in the phases in condition 3.5.1, $\zeta_2(-a,y) = \zeta_3(-a,y)$, $0 \leq y \leq b$, using the Galerkin technique, for increasing values of N. $\Delta = |\mathrm{Arg}(\zeta_2) - \mathrm{Arg}(\zeta_3)|$.

y/b	N = 2		N = 4		N = 6		N = 8	
	Δ	%	Δ	%	Δ	%	Δ	%
0	0	0	0	0	0	0	0	0
1/10	.006	0	0	0	0	0	0	0
2/10	.005	0	0	0	0	0	0	0
3/10	.014	.09	0	0	0	0	0	0
4/10	.010	.08	0	0	0	0	0	0
5/10	.005	0	0	0	0	0	0	0
6/10	.021	.16	.008	.05	0	0	0	0
7/10	.024	.17	0	0	0	0	0	0
8/10	.006	0	0	0	0	0	0	0
9/10	.023	.14	0	0	0	0	0	0
1	.044	.27	.02	.13	.01	.09	.01	.06

TABLE 6.2: The error in the amplitudes of condition 3.5.2, $h_2u_2(-a,y) = h_3u_3(-a,y)$, $0 \leq y \leq b$, using the Galerkin technique, for increasing values of N.

$\Delta = \big|\, |h_2u_2| - |h_3u_3| \,\big|$.

$\lvert x/a \rvert$	N = 2		N = 4		N = 6		N = 8	
	Δ	%	Δ	%	Δ	%	Δ	%
0	.029	3.78	.010	1.37	.006	.73	.003	.46
1/12	.023	3.12	.004	.55	.001	.11	.002	.31
2/12	.006	.83	.008	1.24	.006	.87	.001	.15
3/12	.016	2.75	.010	1.82	.003	.43	.004	.61
4/12	.033	6.92	.001	.20	.005	1.15	.004	.78
5/12	.035	10.36	.013	3.59	.005	1.38	.001	.24
6/12	.020	9.99	.009	4.06	.006	2.46	.004	1.58
7/12	.006	9.17	.007	12.65	.007	10.48	.005	8.84
8/12	.044	56.77	.020	16.95	.003	3.01	.004	4.54
9/12	.060	28.75	0	0	.004	5.50	.001	.58
10/12	.043	12.27	.032	8.74	.003	.70	.011	2.74
11/12	.028	5.59	.020	4.19	.027	5.50	.022	4.28
1	.163	24.96	.104	16.05	.080	12.33	.066	10.21

TABLE 6.3a: The error in the amplitude in condition 3.5.3, $\zeta_1(x,0) = \zeta_2(x,0)$, $-a \leq x \leq 0$, using the Galerkin technique, for increasing values of N.

$\Delta = \left| \, |\zeta_2| - |\zeta_1| \, \right|$

$\left\|x/a\right\|$	N = 2		N = 4		N = 6		N = 8	
	Δ	%	Δ	%	Δ	%	Δ	%
0	.021	1.03	.005	.24	.002	.10	.001	.05
1/12	.010	.51	0	0	.001	.07	.001	.05
2/12	.004	.18	.005	.24	0	0	.001	.06
3/12	.018	.92	.002	.10	.004	.18	0	0
4/12	.029	1.44	.008	.40	.002	.08	.008	.13
5/12	.019	1.35	.017	.86	.007	.37	.004	.19
6/12	.008	.39	.008	.40	.002	.11	.002	.11
7/12	.383	16.16	.219	7.60	.161	6.06	.092	3.60
8/12	.004	.05	.084	1.13	.035	.47	.006	.08
9/12	.010	.14	.027	.34	.004	.05	.009	.11
10/12	.019	.25	.013	.17	.013	.16	.006	.07
11/12	.031	.41	.010	.13	0	0	.004	.05
1	.009	.13	.005	.07	.004	.05	0	0

TABLE 6.3b: The error in the phases in condition 3.5.3, $\zeta_1(x,0) = \zeta_2(x,0)$, $-a \leq x \leq 0$, using the Galerkin technique, for increasing values of N. $\Delta = \left|\mathrm{Arg}(\zeta_2) - \mathrm{Arg}(\zeta_1)\right|$.

y/b	0	1/10	2/10	3/10	4/10	5/10	6/10	7/10	8/10	9/10	1
N = 2	.0038	.0023	.0006	.0033	.0041	.0021	.0020	.0059	.0061	.0012	.0189
N = 4	.0012	.0001	.0012	.0005	.0012	.0009	.0014	.0015	.0021	.0029	.0106
N = 6	.0006	.0003	.0003	.0006	.0003	.0005	.0009	.0005	.0009	.0025	.0073
N = 8	.0003	.0003	.0002	.0001	.0001	.0003	.0005	.0007	.0009	.0014	.0056

TABLE 6.4: Values of $|u_2(0,y)|$, calculated using the Galerkin technique, for increasing values of N.

$\left\|x/a\right\|$	0	1/12	2/12	3/12	4/12	5/12	6/12	7/12	8/12	9/12	10/12	11/12	1
N = 2	.0014	.0013	.0006	.0007	.0018	.0021	.0013	.0005	.0025	.0037	.0027	.0017	.0101
N = 4	.0004	.0003	.0003	.0006	0	.0007	.0005	.0005	.0011	0	.0018	.0011	.0057
N = 6	.0002	0	.0003	.0001	.0003	.0002	.0003	.0004	.0002	.0007	.0001	.0013	.0039
N = 8	.0001	0	.0001	.0002	.0002	0	.0002	.0003	.0002	.0001	.0005	.0010	.0030

TABLE 6.5: Values of $|v_1(x,-d)|$, calculated using the Galerkin technique, for increasing values of N.

(3) Tables 6.3a and b indicate the error in condition 3.5.3, $\zeta_1(x,0) = \zeta_2(x,0)$, $-a \leq x \leq 0$. The residuals of this condition are also seen to decrease as N is increased, however, a comparison with Table 6.1 shows that the convergence is slower than for condition 3.5.1. Except near $x = -a$, there is error only in the 3rd decimal place when $N = 8$, but the percentage error is still high; this is because of the small amplitude region associated with the amphidromic point as seen in Figure 6.5, which shows the co-amplitude and co-phase lines for the M_2 tide. Once again, the largest error in the amplitude occurs at $(-a,0)$.

(4) Table 6.4 shows the error in condition 3.5.4, $u_2(0,y) = 0$, $0 \leq y \leq b$. Satisfactory convergence is obtained as N is increased.

(5) The error in condition 3.5.5, $v_1(x,-d) = 0$, $-a \leq x \leq 0$, is shown in Table 6.5. This also shows satisfactory convergence as the value of N is increased.

The condition $h_1v_1(x,0) = h_2v_2(x,0)$ is satisfied exactly in Section 3.4 and the error was correspondingly found to be zero.

6.2.2 Convergence Using the Collocation Method

Since the mathematical manipulation using the Collocation method is less work than for the Galerkin technique, the same situation was programmed, using this simpler method, to compare the rates of convergence. The results for conditions 3.5.1 and 3.5.3 are shown in Tables 6.6 and 6.7 respectively. Whereas the errors do decrease as N is increased, the rate of convergence is slower than for the Galerkin technique. The zero entries in these tables correspond to chosen Collocation points.

The figures in brackets in Table 6.7 for $N = 2$ are calculated according to the ratio $\Delta/|\zeta_1|$ instead of $\Delta/|\zeta_2|$ since the latter ratio gave an error of greater than 100%, distorting the indication of accuracy.

y/b	N = 2		N = 4		N = 6		N = 8	
	Δ	%	Δ	%	Δ	%	Δ	%
0	0	0	0	0	0	0	0	0
1/10	.084	11.0	.076	9.98	.050	6.67	.022	3.01
2/10	.104	12.83	.032	4.09	.019	2.56	.021	2.81
3/10	.082	9.87	.023	2.98	.013	1.71	.014	1.79
4/10	.040	4.85	.028	3.53	.016	1.93	.006	.79
5/10	0	0	0	0	0	0	0	0
6/10	.025	3.04	.016	1.92	.009	1.08	.004	.42
7/10	.031	3.74	.008	.89	.004	.49	.004	.51
8/10	.023	2.73	.006	.66	.003	.36	.003	.37
9/10	.010	1.17	.007	.78	.004	.43	.002	.17
1	0	0	0	0	0	0	0	0

TABLE 6.6: Errors in the amplitudes in condition 3.5.1, $\zeta_2(-a,y) = \zeta_3(-a,y)$, $0 \leq y \leq b$, as calculated using Collocation, for increasing values of N. $\Delta = \left| \, |\zeta_2| - |\zeta_3| \, \right|$.

$\left\lvert x/a \right\rvert$	N = 2		N = 4		N = 6		N = 8	
	Δ	%	Δ	%	Δ	%	Δ	%
0	0	0	0	0	0	0	0	0
1/12	.007	.96	.004	.51	.002	.30	.001	.16
2/12	.026	3.82	.008	0	0	0	.003	.38
3/12	.047	7.98	0	0	.008	1.26	0	0
4/12	.056	12.02	.018	3.63	0	0	.006	1.18
5/12	.042	12.63	.024	6.48	.014	4.06	.008	2.13
6/12	0	0	0	0	0	0	0	0
7/12	.026	41.63	.026	57.30	.017	27.14	.010	19.44
8/12	.143	200.48 (66.51)	.052	35.90	0	0	.018	16.98
9/12	.201	101.24 (50.0)	0	0	.043	15.08	0	0
10/12	.213	63.32	.090	24.34	0	0	.034	8.28
11/12	.152	30.93	.128	26.74	.093	19.16	.056	11.36
1	0	0	0	0	0	0	0	0

TABLE 6.7: Errors in the amplitude in condition 3.5.3, $\zeta_1(x,0) = \zeta_2(x,0)$, $-a \leq x \leq 0$, using the Collocation method, for increasing values of N. $\Delta = \left|\, |\zeta_1| - |\zeta_2| \,\right|$.

The comparison of Table 6.1 with 6.6 and Table 6.3 with 6.7 justify the use of the more complicated Galerkin technique.

6.2.3 The Frequency Response of the Gulf

Williams (1972), using a Gulf width of $a = 480$ km, found the resonant periods of the Gulf to be 7.86 hrs, 10.35 hrs and 16.0 hrs. His frequency-response curve is based on the amplitude at Karumba and is shown in Figure 6.3. It displays a broad maximum over the periods 15.5 hrs to 17.0 hrs rather than a resonance peak. On the basis of this figure, he uses a period of 11.8 hrs for the semi-diurnal tide rather than 12.4 hrs.

Since bottom friction will tend to damp out oscillations, and in order to find a Gulf width which produces a response which agrees with the observed resonance oscillations of 10.6 hrs and 16.0 hrs (Melville and Buchwald (1976)), the frequency response curves were determined for several different Gulf widths. These curves represent the amplitude at Karumba in response to a unit amplitude at Jensen Bay. The results for $a = 468$ km, 520 km and 546 km are presented in Figure 6.4. Each curve shows a marked resonance near 8.5 hrs, the peak values being

22.2 m at 8.3 hrs for $a = 468$ km

26.3 m at 8.5 hrs for $a = 520$ km

24.6 m at 8.6 hrs for $a = 546$ km.

Melville and Buchwald (1976) indicate that there is some evidence of resonance activity at a period of about 8.0 hrs. Using Figure 6.4, the width of the Gulf was chosen as 468 km since this gives the best agreement with observed resonant frequencies as well as a low amplitude for the period of 12.4 hrs.

The co-amplitude and co-phase lines are shown for the M_2 tide in Figure 6.5 and for the K_1 tide in Figure 6.6.

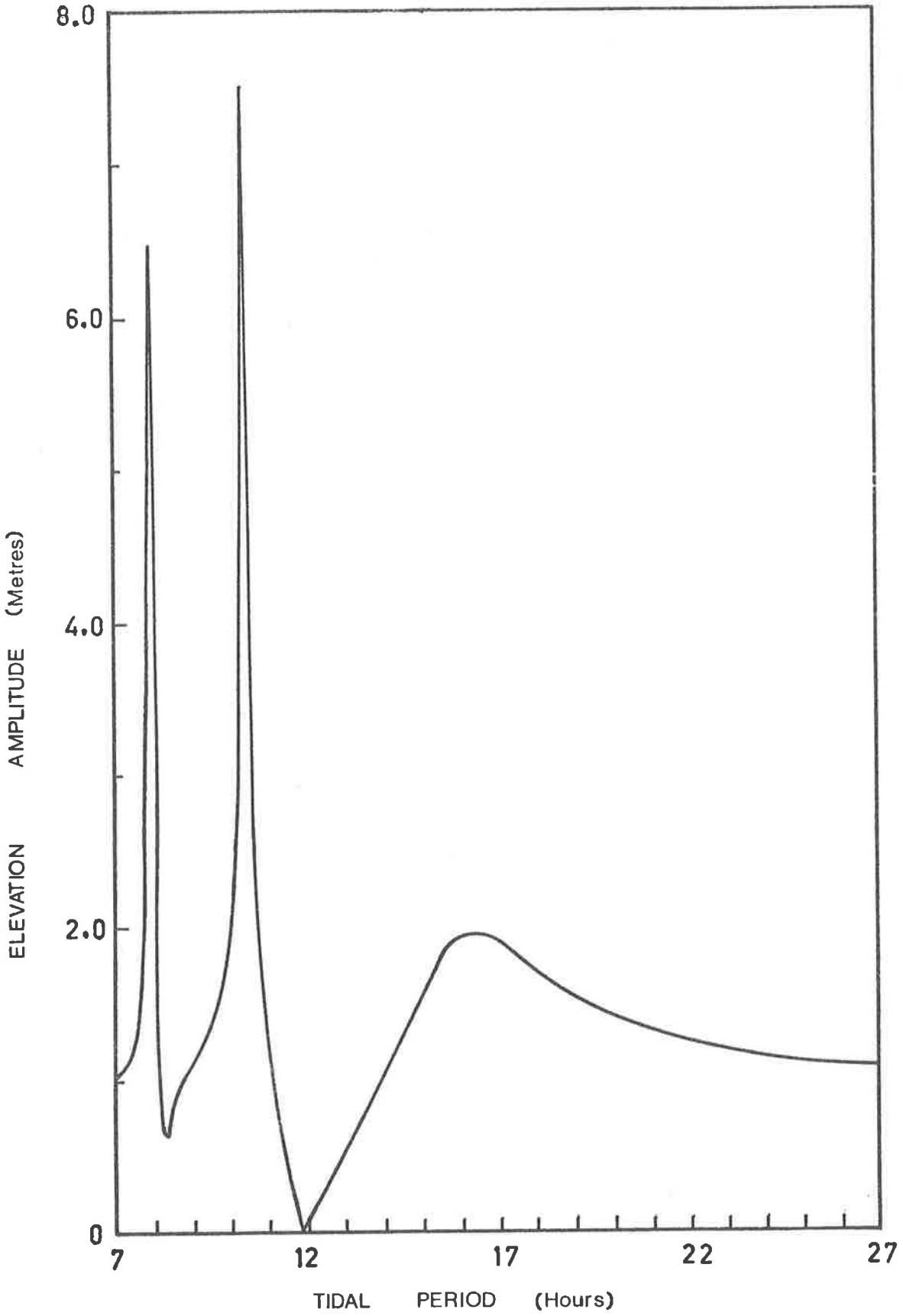

FIGURE 6.3: The frequency response at Karumba according to Williams (1972), with a = 480 km.

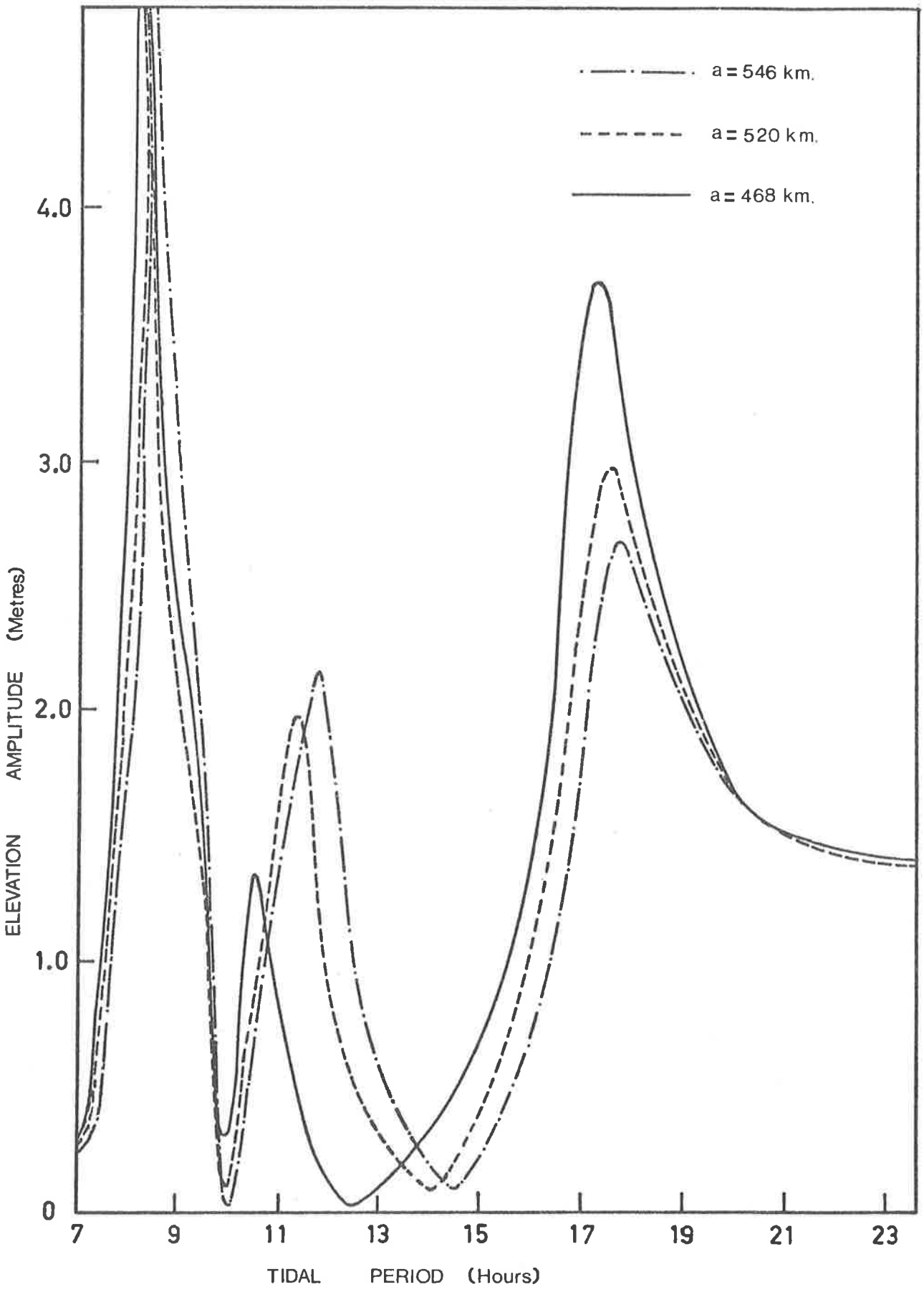

FIGURE 6.4: The frequency response at Karumba for various Gulf widths.

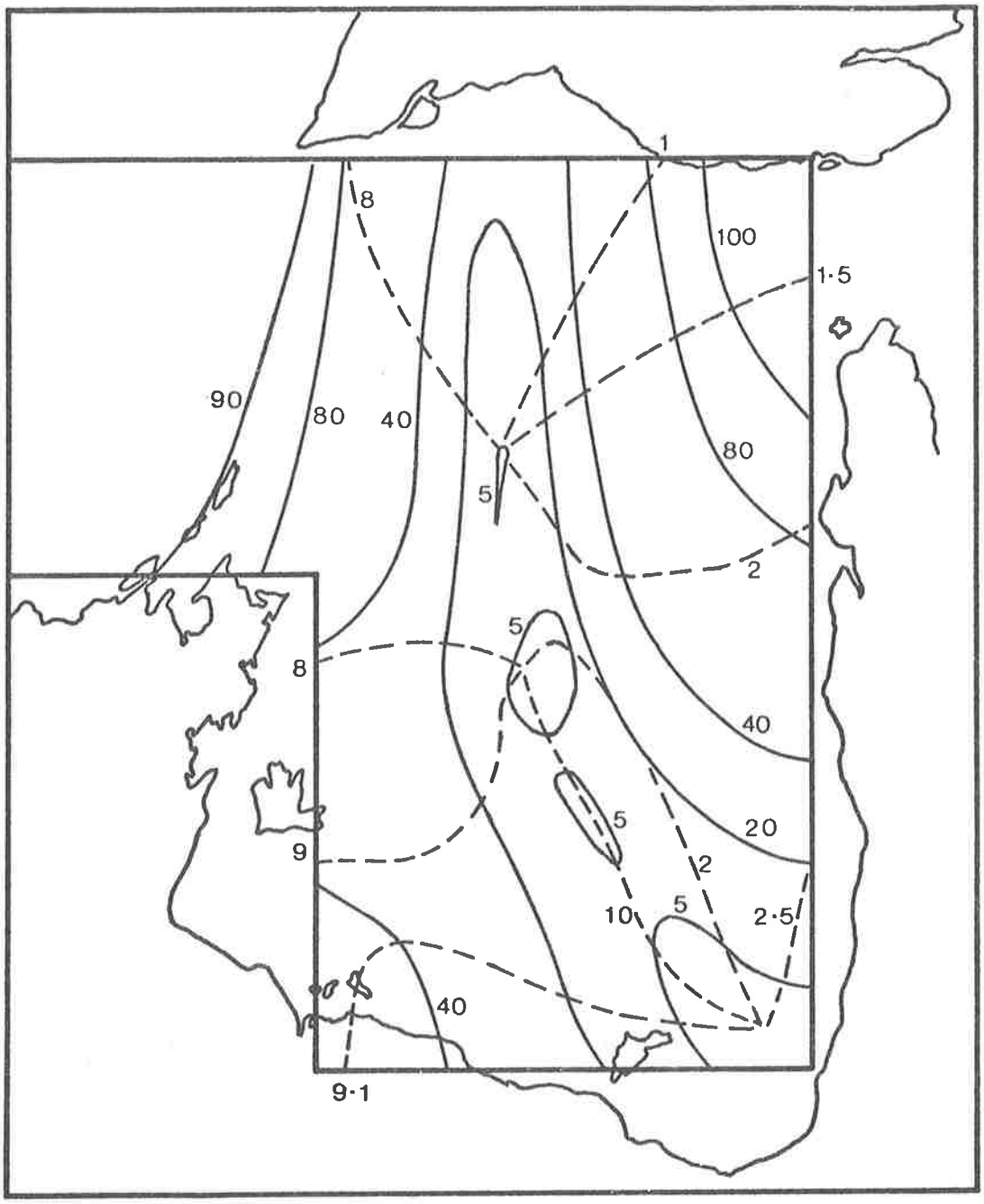

FIGURE 6.5: The co-amplitude and co-phase lines for the M_2 tide according to the analytic model of Chapter 3. The amplitude, ———, is shown in centimetres and the phase, -----, in hours.

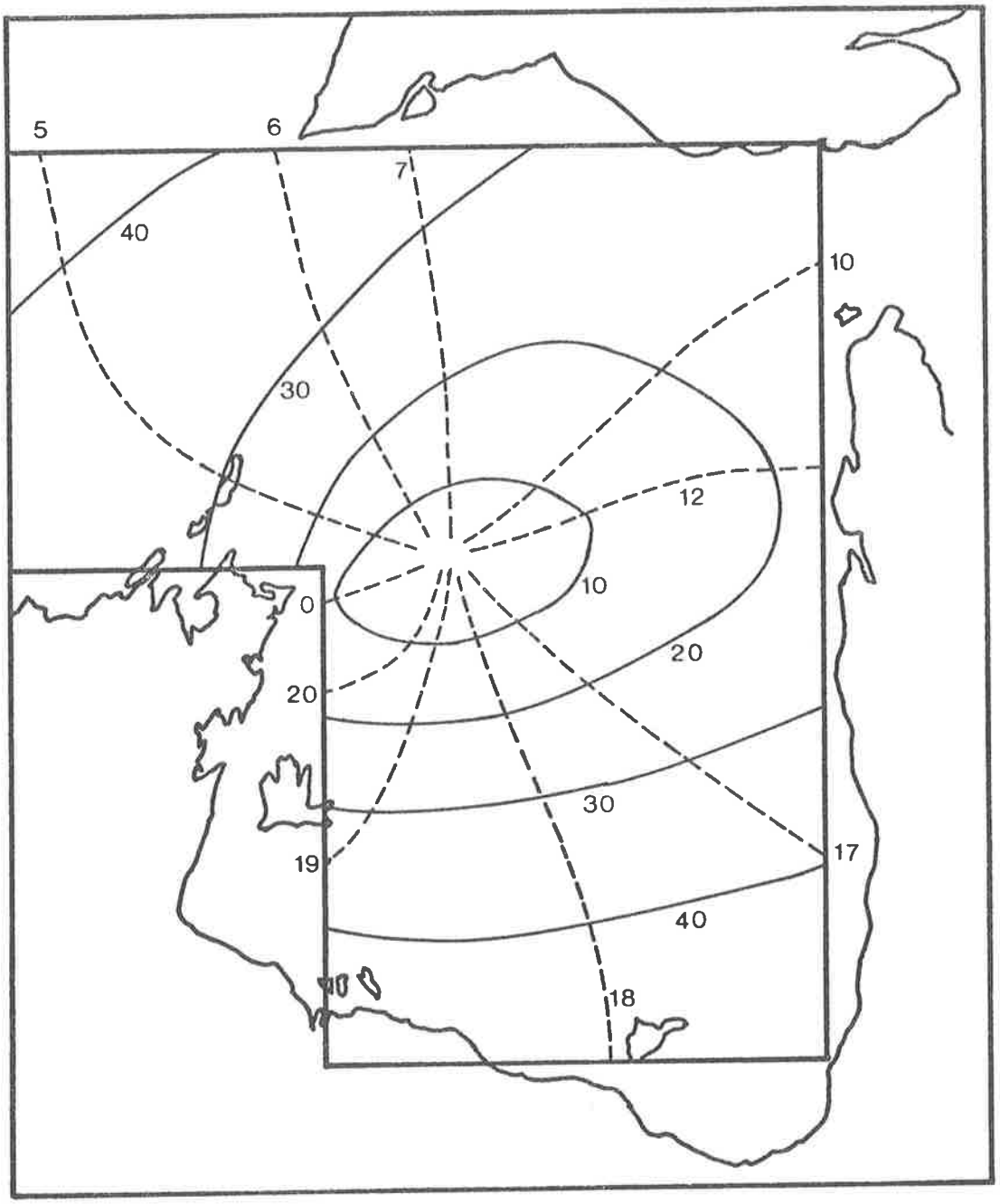

FIGURE 6.6: The co-amplitude and co-phase lines for the K_1 tide according to the analytic model of Chapter 3.

6.3 The Analytic Model of Chapter 4

As well as the constants specified in the previous section, the values

$$w_1 = 156 \text{ km}$$

$$w_2 = 234 \text{ km}$$

$$h_4 = 10 \text{ m}$$

$$\nu_{m_4} = .70 \text{ ms}^{-1}$$

were chosen for the model which considers the effect of tidal forcing from Torres Strait. In the manner described previously, the effective length of the input channel is required to be greater than 57 km. If the channel is extended out to the islands and reefs on the Eastern side of Torres Strait, the channel length may be considered as greater than 100 km, so that, once again, the Kelvin wave is a reasonable approximation to the input wave in this channel.

The method described in Chapter 4 is applied to the region depicted in Figure 6.2, so that the second connecting channel occupies the region $w_2 \leq y \leq b$.

The reference point chosen for evaluation of condition 4.3.1 is Wednesday Island.

6.3.1 Convergence using the Galerkin Technique

The residuals of the condition (i) to (v) in Section 4.2 showed, as would be expected, the same convergence as those in Section 6.2.1 and so the results are not presented here.

The errors in condition 4.2.7, $\zeta_2(0,y) = \zeta_4(0,y)$, $w_2 \leq y \leq b$ are shown in Table 6.8. The residuals of this condition appear to be smaller towards the centre of the channel for $N = 4$ than for $N = 6$; this is due to the manner of choosing points for presentation in the table

y/b	N = 2		N = 4		N = 6	
	Δ	%	Δ	%	Δ	%
6/10	.007	.63	.006	.52	.003	.29
7/10	.005	.43	0	0	.001	.12
8/10	.004	.35	.001	.05	.003	.14
9/10	.007	.59	.001	.08	.003	.24
1	.023	1.99	.008	.68	.006	.51

TABLE 6.8: The errors in the amplitudes in Condition 4.2.7, $\zeta_2(0,y) = \zeta_4(0,y)$, $w_2 \leq y \leq b$, using the Galerkin technique, for increasing values of N. $\Delta = \big|\, |\zeta_2| - |\zeta_4| \,\big|$.

y/b	N = 2		N = 4		N = 6	
	Δ	%	Δ	%	Δ	%
6/10	3.011	57.90	2.600	49.57	2.784	51.74
7/10	1.962	36.81	.061	1.17	.243	4.76
8/10	.649	12.09	.426	8.0	.287	5.39
9/10	.762	14.13	.273	4.85	.455	7.99
1	1.929	34.12	.335	6.09	.624	11.5

TABLE 6.9: The errors in the Condition 4.2.8, $h_2u_2(0,y) = h_4u_4(0,y)$, $w_2 \leq y \leq b$, using the Galerkin technique, for increasing values of N. $\Delta = \big|h_2|u_2| - |h_4|u_4|\big|$.

y/b	N = 2	N = 4	N = 6
0	.0059	.0053	.0043
1/10	.0046	.0001	.0021
2/10	.0021	.0058	.0025
3/10	.0033	.0004	.0051
4/10	.0102	.0088	.0039
5/10	.0211	.0044	.0024

TABLE 6.10: The values of $|u_2(0,y)|$, $0 \leq y < w_2$, using the Galerkin technique, for increasing values of N .

(spacing of 39 km across the channel, the same as in the previous tables). In fact, the error is comparable for $N = 4$ and $N = 6$, the convergence being very slow. However, the error at the channel walls is smaller as N increases, so that the overall error may be considered to decrease with increasing N.

The convergence for part of condition 4.2.8, that is, $h_2u_2(0,y) = h_4u_4(0,y)$, $w_2 \leq y \leq b$, is slow, as shown in Table 6.9, though the error is less than 10% away from the sides of the channel for $N \geq 4$. Once again, the higher errors for $N = 6$ are a little misleading as the overall error is similar to that for $N = 4$. The large error at $y = w_2$ is probably caused by the condition on the velocities at this corner which is similar to the condition at the corner $(-a,0)$. The errors at this junction, $w_2 \leq y \leq b$, are generally higher than for the other matching conditions. This is possibly due to the large relative change in depth, being 82% at this boundary but only 34% at the boundary between region 2 and region 3. However, the other part of condition 4.2.8, $u_2(0,y) = 0$, $0 \leq y < w_2$, shows satisfactory convergence as N is increased as indicated by Table 6.10. The percentage figures in Tables 6.8, 6.9 are calculated with reference to the values in Region 2.

The case of $N = 8$ for these conditions is not shown as it requires over 200K words of Central Memory on the computer.

6.3.2 Convergence using the Collocation Method.

Because of the slow convergence of condition 4.2.8 using the Galerkin technique, it was decided to try Collocation for comparison, as, intuitatively,better results may be expected from the latter method for this, virtually, two-in-one condition. However, as for the results in Section 6.2, the errors were larger and the convergence slower when Collocation was used.

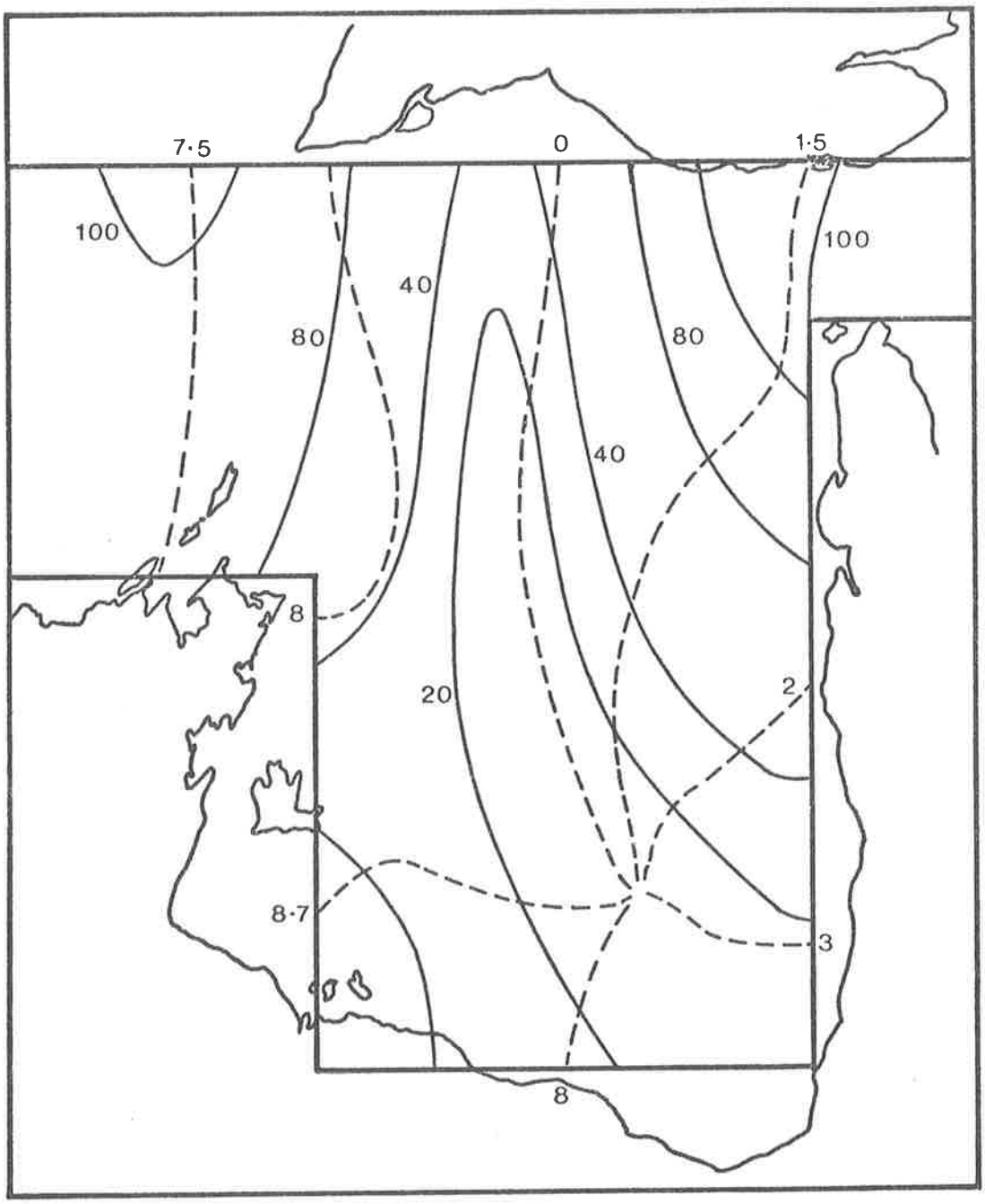

FIGURE 6.7: The co-amplitude and co-phase lines for the M_2 tide according to the analytic model of Chapter 4.

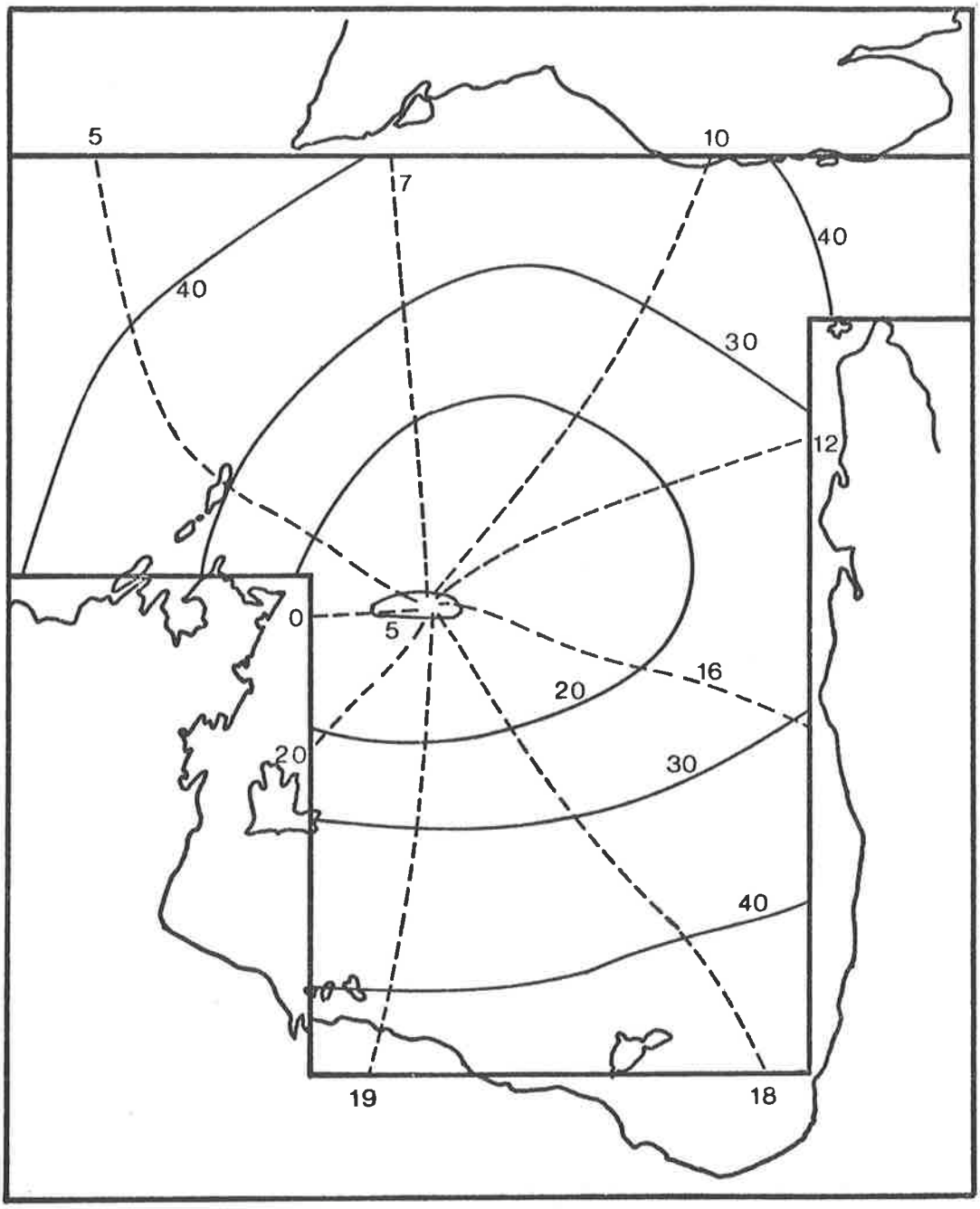

FIGURE 6.8: The co-amplitude and co-phase lines for the K_1 tide according to the analytic model of Chapter 4.

The co-amplitude and co-phase lines for the M_2 and K_1 tides, for the model of Chapter 4, are shown in Figures 6.7 and 6.8 respectively.

6.4 The Linear Numerical Model

The boundary configuration of the numerical model is a closer approximation to the coastline than that for the analytic model. This can be seen in Figure 6.11. This figure shows the coastal boundary approximation used for the numerical models and also the position of the open boundaries at which the tidal inputs are specified. With reference to Table 5.1, the element labels associated with this configuration are shown in Figure 6.9. The depths, assigned at ζ-points, are shown in Figure 6.10. Δx is taken to be 13 km and Δy to be 39 km.

The boundary approximation shown in Figure 6.11 was found to be the one which gave the closest results to the observed tidal phenomena. The seemingly poor approximation on the Western side of the Gulf is consistent with Teleki et al's (1973) observation that "most of Limmen Bight, between Groote Eylandt and the Edward Pellew Group, is a shallow area where the bays and river mouths remain choked with sediment most of the year. This is a low energy coast." An idea of the islands, shoals and sand or mud banks in the area may be obtained from Aus Chart 410. The area to the South-East, near Karumba, is modelled as being wider and shallower than it is in reality. This is to try to account for the dissipation in the M_2 tide. There is a long sand-bank in this area, shown on Aus Chart 410.

The input along the open boundary for the numerical model is obtained from the analytic model, there being no data available across the input channel. It could be possible to determine input values from co-tidal and co-range charts as given by Easton (1970), but such

data would be interpolations on diagrams which are themselves obtained by interpolation and extrapolation, and hence the input is not likely to be very accurate.

The convergence of the model is tested by modelling the exact system described in Chapter 3 and comparing the outputs for the M_2 tide with that obtained from the analytic model. The appropriate form of the friction parameter, 5.4.1, uses $\nu_m = .35\ ms^{-1}$. The results for the amplitudes are given in Table 6.11 and for the phases in Table 6.12.

The largest discrepancies occur at the corner $x = -a$, where the analytic model incurred the largest errors in the matching conditions, and in regions affected by the amphidromic points (compare with Figure 6.5), particularly in the bottom right-hand corner of each table. Away from these regions, the results are in good agreement, the maximum error in the amplitudes being about 3% and for the phases about 5% if the phase is larger than 2 hours. Sometimes the percentage error is larger than this for phases smaller than 2 hours, but the maximum absolute error is comparable to that for the larger phases, being about 18 minutes.

Hence, accepting the fact that amphidromic points are singular regions in which any linear depth-integrated model is likely to be inaccurate (see Nihoul (1977)), the otherwise favourable agreement of the numerical model with the analytic model indicates that the solution provided by the linear numerical model is likely to be convergent to the true solution for the situation of a more complicated boundary and bottom topography.

The results, incorporating the input from Torres Strait, are shown in Figure 6.11 for the M_2 tide and in Figure 6.12 for the K_1 tide. The results for the linear numerical model which uses the iterated form of the friction parameter, as given by 5.4.2, are shown in

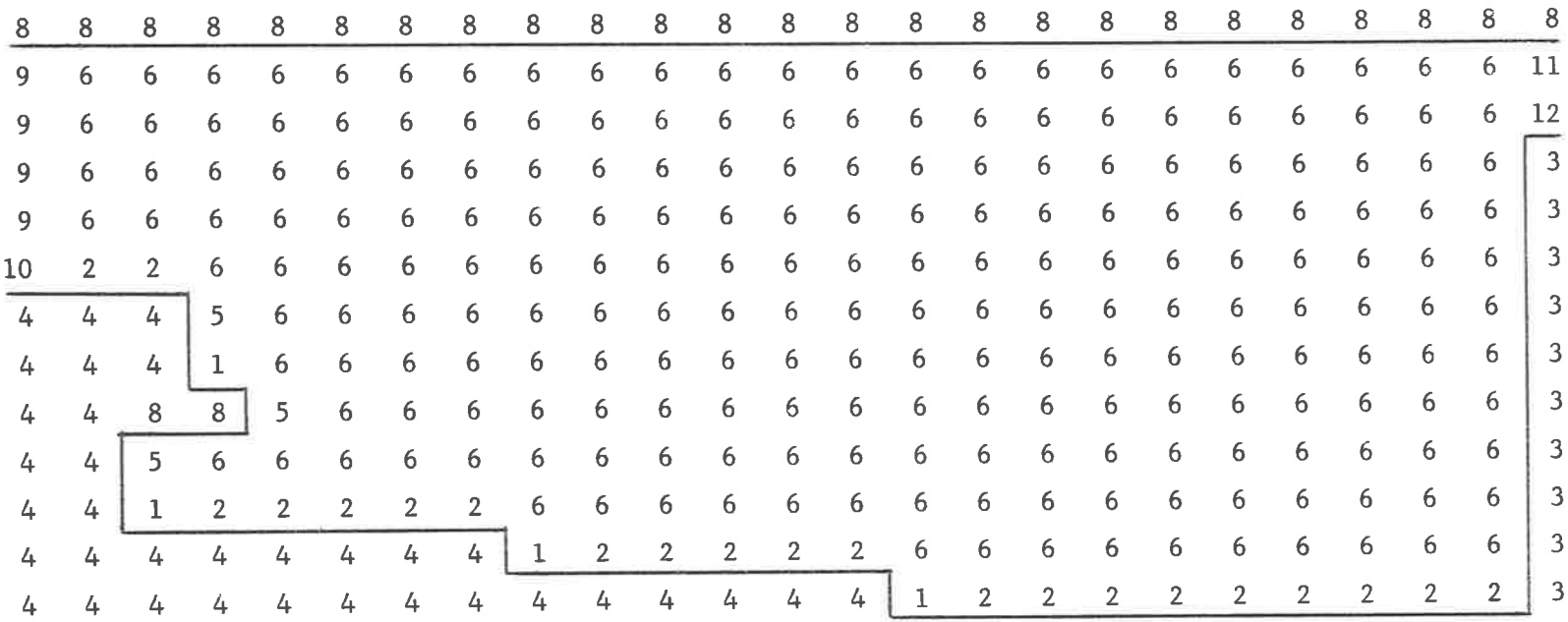

FIGURE 6.9: The element labels for the linear numerical model associated with the boundary configuration in Figure 6.11.

*	*	*	*	*	*	*	*	*	*	*	*	*	*	*	*	*	*	*	*	*	*	*	*	*
65	65	60	60	50	50	40	40	40	40	40	40	40	40	40	40	40	40	30	20	10	10	9	9	10
65	60	55	55	55	55	55	55	55	55	55	55	50	50	50	50	50	45	45	40	30	20	10	10	10
70	70	65	65	65	60	60	57	57	55	55	55	55	55	55	55	55	50	50	45	40	30	20	10	*
50	30	50	50	50	55	55	55	55	55	50	50	55	55	60	60	60	60	60	55	50	40	30	20	*
50	30	30	45	50	50	55	55	55	60	60	60	65	65	65	60	65	70	70	70	60	50	40	30	*
*	*	*	35	50	50	55	55	55	55	60	60	60	60	65	65	65	65	60	60	55	50	45	30	*
*	*	*	40	45	50	55	55	55	55	60	60	60	60	60	60	60	60	60	60	55	50	40	30	*
*	*	*	*	20	40	50	55	55	58	60	62	65	65	65	66	65	60	54	50	45	40	30	20	*
*	*	10	30	35	40	50	50	50	55	55	55	55	55	55	55	55	50	45	45	40	35	20	15	*
*	*	10	20	20	25	25	35	40	45	50	50	55	55	50	45	45	40	40	40	35	25	20	15	*
*	*	*	*	*	*	*	*	20	25	30	30	30	30	30	35	35	35	30	30	25	25	15	10	*
*	*	*	*	*	*	*	*	*	*	*	*	*	*	5	5	5	5	5	5	5	5	5	5	*
														*	*	*	*	*	*	*	*	*	*	*

FIGURE 6.10: The depths in m, specified at ζ-points, for the numerical model with configuration shown in Figure 6.11. The *'s show land, and the depths correspond to the bathymetry shown in Figure 6.1.

y-Distance from Boundary y = b (km)	x-Distance from Input Boundary (km)											
	0	52	104	156	208	260	312	374	416	468	520	572
39	.991 .991	.970 .975	.900 .910	.734 .756	.505 .537	.275 .326	.256 .297	.486 .497	.737 .735	.948 .940	1.095 1.083	1.164 1.150
117	.965 .965	.943 .946	.870 .877	.703 .717	.467 .489	.211 .252	.179 .211	.437 .440	.692 .685	.903 .891	1.050 1.036	1.122 1.106
195	.940 .940	.915 .917	.842 .845	.675 .683	.443 .455	.180 .204	.121 .138	.388 .383	.645 .624	.837 .822	.978 .962	1.049 1.031
273	.916 .916	.886 .887	.808 .808	.641 .643	.419 .422	.171 .178	.087 .087	.339 .331	.567 .555	.753 .739	.883 .868	.949 .933
351	.899 .899	.858 .859	.753 .759	.572 .570	.374 .370	.162 .157	.072 .066	.287 .282	.489 .480	.655 .643	.770 .758	.830 .817
429	* *	* *	* *	.414 .376	.300 .276	.142 .128	.042 .046	.225 .225	.395 .392	.537 .532	.638 .632	.688 .683
507	* *	* *	* *	.319 .297	.256 .237	.147 .133	.014 .017	.140 .144	.280 .281	.398 .396	.483 .482	.525 .525
585	* *	* *	* *	.323 .311	.278 .266	.196 .185	.092 .083	.053 .051	.157 .158	.254 .255	.324 .326	.359 .363
663	* *	* *	* *	.376 .368	.336 .328	.267 .258	.177 .167	.081 .067	.052 .038	.122 .121	.180 .184	.209 .218
741	* *	* *	* *	.432 .427	.394 .388	.330 .324	.248 .240	.156 .148	.069 .060	.027 .031	.071 .083	.095 .113
819	* *	* *	* *	.467 .463	.430 .426	.367 .363	.288 .284	.200 .198	.114 .118	.041 .062	.011 .060	.034 .075

TABLE 6.11: Comparison of the amplitudes (in m), for the M_2 tide, given by analytic model in Chapter 3 and the linear numerical model. For each (x,y) value the analytic result is given above the numerical result, the * indicating land.

y-Distance from Boundary y = h (km)	x-Distance from Input Boundary (km)											
	0	52	104	156	208	260	312	374	416	468	520	572
39	7.51 7.51	7.64 7.67	7.79 7.83	8.01 8.09	8.40 8.53	9.41 9.53	11.90 11.61	.66 .42	1.04 .88	1.23 1.11	1.33 1.23	1.38 1.29
117	7.52 7.52	7.62 7.65	7.72 7.78	7.87 7.97	8.14 8.31	8.93 9.20	12.39 11.96	1.00 .77	1.26 1.13	1.39 1.29	1.46 1.38	1.49 1.42
195	7.53 7.53	7.60 7.63	7.67 7.73	7.76 7.87	7.90 8.08	8.30 8.70	.70 .07	1.35 1.15	1.50 1.39	1.57 1.50	1.62 1.56	1.65 1.60
273	7.54 7.54	7.58 7.61	7.63 7.68	7.68 7.78	7.73 7.90	7.78 8.19	1.65 .90	1.68 1.52	1.72 1.65	1.75 1.72	1.79 1.77	1.82 1.80
351	7.55 7.55	7.56 7.59	7.58 7.63	7.63 7.72	7.66 7.81	7.53 7.87	2.47 1.87	1.95 1.85	1.91 1.89	1.92 1.93	1.95 1.97	1.98 2.01
429	* *	* *	* *	7.74 7.90	7.79 7.99	7.72 8.03	2.81 2.15	2.07 2.05	2.04 2.08	2.06 2.13	2.09 2.17	2.14 2.22
507	* *	* *	* *	8.20 8.41	8.26 8.49	8.37 8.65	10.05 11.56	1.95 2.05	2.07 2.21	2.14 2.29	2.21 2.36	2.28 2.43
585	* *	* *	* *	8.72 8.93	8.76 8.96	8.89 9.07	9.38 9.52	.76 1.31	1.91 2.25	2.15 2.45	2.28 2.56	2.39 2.67
663	* *	* *	* *	9.01 9.18	9.02 9.17	9.09 9.19	9.26 9.27	9.89 9.58	.75 2.07	1.99 2.72	2.30 2.88	2.49 3.01
741	* *	* *	* *	9.10 9.24	9.10 9.21	9.11 9.18	9.16 9.13	9.28 9.03	9.70 8.64	.66 4.62	2.24 3.73	2.58 3.71
819	* *	* *	* *	9.10 9.23	9.07 9.18	9.05 9.11	9.03 9.00	9.02 8.81	9.04 8.39	9.13 7.23	2.32 5.47	2.79 4.87

TABLE 6.12: Comparison of the phases (in hrs), for the M_2 tide, given by the analytic model in Chapter 3 and the linear numerical model. For each (x,y) value, the analytic result is given above the numerical result, the * indicating land.

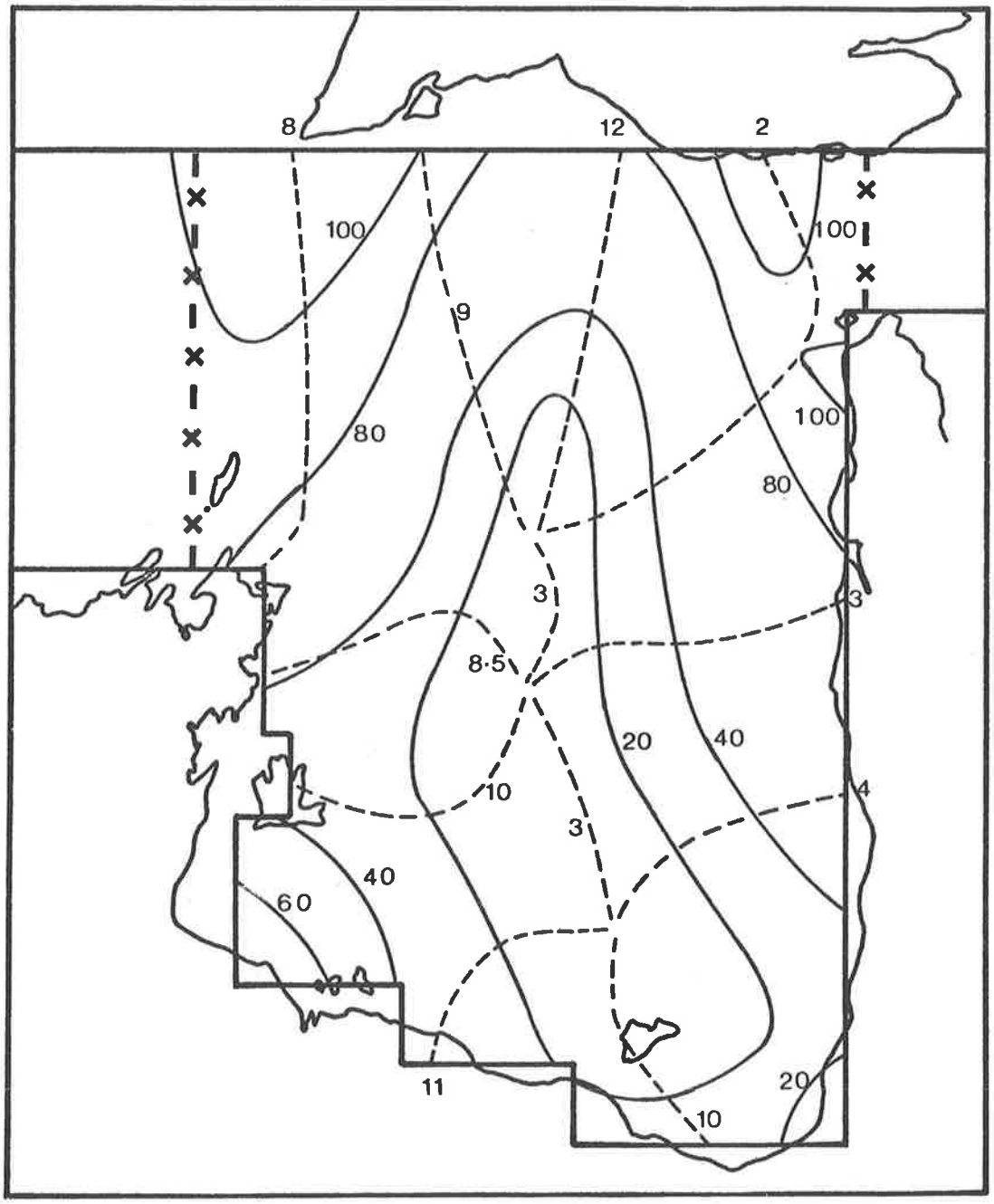

FIGURE 6.11: The co-amplitude and co-phase lines for the M_2 tide according to the linear numerical model which uses the non-iterated form of the friction parameter. The open boundaries are indicated, with a ✖ representing the position of a ζ grid point.

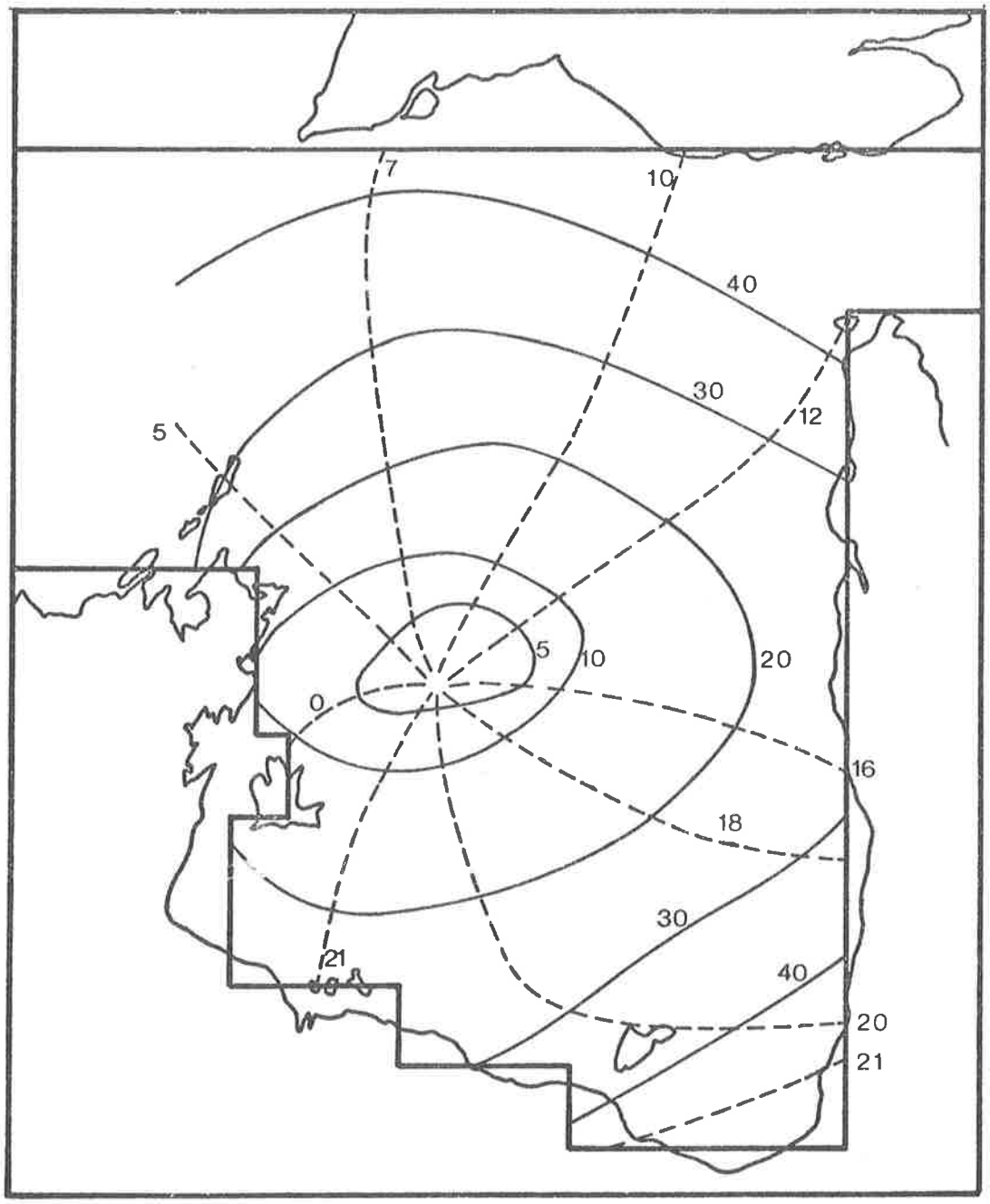

FIGURE 6.12: The co-amplitude and co-phase lines for the K_1 tide according to the linear numerical model which uses the non-iterated form of the friction parameter.

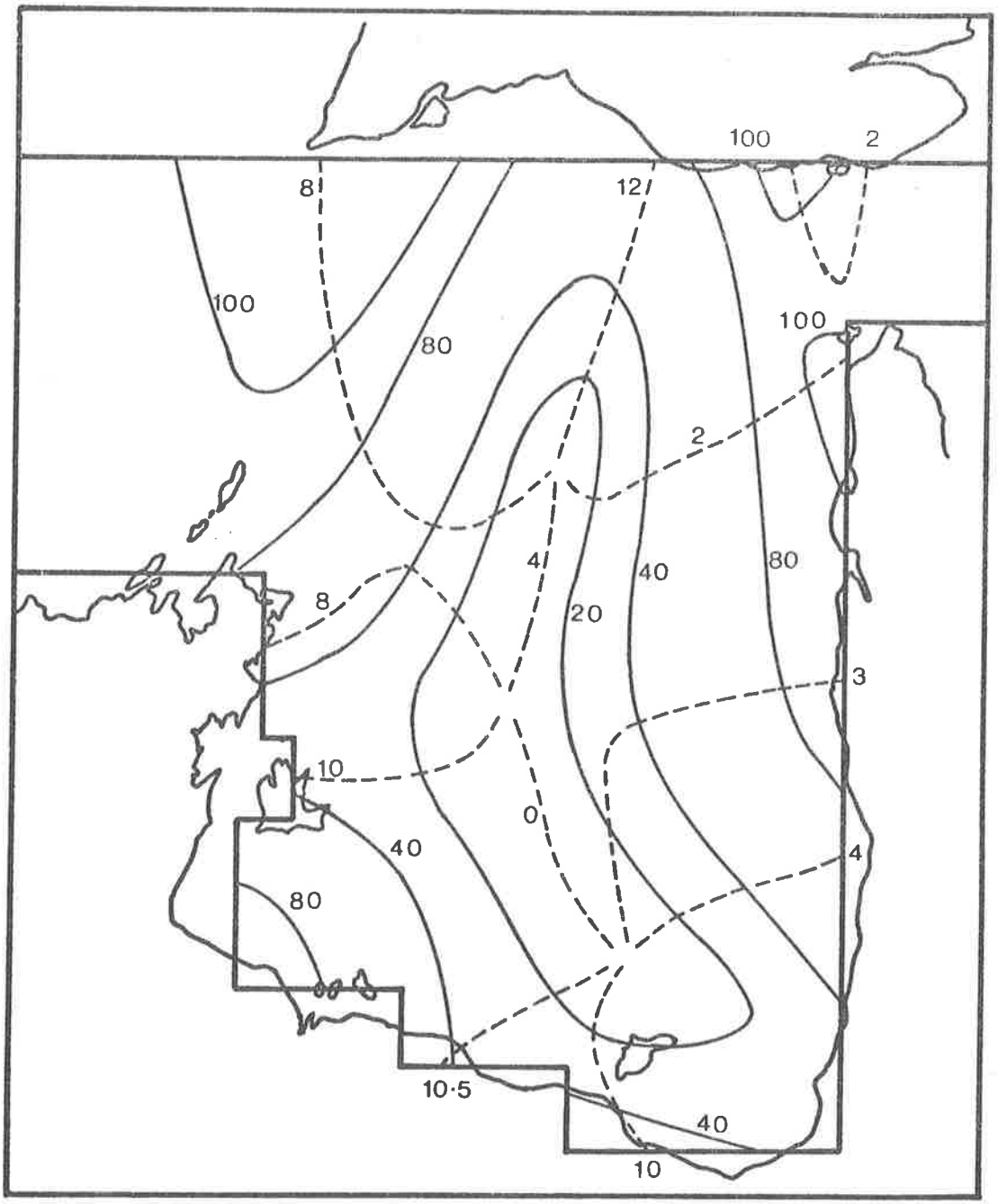

FIGURE 6.13: The co-amplitude and co-phase lines for the M_2 tide according to the linear numerical model which uses the iterated form of the friction parameter.

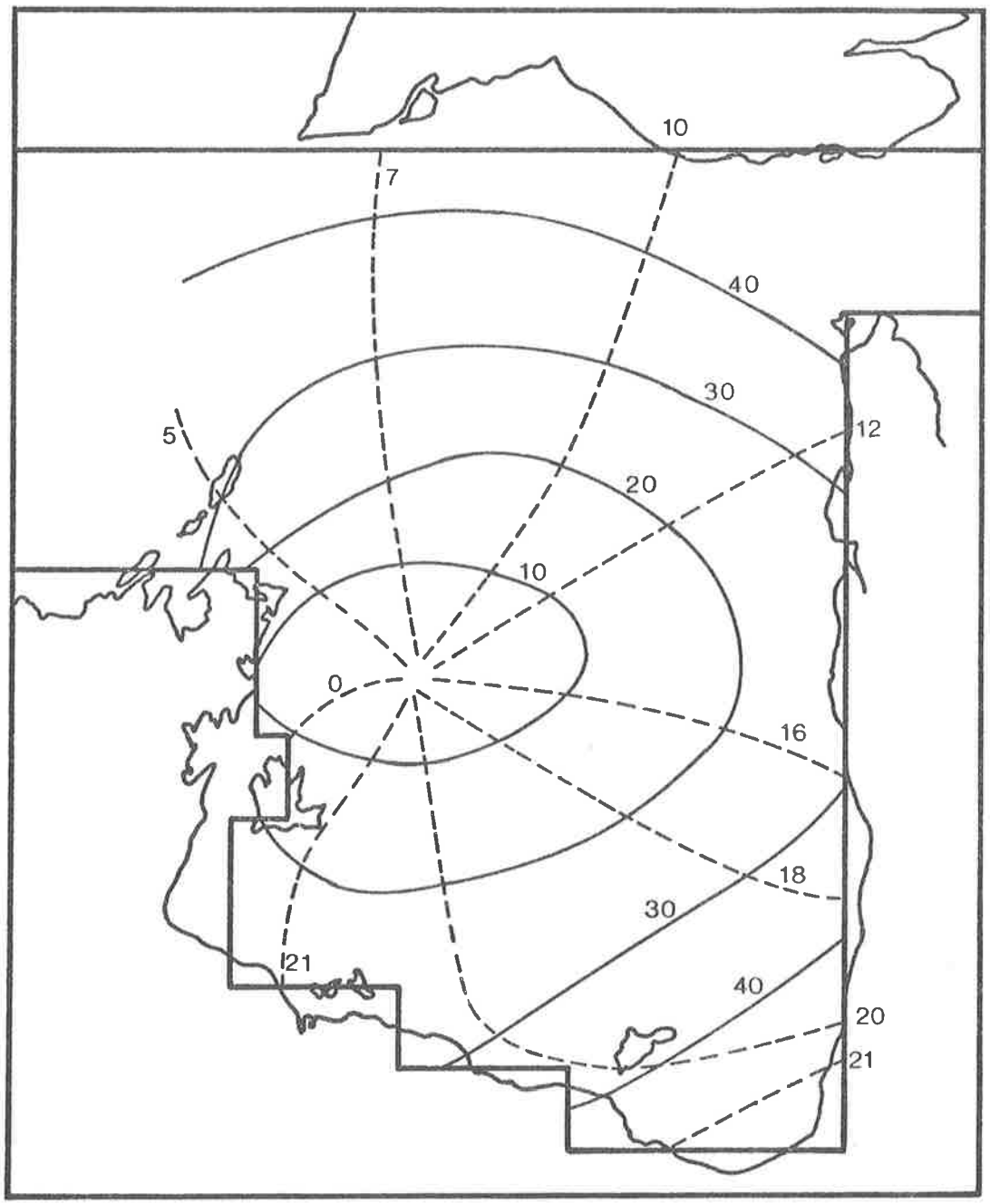

FIGURE 6.14: The co-amplitude and co-phase lines for the K_1 tide according to the linear numerical model which uses the iterated form of the friction parameter.

Figures 6.13 and 6.14. For the M_2 tide, which has the dominant velocity component in the region studied, the friction parameter converged at each velocity grid-point after 11 iterations. For both linear models, the maximum error in the end-condition, after the EVP solution had been determined, was 2×10^{-5} .

6.5 The Non-linear Numerical Model

The labels in Figure 6.9 and the depth array in Figure 6.10 are also used for the non-linear model.

The value of λ , in the friction parameter form of 5.5.3, is taken to be .00878, corresponding to a value of .030 for Manning's n. The time increment which satisfies the stability condition 5.6.4 is taken to be 120 secs for the M_2 tide and 239 secs for the K_1 tide, the number of time-steps per tidal cycle being roughly the same in both cases. As for the linear model, the input data was obtained from the analytic results. The model took 13 tidal cycles to iteratively converge, that is, if p is the number of steps per tidal cycle,

$$|Z_{\ell,j}^{(\nu + p)} - Z_{\ell,j}^{(\nu)}| < .001, \quad \ell = 1,\ldots,m; \; j = 1,\ldots,n; \qquad 6.5.1$$

when $\nu/p = 13$. The output during the 14th tidal cycle is stored on a random-access file, using the Random Mass Storage package on the computer, and later Fourier-analyzed to obtain the fundamental frequency (and harmonics, if desired) using the efficient program detailed in Ralston and Wilf (1960).

At first it was thought that the long model time required for iteration convergence may be due to the method of modelling the advection terms, but removal of these terms from the equations had no effect on the time for convergence. This is reassuring from the point of view that

the advection terms should not have a very large effect on the results (see Flather and Heaps (1975)).

The iteration convergence time seems to be dependent more on the type of area being modelled than on the manner in which the PDE is approximated by the FDA. The model of Morecambe Bay developed by Flather and Heaps (1975) takes 11 tidal cycles to iteratively converge in the manner of 6.5.1.

The long model-time for convergence in this study is probably due to two factors:-

(i) the large model region

and (ii) the input wave has to sweep around the corner into the resonator region and, because of this, the transient motion associated with the wave and its reflection may take a while to die away.

The truncation convergence, that is, the property of convergence discussed in Sections 5.3.3 and 5.6, is investigated by comparing the results for the M_2 tide with the results obtained from the linear numerical model which used the iterated friction parameter. The agreement between the two, shown by a comparison of Figure 6.13 with 6.15, is excellent. The only discrepancy is in the South-Eastern corner where depths are only 5 m and the advection terms are likely to be of more importance than elsewhere in the Gulf. Such a comparison shows not only the convergence of the non-linear model, but also the value of the simple linear model.

The result for the K_1 tide is shown in Figure 6.16. This shows favourable agreement with Figure 6.14, any differences arising from the fact that the linear model accounts for interaction with the M_2 component, through the manner in which friction parameter is modelled, while the non-linear model does not.

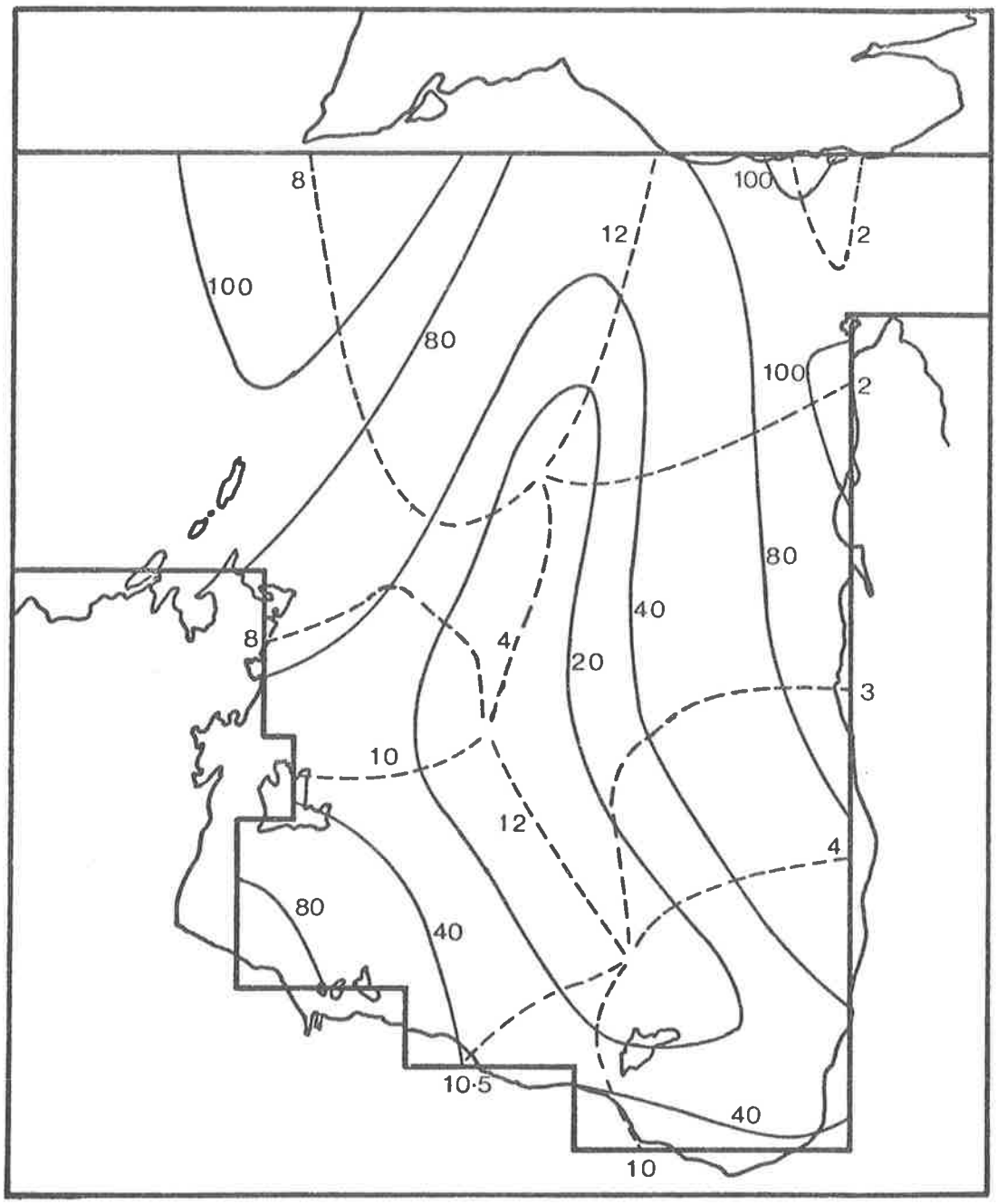

FIGURE 6.15: The co-amplitude and co-phase lines for the M_2 tide according to the non-linear numerical model.

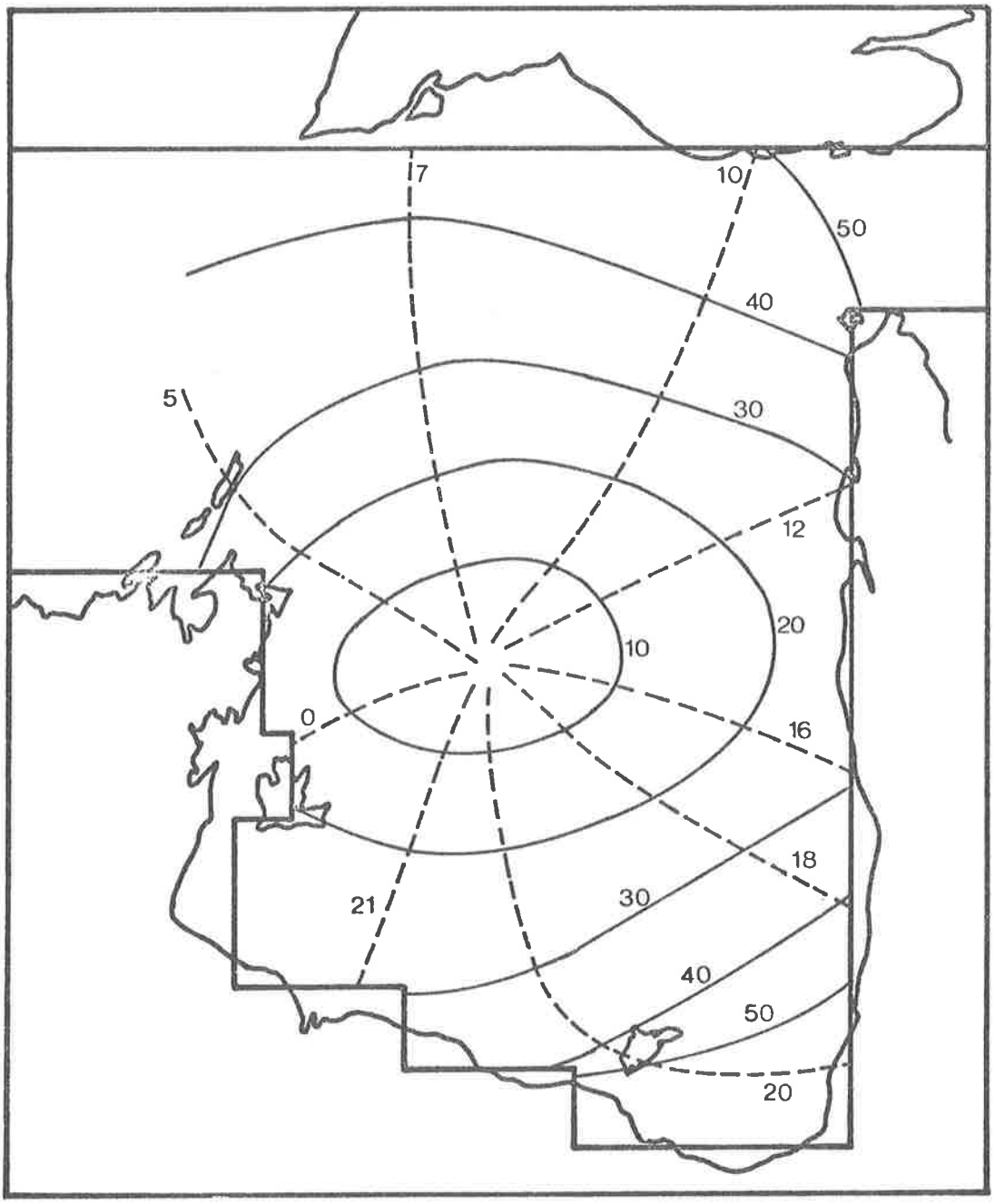

FIGURE 6.16: The co-amplitude and co-phase lines for the K_1 tide according to the non-linear numerical model.

MODEL	TIME (secs)	CENTRAL MEMORY (K words)
LINEAR ANALYTIC		
Torres Strait closed	53	100.2
Torres Strait open	72	140
LINEAR NUMERICAL		
simple friction	6.4	60
iterated friction	21.8	60
NON-LINEAR NUMERICAL		
basic program - 14 cycles	1024.1	54
Fourier analysis	5.4	60

TABLE 6.13: Details of the requirements of each model on the CDC Cyber 173 Computer.

6.6 The Programs

The programs for all the models described were written in Fortran IV and run on the CDC Cyber 173 computer at the University of Adelaide. The results for the analytic models were obtained using $N = 6$. Table 6.13 indicates the time required (in secs) to run each program and the length of Central Memory needed(in Kilowords).

6.7 The Response of the Gulf to Tidal Forcing

The tidal response predicted by the models is now discussed in more detail.

6.7.1 The Semi-diurnal Response

The semi-diurnal response of the system is investigated with reference to the M_2 tide which has a period of 12.4 hours.

The response predicted by the analytic model of Chapter 3 is shown in Figure 6.5. It features three amphidromic points, one in the junction which is clockwise and two in the resonator, the one near Karumba in the South-East being clockwise, the other anti-clockwise. This agrees fairly well with the results of Williams (1972) with the difference that the features that he suggests should appear in his results (namely, that the amphidromic point in the junction should be nearer to the resonator than to the boundary $y = b$, and the existence of the amphidromic point near Karumba) in fact do appear in Figure 6.5.

Figure 6.7 shows the M_2 tidal response when flow through Torres Strait is allowed. This flow forces the three amphidromic points to contract to one, near Karumba. Apart from this, the response is similar to that of Figure 6.5. This result is analogous to the effect of allowing flow through the Straits of Dover in a North Sea model (see Nihoul and

Ronday (1976)) where the overall response is similar when the Strait is opened or closed but the position of the amphidromic point is changed when the Strait is opened. The phase distribution varies accordingly.

Figures 6.11, 6.13 and 6.15 show the response as predicted by the numerical models which more accurately approximate the boundaries and the depth contours. The three amphidromic points reappear. That the first analytic model agrees so well in this respect with the numerical models is deemed to be completely fortuitous. It may be personal interpretation by interpolation since the region inside the .2m contour contains a very narrow region of amplitudes less than .1m in both analytic models. The three amphidromes which appear in the numerical model (and thus the features suggested by Williams (1972))are likely to be due to the bottom topography which causes this region of small amplitudes to bend away from the deeper water to the North-East of the resonator. The linear model which uses the simple friction parameter agrees well with the other numerical models. It, in fact, gives a more accurate response at Karumba, predicting an amplitude of .18m, while the other two models predict an amplitude of .4m (the measured value is .17m).

All models predict the peak amplitude of the Gulf to be at the point (0,0) as well as high amplitudes in the South-West of the Gulf.

The amplitudes and phases for selected positions,as given in the Australian National Tide Tables for 1978, are shown in Table 6.14. Keeping in mind that these observations are made at sites which may be subject to local influences not capable of resolution in the model (one grid element represents a surface area of 2028 km^2), the following observations may be made:

(1) The movement of the tide around the perimeter of the resonator agrees with observation in that the tide at Weipa lags behind that at Karumba and the tide in the Northern region around Caledon Bay lags behind that at Port McArthur in the South.

LOCATION	M_2		K_1	
	PHASE (hrs)	AMPLITUDE (m)	PHASE	AMPLITUDE
JENSEN BAY	7.5	.91	5.0	.32
MELVILLE BAY	8.3	.80	5.8	.26
CALEDON BAY	9.0	.50	2.7	.2
PORT LANGDON	9.2	.26	23.2	.15
PORT McARTHUR	1.6	.41	23.6	.41
KARUMBA	6.2	.17	22.0	.91
WEIPA	5.1	.36	14.4	.46
WEDNESDAY IS.	1.3	.40	14.1	.56

TABLE 6.14: The amplitudes and phases for the M_2 and K_1 tides at selected sites, as given in the Australian National Tide Tables, 1978.

(2) The amplitude response at Weipa is too high in all models. This site is located near a relatively steep bottom slope and a better representation of the bathymetry in this area may improve the results. The amplitude along the perimeter in the Southern half of the Gulf is generally in good agreement with data in the analytic results but too high in the numerical results. This is surprising, as a closer approximation to the boundaries and bottom topography should give more accurate results.

Using the input from an analytic model with a different Gulf width produced no significant change in the response of the numerical models. Increasing the value of the friction parameter will decrease the amplitudes in the South of the Gulf, but this has a detrimental effect on the amplitude of the diurnal tide and is hardly justifiable on the results of the analytic model. It is probable that the input provided by the analytic model is still not accurate enough. This could be improved if the reference point for the scaling of the response could be chosen away from the mainland or islands. However, no data is available at such sites and so this could not be tested. The reference points were changed to other mainland sites but Jensen Bay and Wednesday Island gave the best results.

6.7.2 The Diurnal Response

The response of the system of Chapter 3 for the K_1 tide is shown in Figure 6.6. There is a single amphidromic point about which the rotation is clockwise, in keeping with observations. With the opening of Torres Strait, the location of the amphidrome moves South from just outside the resonator to just inside. This is shown in Figure 6.8. The bathymetry introduced in the numerical model moves the amphidromic point further South-East. This is in agreement with William's (1972) suggestion

that the amphidrome lies 240 km in a direction East-South-East of the position, towards the centre of the channel-junction boundary, predicted by his model. As the amphidrome moves further into the resonator, the phases in the Western and Southern parts of the Gulf change accordingly, providing better agreement with observed values.

Comparison with Table 6.14 shows that the amplitude at Weipa, Karumba and Port McArthur is too small while the agreement in phase is quite good. The phase and amplitudes at Port Langdon and positions north of this agree quite well with observations.

The results of the S_2 tide were similar to those of the M_2 tide, and the O_1 tide similar to the K_1 tide; hence the results are not presented here.

Since no data is yet available away from the mainland or islands, there is no conclusive evidence as to the quantitative accuracy of the models in the interior of the Gulf. However, there is good agreement amongst the models, giving an indication as to the main features of the response of the Gulf to tidal forcing. The discrepancies with regard to specific observed tidal phenomena may possibly be due to lack of detail in coastal boundaries and in the bottom topography near the coast. As mentioned in Chapter 1, the water motion in the Gulf is influenced by a variety of factors and it may be necessary to incorporate some of these, for example, a horizontal density gradient from South to North, or the effect of winds, to more accurately predict the tidal motion in the Gulf.

The results of the models in this thesis could be used in more localized studies with a grid refinement such as used by Ramming (1976), giving a better approximation to coastal boundaries and bathymetry. Thus, if a model of the Gulf included more detail of Limmen Bight, a more accurate study of this area could be obtained by using a finer grid and inputs from some outer boundary to the East of Groote Eylandt, the interaction between

the coarse and fine grids being accounted for in the manner described by Ramming. The fine grid model would, of necessity, be a non-linear model because of the importance of the advection terms in shallow coastal areas.

Whereas it is possible, by including features and refinements as described above, to improve the models in this thesis, it is considered that one of the factors limiting the accuracy of the numerical models may still be the input along the open boundary. If the reference locations of the analytic model could be more ideally chosen, a more accurate input for the numerical models could be obtained.

CHAPTER 7

CONCLUSION

Two analytic models to determine the tidal propagation in a resonator-channel system have been developed in this thesis. They are based on the two-dimensional depth-integrated equations of continuity and momentum conservation which govern fluid flow. The models have been applied to the Gulf of Carpentaria, Australia. The second model accounts for flow through Torres Strait and shows the influence of this Strait on the position of amphidromic points and the subsequent effect on the phase distribution in the Gulf. There is little change in the amplitude response of the Gulf with the inclusion of this second channel.

As well as giving a good indication of the general features of the tidal response of the Gulf, these models are useful in providing a comparison for the two numerical models which are developed to approximate the boundaries and bottom topography more accurately. The second analytic model also provides the input along the open boundaries for the numerical models since there is inadequate measured data available.

The two numerical models use finite-difference approximations to the two-dimensional equations, the first being linear and the second, non-linear. The results of the linear model agree very well with those of the non-linear model, indicating the usefulness of linear schemes which model the friction parameter judiciously. They also indicate, as would be expected, that the advection terms are not important in the interior of the Gulf.

Table 6.13 supports the usefulness of the linear model, which, as well as providing good results, has a much smaller running time on the computer than the non-linear model. It, thus, would be an ideal model to provide inputs for more localized studies utilizing a finer grid resolution. These localized studies would use the non-linear numerical model to give better quantitative agreement with the data available near the mainland.

APPENDIX 1.

The Representation of Bottom Friction

Integration of the general three-dimensional equations over depth introduces the surface and bottom stresses (see, for example, Dronkers (1964),Nihoul (1975)). The generally accepted formula used for the latter is (see Groen and Groves (1962), Nihoul (1977))

$$\underset{\sim}{\tau}_b = - m\underset{\sim}{\tau}_s + \gamma\rho|\underset{\sim}{q}|\underset{\sim}{q}$$

where $\underset{\sim}{\tau}_b$ and $\underset{\sim}{\tau}_s$ are the bottom and surface stresses, respectively, m and γ are empirical constants and $\underset{\sim}{q}$ is the horizontal velocity at some reference height above the bottom (henceforth termed the "bottom velocity") or the depth-averaged velocity and ρ is the density of the fluid. This formula includes a stress exerted on the bottom even at times when $\underset{\sim}{q} = 0$. However, in tidal models where the effects of wind are neglected, $\underset{\sim}{\tau}_s$ is taken to be zero.

(a) The Non-linear Representation, $k|\underset{\sim}{q}|\underset{\sim}{q}$.

Since, in two-dimensional models, the value of the bottom velocity is not known, non-linear equations use the form

$$\underset{\sim}{F}_b (= \underset{\sim}{\tau}_b/\rho H) = k|\underset{\sim}{q}|\underset{\sim}{q} \qquad \text{A1.1}$$

where H is the water depth and k has dimensions m^{-1} in mks units.

As a first estimation, k may be given a constant value, equivalent to considering a region of constant depth. Thus

$$k = \gamma/h$$

where h is the depth of undisturbed water and γ is dimensionless. Taylor's (1920b) study of dissipation in the Irish Sea used $\gamma = .002$.

Grace (1936, 1937) attempted to determine appropriate values for γ by using measurements of tidal elevations along the coasts of the Bristol and English Channels. He found values of γ ranging from .0014 to .0041 (average value of .0026) for various sections of the Bristol Channel, and from .0024 to .021 (average value of .0093) for various sections of the English Channel. The larger values for the English Channel were associated with large apparent phase differences between the current and the frictional stress and, according to Bowden and Fairbairn (1952), are "probably less significant than the Bristol Channel results." Bowden and Fairbairn give a value of $\gamma = .0018$ when using the mean current in a water depth of about 19m in their investigation off Anglesey, whereas, in a later paper (1956), they find an average value for γ of .0024 when using the current at a specified height above the bottom, the depths ranging from 12m to 22m.

Numerical models often use (see, for example, Flather (1976))

$$k = \gamma/H$$

with $H = h + Z$, the total depth of water. Values for γ which are commonly used lie in the range

$$.0024 \leqslant \gamma \leqslant .0030$$

(see Dronkers (1964), Nihoul and Ronday (1976)).

A perhaps more realistic formula considers the roughness of the bottom material. It is a combination of the de Chèzy and the Manning formulae (see Dronkers (1964, p.156)) which were originally developed for the study of channel flows:

$$k = \frac{g}{C^2 H} \qquad \text{A1.2}$$

where

$$C = \frac{1.003\ R^{1/6}}{n}\ m^{\frac{1}{2}} s^{-1}$$

R is the hydraulic radius (usually approximated by H for a shallow sea)

n is Manning's roughness coefficient which varies with position according to the roughness of the bottom material.

Wang and Connor (1975) give $.025 \leqslant n \leqslant .040$ and their subsequent calculations of the bottom friction parameter for different depths ($1 \leqslant h \leqslant 100m$) and different types of bottom material yield values of k in the range .0013 - .0095. Harleman and Lee (1969) use values of n as low as .020.

Using R = H, A1.2 can be written

$$k = \lambda/H^{4/3} \qquad \text{A1.3}$$

where λ depends on n.

In channel or river flow studies where the region of interest may be divided into a series of one-dimensional sections, the value of n may be varied in each section until the results obtained agree with observations. This is the approach of Harleman and Lee (1969). However, such systematic variation of n, in the case of a two-dimensional shallow sea model, is not always feasible and λ is usually given a constant value. A1.3 is used by Teubner (1976),who considers a value of λ corresponding to n = .030, and Prandle (1978),who uses n = .025.

Leendertse (1967) says that when the bottom roughness has a considerable influence on water movement "the parameter C has to be found in an iterative manner by comparing results with actual field measurements." He obtains

$$C = 19.4\ \ell n[0.9H]$$

experimentally from computations of his Haringvliet model. However, as previously stated, such experimental evaluation of C is not always feasible, especially when there is a paucity of field data available.

Some, more sophisticated, models return to the definition which employs the bottom velocity. Using vertical velocity profiles adjusted to observations, the reference velocity can be expressed in terms of the depth-averaged velocity. Thus,Nihoul and Ronday (1976) quote Ronday (1976) as using

$$\gamma = \frac{\alpha_0}{(1.23+\ell n \frac{0.14H}{z_0})^2}$$

where α_0 is a constant and z_0 is a roughness length. This can be obtained from a velocity profile of the type due to von Karman (see Dronkers (1964, p.156)). Dronkers gives $z_0 = .03d$, where d is a scale for the height of the irregularities of the bottom.

The non-linearity of the friction term $k\|\underset{\sim}{q}\|\underset{\sim}{q}$ provides one mechanism for the interaction between different tidal constitutents and for the generation of harmonics. This effect of the quadratic law has been studied by, amongst others, Dronkers (1961) for the case of a two-dimensional mono-periodic tide, and by Le Provost (1976) for the case of a multi-periodic tide. Le Provost's investigation of the components of the friction in the English Channel lead him to conclude that "for a first approximation, the M_2 component could be studied alone upon a given area, but that to study a secondary wave, S_2,N_2,K_2, it is necessary to consider their propagation together with the M_2 component....; a simulation taking together M_2 and S_2 or M_2,S_2 and N_2 gave a better representation of the component M_2 ." His analysis depends on the presence of a dominant tidal component. However, such a dominant component may not always exist, and, in such a case, a complete picture of

the tidal motion can probably only be obtained by considering the whole tide, a Fourier analysis of the results providing the components if these are required. The main deterrent against such studies is not only the lack of adequate data along open boundaries, but also, if such information did exist, the data over about 15 or 29 days would be needed as input for a model (see Defant (1961, p.304)). This is necessary to account for the effects of such factors as the semi-monthly inequality and the contrast between the spring and the neap tides. Then, not only would the model have to be run long enough to converge numerically, but it would also have to be run for a further period to provide the necessary output. Time and cost obviously preclude such a study. One of the advantages of a linear representation of the frictional force (in linear equations of motion) is that the complete tide may be estimated from the superposition of the solutions for the individual constitutents.

(b) The Linear Representation of $k\|q\|q$

Many models have linearized the quadratic bottom friction law for the sake of simplicity, taking

$$\underset{\sim}{F}_b = \frac{r}{h}\underset{\sim}{q} \quad \text{or} \quad \underset{\sim}{F}_b = \frac{r}{H}\underset{\sim}{q} \quad . \qquad \text{A1.4}$$

In MKS units, r has dimensions ms^{-1}. This linear representation is essential for analytic methods of solution which do not rely on perturbation or iterative techniques. The second expression of A1.4 is sometimes used in linear numerical models which still retain explicit time dependence.

Most studies take r to be a constant, for example, Heaps (1969) uses $r = .0024\ ms^{-1}$ while Flather (1972) uses a value of .0014. Realistically, the value of r will not be constant, but will vary with position.

The linear expression $\frac{r}{h}\underset{\sim}{q}$ can be related to the quadratic law $\frac{\gamma}{h}\|\underset{\sim}{q}\|\underset{\sim}{q}$. The Lorentz approximation for r, in the one-dimensional case, is found by equating the dissipation over a tidal cycle given by each of the expressions (see Proudman (1953)). Thus, it is found

$$r = \frac{8}{3\pi}\gamma U$$

where $q = U \cos \omega t$.

Harleman and Lee (1969) use

$$r = \frac{8}{3\pi}\frac{g}{C^2}u_{max}$$

where C is the Chèzy coefficient which can vary with position and u_{max} is an over-all estimate of the maximum velocity. Dronkers (1964, p.191) gives the two-dimensional version of this,

$$r = \frac{8}{3\pi}\frac{g}{C^2}\nu_m \qquad \text{A1.5}$$

where ν_m is the mean value of the maximum magnitudes of the velocities, if it may be assumed that ν_m does not vary greatly. If C is given a constant value, A1.5 may be used as an estimate of r in an analytic analysis of a tidal region.

Dronkers (1961), produces a linearized form of the quadratic friction term for the two-dimensional case of a mono-periodic tide and shows that, not only the magnitude of the velocity, but also the relative phases of the two velocity components should be taken into account. Using

$$u = U \cos(\omega t+\alpha)$$

$$v = V \cos(\omega t+\beta)$$

he finds, on neglecting the harmonics which arise from the quadratic law

$$u(u^2+v^2)^{\frac{1}{2}} = \lambda u + m \frac{\partial v}{\partial t}$$

$$v(u^2+v^2)^{\frac{1}{2}} = \lambda v - m \frac{\partial u}{\partial t} \quad ,$$

where λ and m are quite complicated functions of U,V,α and β. This form is only useful in idealized studies when (for example, if only Kelvin waves are considered) exact values for λ and m may be found. However, use of this linear form is usually precluded by the fact that foreknowledge of U,V,α and β are required and these are, in fact, unknowns of the system.

Prandle (1978) uses a non-linear tidal model in conjunction with a linear model for secondary effects (such as those of wind) and so is able to relate, at each grid-point, the linear friction coefficient $K(=\frac{r}{H})$ of the dominant constituent (say M_2) to the non-linear law. He finds K at a u-velocity grid point by minimizing $\in$ with respect to K, where

$$\in^2 = \int_0^T \left(g \frac{C_0 u(u^2+v^2)^{\frac{1}{2}}}{H^{4/3}} - Ku \right)^2 dt$$

where T is the period of the M_2 tidal constituent,
and C_0 is a frictional coefficient corresponding to $n = .025$.
An analogous expression is used at a v-velocity grid-point.

However, for obvious reasons, this approach cannot be adopted in linear tidal models and the best approximation to the friction coefficient is probably given by A1.5.

The effect of a dominant tidal constituent on other components is easily accounted for with a linear friction representation. Jeffreys (1976) shows that, for two tidal velocity constituents $U_1\cos \omega_1 t$ and $U_2\cos \omega_2 t$, with $U_2/U_1 < \frac{1}{2}$, the frictional component with frequency ω_1 is

$$F_1 = \frac{8}{3\pi} \frac{\gamma}{h} U_1^2 \cos \omega_1 t = \frac{r_1}{h} U_1 \cos \omega_1 t,$$

while the component at frequency ω_2 is

$$F_2 = \frac{4}{\pi}\frac{\gamma}{h} U_1 U_2 \cos \omega_2 t = \frac{r_2}{h} U_2 \cos \omega_2 t.$$

Hence, if r_1 is a frictional coefficient for a dominant tidal constituent, the appropriate linear friction factor for any other constituent is

$$r_2 = 1.5\ r_1 \quad . \qquad \text{A1.6}$$

Garrett (1972) states that this result is readily extended to the two-dimensional case when "tidal ellipses (are) of the same eccentricity for all constituents being considered." This interaction of constituents is not so easily taken into account with a non-linear friction law.

(c) Comparison between the two representations

Although, according to Nihoul and Ronday (1976), "it is now commonly admitted that a quadratic law must be used", Durance (1975) justifies his use of the linear law thus: "Although there is evidence to suggest that the bottom friction does depend quadratically on the velocity near the bottom, there is no direct relationship betweem the near-bottom velocity and the mass transport, and in some situations they can be in opposite directions. In addition, the bottom friction coefficient is likely to depend on position because of both the general bathymetry and the variation in bottom roughness." The investigation of velocity profiles by Johns (1976) and Nihoul (1977) would seem to substantiate that, about the time of tide reversal, the validity of the quadratic law is questionable; however, Nihoul shows that the discrepancy does not affect the results significantly.

Flather (1972) compares the results of a linear scheme to the results of a non-linear scheme applied to the computation of the M_2 tide in a rectangular sea 65m deep. He finds large differences in the M_2

amplitudes obtained by the two models, but says that this is "probably due largely to the choice of friction parameters" (he uses $r = .0014$ and $\gamma = .0025$). Noye and Tronson (1978) show that with a judicious choice (through trial and error) of the value of the linear parameter, good agreement can be obtained between the results produced by the two models.

Apart from simplicity and the possibility of superposition of solutions, the linear friction coefficient has the advantage of being more easily able to include the effect (shown by Jeffreys (1976) and Le Provost (1976)) of a dominant tidal constituent on the other constituents. However, if the non-linear effects in shallow water are of special interest, it seems more important, in some cases, to include a non-linear friction law than to include the non-linear advection terms (see, for example, Flather and Heaps (1975)).

In some cases, as in Leendertse's (1967) Haringvliet study (where the maximum depth is 13m), the bottom roughness influences the water movements to a considerable extent and it would be expected that a quadratic law would be essential. Even for the non-linear representation, careful estimates of the friction parameter are necessary and usually have to be found in an iterative manner, comparing computed results with actual field measurements.

No matter which form is chosen for the representation of the bottom frictional force, no matter how complicated the analysis used to obtain it, there is always some empirical factor associated with it; and it seems that the justification for any choice of parameterization lies solely in the accuracy of the results obtained by the model.

APPENDIX 2.

The Galerkin and Collocation Methods

The exact solution to a differential equation and its boundary conditions cannot always be found and an approximate solution must be sought, either by analytical methods or by numerical methods. An analytical approximation may be obtained by the Method of Weighted Residuals (see Finlayson (1972)). The two techniques discussed here, the Collocation and the Galerkin methods, belong to this class.

The classic approach of these two methods is to find an infinite series of, for example, trigonometric functions which satisfy at least some of the boundary conditions exactly, and to proceed to solve for a finite number of unknown coefficients in the series by approximately satisfying the differential equation and any remaining boundary conditions. The Galerkin technique used in this manner is described in detail by Fletcher (1978).

However, if it is possible to find a solution to the differential equation, Shuleshko (1961a, 1961b) has shown that better results are obtained if the approximation method is applied to the boundary condition rather than to the differential equation. This is the technique used here.

Consider the Helmholtz equation

$$(\nabla^2+\chi^2)\zeta = 0 \qquad \text{A2.1}$$

with its boundary conditions

$$M_p[\zeta(x,y)] = \phi_p(x,y) \quad \text{along} \quad s_p, \quad p = 1,\ldots,P$$

where M_p are linear differential operators and s_p is the pth portion of the boundary. The solution to the differential equation may be written as

$$\zeta(x,y) = \sum_{j=1}^{P} \sum_{n=0}^{\infty} a_{jn}\, \zeta_{jn}(x,y)$$

where a_{jn} are unknown coefficients and each term, ζ_{jn}, in the series satisfies A2.1 exactly. It is also required that

$$M_p \left[\sum_{j=1}^{P} \sum_{n=0}^{\infty} a_{jn}\, \zeta_{jn} \right] - \phi_p = 0 \quad \text{along} \quad s_p, \quad p = 1,\ldots,P. \qquad \text{A2.2}$$

For some boundary conditions it may be possible to find a simple relation between the a_{jn} such that A2.2 is satisfied exactly; but, if not, an approximate solution may be found by truncating the infinite series; in which case

$$M_p [\tilde{\zeta}(x,y)] - \phi_p(x,y) = r_p(x,y), \text{ along } s_p, \; p = 1,\ldots,P$$

where

$$\tilde{\zeta} = \sum_{j=1}^{P} \sum_{n=0}^{N} a_{jn}\, \zeta_{jn}$$

and r_p is the residual, or the error in the pth boundary condition. It is expected that the residual be small in some measure and that the effect of obtaining a new solution with N increased should cause a reduction in r_p in some average sense along s_p. When $r_p = 0$, for all p, the exact solution has been found.

The method proceeds to solve for the a_{jn} by imposing an orthogonality condition on the $r_p(x,y)$,

$$\int_{s_p} r_p(x,y) w_{np}(x,y)\, ds = 0, \; n = 0,\ldots,N \text{ for } p = 1,\ldots,P \qquad \text{A2.3}$$

where ds is a line increment along s_p and w_{np} is some chosen weighting function. If, as $N \to \infty$, $\{w_{np}\}$ is a complete set, then $r_p \equiv 0$ and $\tilde{\zeta}$ is the exact solution. If

$$w_{np} = \delta(x - x_{np}, y - y_{np})$$

where $\delta(x,y)$ is the Dirac delta function and (x_{np},y_{np}) $(n = 0,\ldots,N)$ are points along s_p, use of A2.3 is called the Collocation Method. If

$$w_{np} = M_p[\zeta_{jn}], \quad j \in \{1,\ldots,P\} \quad \text{for} \quad n = 0,\ldots,N,$$

then use of A2.3 is called the Galerkin technique.

Application of A2.3 results in a set of linear simultaneous equations which may be solved for the a_{jn}.

The advantage of Collocation is its simplicity; no integration or mathematical manipulation is required to set up the simultaneous equations. However, the accuracy of the solution depends on the position of the Collocation points (see Shuleshko (1961a)). Chapter 6 shows that the overall accuracy and convergence using the Galerkin method is better than that obtained by Collocation. Since the mathematical manipulation for the Galerkin method need to be done only once, even if physical constants are varied, it is the Galerkin method which has been adopted for the analytical approximations in Chapters 3 and 4.

APPENDIX 3.

Evaluation of the Integral Form for $\zeta_2(x,y)$

In Chapter 3, $\zeta_2(x,y)$ is expressed in integral form by 3.4.13, that is,

$$\zeta_2(x,y) = \frac{\Omega}{2\pi}\left[-\int_{-\infty}^{\infty} e^{-i\lambda x}\,\frac{\{\lambda g_0 + iK_1 f_0\}}{\lambda^2+K_1^2}\,\Phi(\lambda)d\lambda\right.$$

$$+\int_{-\infty}^{\infty} e^{-i\lambda(x+a)}\{g_0[\lambda\cosh K_1 a - iK_1\sinh K_1 a]$$

$$-\ f_0[\lambda\sinh K_1 a - iK_1\cosh K_1 a]\}\frac{\Phi(\lambda)}{\lambda^2+K_1^2}\,d\lambda$$

$$-\sum_{n=1}^{\infty}\int_{-\infty}^{\infty} e^{-i\lambda x}\,\frac{\{\lambda g_n + i\frac{n\pi}{a} f_n\}}{\lambda^2 - (\frac{n\pi}{a})^2}\,\Phi(\lambda)d\lambda$$

$$\left.+\sum_{n=1}^{\infty}(-1)^n\int_{-\infty}^{\infty} e^{-i\lambda(x+a)}\,\frac{\{\lambda g_n + i\frac{n\pi}{a} f_n\}}{\lambda^2 - (\frac{n\pi}{a})^2}\,\Phi(\lambda)d\lambda\right] \qquad \text{A3.1}$$

with

$$\Phi(\lambda) = \frac{\lambda\theta\sinh s(y-b) + s(1+i\phi_2)\cosh s(y-b)}{\{\lambda^2\theta^2 - s^2(1+i\phi_2)^2\}\sinh sb},$$

$$-a \leqslant x \leqslant 0$$

and $$s^2 = \lambda^2 - \chi_2^2 \ .$$

This may be written as

$$\zeta_2(x,y) = \frac{\Omega}{2\pi}\{-I_{Uo} + I_{Lo} + \sum_{n=1}^{\infty}(-I_{Un} + I_{Ln})\}, \qquad \text{A3.2}$$

where $I_{Un}\ (n \geqslant 0)$ is an integral associated with $e^{-i\lambda x}$ and is evaluated using a contour closed in the upper half-plane; and $I_{Ln}\ (n \geqslant 0)$ is an integral associated with $e^{-i\lambda(x+a)}$ and is evaluated using a contour closed in the lower half-plane.

For I_{Uo}, I_{Lo}, the poles of the integrand are given by

$$\lambda = \pm iK_1, \quad (s = i(K_1^2 + \chi_2^2)^{\frac{1}{2}} = s_0) \qquad \text{A3.3a}$$

$$\lambda = \pm k_2^{(0)} = \pm\left[\frac{\omega^2}{gh_2}(1+i\phi_2)\right]^{\frac{1}{2}}, \left(s = \theta\left[\frac{\omega^2}{gh_2}\frac{1}{(1+i\phi_2)}\right]^{\frac{1}{2}} = K_2\right) \qquad \text{A3.3b}$$

$$\lambda = \pm k_2^{(\ell)} = \pm\left[\chi_2^2 - \left(\frac{\ell\pi}{b}\right)^2\right]^{\frac{1}{2}}, \quad \left(s = i\,\frac{\ell\pi}{b}\right), \ \ell > 0 \qquad \text{A3.3c}$$

where the appropriate value of s is defined as shown and the branch chosen for A3.3b,c is such that $\mathrm{Im}(k_2^{(\ell)}) > 0$, $\ell \geq 0$.

The poles associated with I_{Un}, I_{Ln} $(n \geq 1)$ are given by

$$\lambda = \pm \frac{n\pi}{a}, \quad \left(s = \left[\left(\frac{n\pi}{a}\right)^2 - \chi_2^2\right]^{\frac{1}{2}} = s_n\right)$$

$$\lambda = \pm k_2^{(0)}$$

$$\lambda = \pm k_2^{(\ell)}, \ \ell > 0.$$

Noting that $\mathrm{Im}(iK_1) \leq 0$, A3.2 may be written as a sum of residues

$$I_{Uo} = 2\pi i\left\{\mathrm{Res}(-iK_1) + \mathrm{Res}(k_2^{(0)}) + \sum_{\ell=1}^{\infty} \mathrm{Res}(k_2^{(\ell)})\right\}$$

$$= -2\pi i\left\{e^{-K_1 x}\frac{[g_0-f_0][-i\theta K_1 \sinh s_0(y-b) + s_0(1+i\phi_2)\cosh s_0(y-b)]}{2[\theta^2K_1^2 + s_0^2(1+i\phi_2)^2]\sinh s_0 b}\right.$$

$$\left. + \delta_{oo}\, e^{-ik_2^{(0)}x + K_2(y-b)} + \sum_{\ell=1}^{\infty} \delta_{o\ell}\, e^{-ik_2^{(\ell)}x}\left[\cos\frac{\ell\pi y}{b} + \frac{\theta}{(1+i\phi_2)}\frac{b}{\ell\pi}k_2^{(\ell)}\sin\frac{\ell\pi y}{b}\right]\right\}$$

$$I_{Lo} = -2\pi i\left\{\mathrm{Res}(iK_1) + \mathrm{Res}(-k_2^{(0)}) + \sum_{\ell=1}^{\infty} \mathrm{Res}(-k_2^{(\ell)})\right\}$$

$$= -2\pi i\left\{e^{K_1 x}\frac{[g_0+f_0][i\theta K_1 \sinh s_0(y-b) + s_0(1+i\phi_2)\cosh s_0(y-b)]}{2[\theta^2K_1^2 + s_0^2(1+i\phi_2)^2]\sinh s_0 b}\right.$$

$$\left. + \in_{oo} e^{ik_2^{(0)}x - K_2(y-b)} + \sum_{\ell=1}^{\infty} \in_{o\ell} e^{ik_2^{(\ell)}x}\left[\cos\frac{\ell\pi y}{b} - \frac{\theta}{(1+i\phi_2)}\frac{b}{\ell\pi}k_2^{(\ell)}\sin\frac{\ell\pi y}{b}\right]\right\}$$

$$I_{Un} = 2\pi i\left\{\mathrm{Res}(k_2^{(0)}) + \sum_{\ell=1}^{\infty}\mathrm{Res}(k_2^{(\ell)}) + \tfrac{1}{2}\mathrm{Res}\left(\frac{n\pi}{a}\right) + \tfrac{1}{2}\mathrm{Res}\left(-\frac{n\pi}{a}\right)\right\}$$

$$= 2\pi i\left\{\delta_{no}\, e^{-ik_2^{(0)}x + K_2(y-b)}\right.$$

$$+ \sum_{\ell=1}^{\infty}\delta_{n\ell}\, e^{-ik_2^{(\ell)}x}\left[\cos\frac{\ell\pi y}{b} + \frac{\theta}{(1+i\phi_2)}\frac{b}{\ell\pi}k_2^{(\ell)}\sin\frac{\ell\pi y}{b}\right]$$

$$+ g_n\frac{\left[-i\frac{n\pi\theta}{a}\sin\frac{n\pi x}{a}\sinh s_n(y-b) + s_n(1+i\phi_2)\cos\frac{n\pi x}{a}\cosh s_n(y-b)\right]}{2\left[(n\pi\theta/a)^2 - s_n^2(1+i\phi_2)^2\right]\sinh s_n b}$$

$$\left. + if_n\frac{\left[\frac{n\pi\theta}{a}\cos\frac{n\pi x}{a}\sinh s_n(y-b) - is_n(1+i\phi_2)\sin\frac{n\pi x}{a}\cosh s_n(y-b)\right]}{2\left[(n\pi\theta/a)^2 - s_n^2(1+i\phi_2)^2\right]\sinh s_n b}\right\}$$

$$I_{Ln} = -2\pi i\left\{\mathrm{Res}(-k_2^{(0)}) + \sum_{\ell=1}^{\infty}\mathrm{Res}(-k_2^{(\ell)}) + \tfrac{1}{2}\mathrm{Res}\left(-\frac{n\pi}{a}\right) + \tfrac{1}{2}\mathrm{Res}\left(\frac{n\pi}{a}\right)\right\}$$

$$= -2\pi i\left\{\in_{no} e^{ik_2^{(0)}x - K_2(y-b)}\right.$$

$$+ \sum_{\ell=1}^{\infty}\in_{n\ell} e^{ik_2^{(\ell)}x}\left[\cos\frac{\ell\pi y}{b} - \frac{\theta}{(1+i\phi_2)}\frac{b}{\ell\pi}k_2^{(\ell)}\sin\frac{\ell\pi y}{b}\right]$$

$$+ g_n\frac{\left[-i\frac{n\pi\theta}{a}\sin\frac{n\pi x}{a}\sinh s_n(y-b) + s_n(1+i\phi_2)\cos\frac{n\pi x}{a}\cosh s_n(y-b)\right]}{2\left[(n\pi\theta/a)^2 - s_n^2(1+i\phi_2)^2\right]\sinh s_n b}$$

$$\left. + if_n\frac{\left[\frac{n\pi\theta}{a}\cos\frac{n\pi x}{a}\sinh s_n(y-b) - is_n(1+i\phi_2)\sin\frac{n\pi x}{a}\cosh s_n(y-b)\right]}{2\left[(n\pi\theta/a)^2 - s_n^2(1+i\phi_2)^2\right]\sinh s_n b}\right\},$$

where $\in_{n\ell}, \delta_{n\ell}$ $(n \geq 0,\ \ell \geq 0)$ are linear combinations of the g_n and f_n, their actual form being immaterial.

Thus, using A3.2 ,

$$\zeta_2(x,y) = \Omega i\Bigg\{\Bigg(\sum_{n=0}^{\infty} \in_{no}\Bigg)e^{i k_2^{(0)} x - K_2(y-b)} + \Bigg(\sum_{n=0}^{\infty} \delta_{no}\Bigg) e^{-i k_2^{(0)} x + K_2(y-b)}$$

$$+ \sum_{\ell=1}^{\infty}\Bigg(\sum_{n=0}^{\infty} \in_{n\ell}\Bigg)e^{i k_2^{(\ell)} x}\left[\cos\frac{\ell\pi y}{b} - \frac{\theta}{(1+i\phi_2)}\frac{b}{\ell\pi}k_2^{(\ell)}\sin\frac{\ell\pi y}{b}\right]$$

$$+ \sum_{\ell=1}^{\infty}\Bigg(\sum_{n=0}^{\infty} \delta_{n\ell}\Bigg)e^{-i k_2^{(\ell)} x}\left[\cos\frac{\ell\pi y}{b} + \frac{\theta}{(1+i\phi_2)}\frac{b}{\ell\pi}k_2^{(\ell)}\sin\frac{\ell\pi y}{b}\right]$$

$$+ g_0\frac{[i\theta K_1 \sinh K_1x \sinh s_0(y-b) + s_0(1+i\phi_2)\cosh K_1x \cosh s_0(y-b)]}{[\theta^2K_1^2 + s_0^2(1+i\phi_2)^2]\sinh s_0b}$$

$$+ f_0\frac{[i\theta K_1 \cosh K_1x \sinh s_0(y-b) + s_0(1+i\phi_2)\sinh K_1x \cosh s_0(y-b)]}{[\theta^2K_1^2 + s_0^2(1+i\phi_2)^2]\sinh s_0b}$$

$$- \sum_{n=1}^{\infty} g_n\frac{[-i\frac{n\pi\theta}{a}\sin\frac{n\pi x}{a}\sinh s_n(y-b) + s_n(1+i\phi_2)\cos\frac{n\pi x}{a}\cosh s_n(y-b)]}{[(n\pi\theta/a)^2 - s_n^2(1+i\phi_2)^2]\sinh s_nb}$$

$$- i\sum_{n=1}^{\infty} f_n\frac{[\frac{n\pi\theta}{a}\cos\frac{n\pi x}{a}\sinh s_n(y-b) - i\,s_n(1+i\phi_2)\sin\frac{n\pi x}{a}\cosh s_n(y-b)]}{[(n\pi\theta/a)^2 - s_n^2(1+i\phi_2)^2]\sinh s_nb}\Bigg\}, \qquad \text{A3.4}$$

where it has been assumed that the order of summation of the series associated with $\in_{n\ell}, \delta_{n\ell}$ may be interchanged.

This expression may be rewritten as

$$\zeta_2(x,y) = E_0\, e^{i k_2^{(0)} x - K_2(y-b)} + G_0\, e^{-i k_2^{(0)} x + K_2(y-b)}$$

$$+ \sum_{\ell=1}^{\infty} E_\ell\, e^{i k_2^{(\ell)} x}\left[\cos\frac{\ell\pi y}{b} - \frac{\theta}{(1+i\phi_2)}\frac{b}{\ell\pi}k_2^{(\ell)}\sin\frac{\ell\pi y}{b}\right]$$

$$+ \sum_{\ell=1}^{\infty} G_\ell\, e^{-i k_2^{(\ell)} x}\left[\cos\frac{\ell\pi y}{b} + \frac{\theta}{(1+i\phi_2)}\frac{b}{\ell\pi}k_2^{(\ell)}\sin\frac{\ell\pi y}{b}\right]$$

$$+ D_0\left[\cosh K_1x \cosh s_0(y-b) + \frac{i\theta K_1}{s_0(1+i\phi_2)}\sinh K_1x \sinh s_0(y-b)\right]$$

$$+ F_0\left[\sinh K_1x \cosh s_0(y-b) + \frac{i\theta K_1}{s_0(1+i\phi_2)}\cosh K_1x \sinh s_0(y-b)\right]$$

$$+ \sum_{\ell=1}^{\infty} D_\ell\left[\cos\frac{\ell\pi x}{a}\cosh s_\ell(y-b) - \frac{i\theta}{(1+i\phi_2)}\frac{\ell\pi}{as_\ell}\sin\frac{\ell\pi x}{a}\sinh s_\ell(y-b)\right]$$

$$+ \sum_{\ell=1}^{\infty} F_\ell\left[\sin\frac{\ell\pi x}{a}\cosh s_\ell(y-b) + \frac{i\theta}{(1+i\phi_2)}\frac{\ell\pi}{as_\ell}\cos\frac{\ell\pi x}{a}\sinh s_\ell(y-b)\right], \qquad \text{A3.5}$$

with

$$(D_0, F_0) = \frac{\Omega\, i\, s_0(1+i\phi_2)}{[\theta^2 K_1^2 + s_0^2(1+i\phi_2)^2]\sinh s_0 b}\,(g_0, f_0)$$

$$(D_\ell, F_\ell) = -\frac{\Omega\, i\, s_\ell(1+i\phi_2)}{[(\ell\pi\theta/a)^2 - s_\ell^2(1+i\phi_2)^2]\sinh s_\ell b}\,(g_\ell, f_\ell),\ \ell \in \mathbb{Z}^+$$

$$k_2^{(0)} = \left\{\frac{\omega^2}{gh_2}(1+i\phi_2)\right\}^{1/2}$$

$$k_2^{(\ell)} = \left\{\chi_2^2 - \left(\frac{\ell\pi}{b}\right)^2\right\}^{1/2}, \ell \in \mathbb{Z}^+$$

$$s_0 = i\left\{K_1^2 + \chi_2^2\right\}^{1/2}$$

$$s_\ell = \left\{\left(\frac{\ell\pi}{a}\right)^2 - \chi_2^2\right\}^{1/2}, \ell \in \mathbb{Z}^+$$

$$K_2 = \theta\left\{\frac{\omega^2}{gh_2}\,\frac{1}{(1+i\phi_2)}\right\}^{1/2}.$$

APPENDIX 4.

The Classes of Elements for the Non-Linear Model and their Associated Finite-Difference Equations

1. 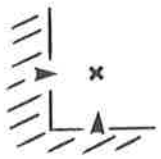

$Z_{\ell,j}^{(n+1)}$ as in equation 5.5.2a

$U_{\ell,j}^{(n+1)} = V_{\ell,j}^{(n+1)} = 0$

2. 

$Z_{\ell,j}^{(n+1)}$ as in equation 5.5.2a

$$U_{\ell,j}^{(n+1)} = U_{\ell,j}^{(n)} - \frac{\Delta t}{4\Delta x} U_{\ell,j}^{(n)} \{U_{\ell+1,j}^{(n)} - U_{\ell-1,j}^{(n)}\} - \frac{\Delta t}{2\Delta y} \bar{\bar{V}}_{\ell,j}^{(n)} \{U_{\ell,j+1}^{(n)} - U_{\ell,j}^{(n)}\}$$
$$- \Delta t\, R_{u_{\ell,j}}^{(n)} U_{\ell,j}^{(n)} + \Delta t\, f\, \bar{\bar{V}}_{\ell,j}^{(n)} - \frac{\Delta t}{2\Delta x} g\{Z_{\ell,j}^{(n+1)} - Z_{\ell-1,j}^{(n+1)}\}$$

$V_{\ell,j}^{(n+1)} = 0$

3. 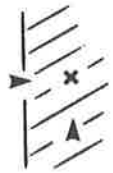

$Z_{\ell,j}^{(n+1)}$, $V_{\ell,j}^{(n+1)}$ not calculated

$U_{\ell,j}^{(n+1)} = 0$

4. 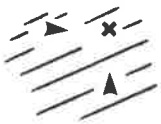

$Z_{\ell,j}^{(n+1)}$, $V_{\ell,j}^{(n+1)}$, $U_{\ell,j}^{(n+1)}$ not calculated

5. 

$Z_{\ell,j}^{(n+1)}$ as in equation 5.5.2a

$U_{\ell,j}^{(n+1)} = 0$

$$V_{\ell,j}^{(n+1)} = V_{\ell,j}^{(n)} - \frac{\Delta t}{2\Delta x} \bar{\bar{U}}_{\ell,j}^{(n+1)} \{V_{\ell+1,j}^{(n)} - V_{\ell,j}^{(n)}\}$$
$$- \frac{\Delta t}{4\Delta y} V_{\ell,j}^{(n)} \{V_{\ell,j+1}^{(n)} - V_{\ell,j-1}^{(n)}\} - \Delta t\, R_{v_{\ell,j}}^{(n)} V_{\ell,j}^{(n)}$$
$$- \Delta t f\, \bar{\bar{U}}_{\ell,j}^{(n+1)} - \frac{\Delta t}{2\Delta y} g\{Z_{\ell,j}^{(n+1)} - Z_{\ell,j-1}^{(n+1)}\}$$

6. 

$Z_{\ell,j}^{(n+1)}$, $U_{\ell,j}^{(n+1)}$, $V_{\ell,j}^{(n+1)}$ as in equations 5.5.2

7. 

$Z_{\ell,j}^{(n+1)}$ not calculated

$U_{\ell,j}^{(n+1)} = V_{\ell,j}^{(n+1)} = 0$

8. 

$Z^{(n+1)}_{\ell,j}$, $U^{(n+1)}_{\ell,j}$ not calculated

$V^{(n+1)}_{\ell,j} = 0$

9. 

(Western open boundary)

$Z^{(n+1)}_{\ell,j} = \mathrm{Re}\{Z_{in_j} e^{-i\omega(n+1)\Delta t}\}$, where Z_{in_j} gives the amplitude and phase of the elevation at $y = j\Delta y$ along the open boundary.

$U^{(n+1)}_{\ell,j}$ not calculated

$$V^{(n+1)}_{\ell,j} = V^{(n)}_{\ell,j} - \frac{\Delta t}{2\Delta x} \bar{\bar{U}}^{(n+1)}_{\ell,j} \{V^{(n)}_{\ell+1,j} - V^{(n)}_{\ell,j}\} - \frac{\Delta t}{4\Delta y} V^{(n)}_{\ell,j} \{V^{(n)}_{\ell,j+1} - V^{(n)}_{\ell,j-1}\} - \Delta t\, R^{(n)}_{v_{\ell,j}} V^{(n)}_{\ell,j} - \Delta t\, f\, \bar{\bar{U}}^{(n+1)}_{\ell,j} - \frac{\Delta t}{2\Delta y} g\{Z^{(n+1)}_{\ell,j} - Z^{(n+1)}_{\ell,j-1}\}$$

$$\bar{\bar{U}}^{(n+1)}_{\ell,j} = \tfrac{1}{2}\{U^{(n+1)}_{\ell+1,j} + U^{(n+1)}_{\ell+1,j-1}\}$$

10. 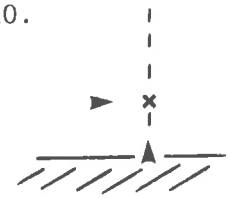

(Western open Boundary)

$Z^{(n+1)}_{\ell,j} = \mathrm{Re}\{Z_{in_j} e^{-i\omega(n+1)\Delta t}\}$, Z_{in_j} as for element 9

$U^{(n+1)}_{\ell,j}$ not calculated

$V^{(n+1)}_{\ell,j} = 0$

12. 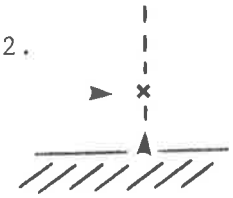

(Eastern open Boundary)

$Z^{(n+1)}_{\ell,j} = \mathrm{Re}\{Z'_{in_j} e^{-i\omega(n+1)\Delta t}\}$, Z'_{in_j} as for Z_{in_j} in elements 9 and 10

$$U^{(n+1)}_{\ell,j} = U^{(n)}_{\ell,j} - \frac{\Delta t}{2\Delta x} U^{(n)}_{\ell,j} \{U^{(n)}_{\ell,j} - U^{(n)}_{\ell-1,j}\} - \frac{\Delta t}{2\Delta y} \bar{\bar{V}}^{(n)}_{\ell,j} \{U^{(n)}_{\ell,j+1} - U^{(n)}_{\ell,j}\} - \Delta t\, R^{(n)}_{u_{\ell,j}} U^{(n)}_{\ell,j} + \Delta t\, f\, \bar{\bar{V}}^{(n)}_{\ell,j} - \frac{\Delta t}{2\Delta x} g\{Z^{(n+1)}_{\ell,j} - Z^{(n+1)}_{\ell-1,j}\}$$

$V^{(n+1)}_{\ell,j} = 0.$

11. (Eastern open Boundary)

$$Z_{\ell,j}^{(n+1)} = \mathrm{Re}\{Z'_{in_j}\ e^{-i\omega(n+1)\Delta t}\}, Z'_{in_j} \text{ as in element 12}$$

$$U_{\ell,j}^{(n+1)} = U_{\ell,j}^{(n)} - \frac{\Delta t}{2\Delta x} U_{\ell,j}^{(n)} \{U_{\ell,j}^{(n)} - U_{\ell-1,j}^{(n)}\}$$

$$- \frac{\Delta t}{4\Delta y} \overline{\overline{V}}_{\ell,j}^{(n)} \{U_{\ell,j+1}^{(n)} - U_{\ell,j-1}^{(n)}\} - \Delta t\ R_{u_{\ell,j}}^{(n)} U_{\ell,j}^{(n)}$$

$$+ \Delta t\ f\ \overline{\overline{V}}_{\ell,j}^{(n)} - \frac{\Delta t}{2\Delta x} g\{Z_{\ell,j}^{(n+1)} - Z_{\ell-1,j}^{(n+1)}\}$$

$$V_{\ell,j}^{(n+1)} = V_{\ell,j}^{(n)} - \frac{\Delta t}{2\Delta x} \overline{\overline{U}}_{\ell,j}^{(n+1)} \{V_{\ell,j}^{(n)} - V_{\ell-1,j}^{(n)}\}$$

$$- \frac{\Delta t}{4\Delta y} V_{\ell,j}^{(n)} \{V_{\ell,j+1}^{(n)} - V_{\ell,j-1}^{(n)}\} - \Delta t\ R_{v_{\ell,j}}^{(n)} V_{\ell,j}^{(n)}$$

$$- \Delta t\ f\ \overline{\overline{U}}_{\ell,j}^{(n+1)} - \frac{\Delta t}{2\Delta y} g\{Z_{\ell,j}^{(n+1)} - Z_{\ell,j-1}^{(n+1)}\}$$

$$\overline{\overline{U}}_{\ell,j}^{(n+1)} = \tfrac{1}{2}\{U_{\ell,j}^{(n+1)} + U_{\ell,j-1}^{(n+1)}\}$$

► indicates a U-velocity grid-point

▲ indicates a V-velocity grid-point

× an elevation grid-point

////// land

– – – – an open boundary.

BIBLIOGRAPHY

BOWDEN, K.F. and FAIRBAIRN, L.A. (1952): *A Determination of the Frictional Forces in a Tidal Current.* Proc.Roy. Soc. Lond. A,214, 371-392.

BOWDEN, K.F. and FAIRBAIRN, L.A. (1956): *Measurements of Turbulent Fluctuations and Reynolds Stresses in a Tidal Current.* Proc. Roy. Soc. Lond. A, 237, 424-438.

BUCHWALD, V.T. and WILLIAMS, N.V. (1975): *Rectangular Resonators on Infinite and Semi-infinite Channels.* J. Fluid Mech. 67, 497-511.

CRESSWELL, G.R. (1971): *Current Measurements in the Gulf of Carpentaria.* C.S.I.R.O. Div. Fish. Oceanog. Rept. No.50.

DEFANT, A. (1961): *Physical Oceanography*, Vol. 2, Pergamon Press, Oxford, 598 pp.

DRONKERS, J.J. (1961): *The Linearization of the Quadratic Resistance Term in the Equations of Motion for a Pure Harmonic Tide in a Sea.* NATO Symposium 1961. Inst. für Meeresk, Univ. Hamburg.

DRONKERS, J.J. (1964): *Tidal Computations in Rivers and Coastal Waters.* North-Holland Publ. Co., Amsterdam, 518 pp.

DURANCE, J.A. (1975): *A Mathematical Model of the Residual Circulation of the Southern North Sea.* Mém. Soc. Roy. Sci. Liège, 6^{e} série, tome VII, 261-272.

EASTON, A.K. (1970): *The Tides of the Continent of Australia.* Horace Lamb Centre for Oceanog. Res., Res. paper No. 37.

FINLAYSON, B.A. (1972): *The Method of Weighted Residuals and Variational Principles.* Academic Press, New York, 412 pp.

FLATHER, R.A. (1972): *Analytic and Numerical Studies in the Theory of Tides and Storm Surges.* Ph. D. Thesis, U. of Liverpool.

FLATHER, R.A. (1976): *A Tidal Model of the North-West European Continental Shelf.* Mém. Soc. Roy. Sci. Liège, 6^{e} série, tome X, 141-164.

FLATHER, R.A. and HEAPS, N.S. (1975): *Tidal Computations for Morecambe Bay.* Geophys. J. Roy. Astr. Soc. 42, 489-517.

FLETCHER, C.A.J. (1978): *The Galerkin Method: An Introduction* in *Numerical Simulation of Fluid Motion* (ed. J. Noye), North-Holland Publ. Co., Amsterdam, 580 pp.

GARRETT, C. (1972): *Tidal Resonance in the Bay of Fundy and Gulf of Maine.* Nature, London 238, 441-443.

GRACE, S.F. (1936): *Friction in the Tidal Currents of the Bristol Channel.* Mon. Not. Roy. Astr. Soc., Geophys. Suppl. 3, 388-395.

GRACE, S.F. (1937): *Friction in the Tidal Currents of the English Channel.* Mon. Not. Roy. Astr. Soc., Geophys. Suppl. 4, 133-142.

GROEN, P. and GROVES, G.W. (1962): *Surges* in *The Sea* (ed. M.N. Hill). Vol. 1, 611-646, Interscience Publ., New York.

HAMBLIN, P.F. (1976): *A Theory of Short Period Tides in a Rotating Basin.* Phil. Trans. Roy. Soc. Lond. A, 281, 97-111.

HANSEN, W. (1962): *Tides* from *The Sea* (ed. M.N. Hill), Vol.1, 764-801, Interscience Publ., New York.

HARLEMAN, D.R.F. and LEE, C.H. (1969): *The Computation of Tides and Currents in Estuaries and Canals.* U.S. Army Corps of Engrs., Comm. Tidal Hydraulics, Tech. Bull. No.16.

HEAPS, N.S. (1969): *A Two Dimensional Numerical Sea Model.* Phil. Trans. Roy. Soc. Lond. A, 265, 93-137.

HENDERSHOTT, M. and MUNK, W. (1970): *Tides.* Ann. Rev. Fl. Mech., 2, 205-224.

JEFFREYS, H. (1976): *The Earth,* 6th ed., Cambridge University Press, 574 pp.

JOHNS, B. (1976): *A Note on the Boundary Layer at the Floor of a Tidal Channel.* Dyn. Atmos. Oceans. 1, 91-98.

LEENDERTSE, J.J. (1967): *Aspects of the Computational Model for Long-Period Water-wave Propagation.* Rand Mem. RM5294-PR.

LE PROVOST, C. (1976): *Theoretical Analysis of the Structure of the Tidal Wave's Spectrum in Shallow Water Areas.* Mém. Soc. Roy. Sci. Liège, 6^{e} série, tome X, 97-111.

MELVILLE, W.K. and BUCHWALD, V.T. (1976): *Oscillations in the Gulf of Carpentaria.* J. Phys. Oceanog. 6, 394-398.

MILLER, G.R. (1966): *The Flux of Tidal Energy Out of the Deep Oceans.* J. Geophys. Res. 71, 2485-2489.

NEWELL, B.S (1973): *Hydrology of the Gulf of Carpentaria.* C.S.I.R.O. Div. Fish. Oceanog, Tech. Pap. No. 35.

NIHOUL, J.C.J. (1975): *Hydrodynamic Models* in *Modelling of Marine Systems* (ed. J.C.J. Nihoul), Elsevier, Amsterdam, 292 pp.

NIHOUL, J.C.J. (1977): *Three-dimensional Model of Tides and Storm Surges in a Shallow Well-mixed Continental Sea.* Dyn. Atmos. Oceans, 2, 29-47.

NIHOUL, J.C.J. and RONDAY, F.C. (1976): *Hydrodynamic Models of the North Sea: A Comparative Assessment.* Mém. Soc. Roy. Sci. Liège, 6^{e} série, tome X, 61-96.

NOYE, B.J. (1978): *An Introduction to Finite Difference Techniques.* in *Numerical Simulation of Fluid Motion* (ed. J. Noye), North-Holland Publ. Co., Amsterdam, 580 pp.

NOYE, B.J. and TRONSON, K. (1978): *Finite Difference Techniques Applied to the Simulation of Tides and Currents in Gulfs.* in *Numerical Simulation of Fluid Motion* (ed. J. Noye), North-Holland Publ. Co., Amsterdam, 580 pp.

PLATZMAN, G.W. (1958): *A Numerical Computation of the Surge of 26th June, 1954, on Lake Michigan.* Geophysica 6, 407-438.

PRANDLE, D. (1978): *Residual Flows and Elevations in the Southern North Sea.* Proc. Roy. Soc. Lond. A, 359, 189-228.

PROUDMAN, J. (1953): *Dynamical Oceanography.* Methuen, London, 409 pp.

RALSTON, A. and WILF, H.S. (1960): *Mathematical Methods for Digital Computers.* Vol. 1, Wiley, New York.

RAMMING, H.G. (1976): *A Nested North Sea Model with Fine Resolution in Shallow Coastal Areas.* Mém. Soc. Roy. Sci. Liège, 6^{e} série, tome X, 9-26.

ROACHE, P.J. (1972): *Computational Fluid Dynamics.* Hermosa Publishers, Alberquerque. 446 pp.

ROCHFORD, D.J. (1966): *Some Hydrological Features of the Eastern Arafura Sea and the Gulf of Carpentaria in August 1964.* Aust. J. Mar. Freshw. Res. 17, 31-60.

RONDAY, F.C. (1976): *Modèles de Circulation Hydrodynamique en Mer du Nord.* Ph.D. Thesis, Liège Univ.

SHULESHKO, P. (1961a): *Comparative Analysis of Different Collocation Methods on the Basis of the Solution of a Torsional Problem.* Aust. J. Appl. Sci. 12, 194-210.

SHULESHKO, P. (1961b): *A Method of Integration over the Boundary for Solving Boundary Value Problems.* Aust. J. Appl. Sci. 12, 393-406.

TAYLOR, G.I. (1920a): *Tidal Oscillations in Gulfs and Rectangular Basins.* Proc. Lond. Math. Soc. (2), 20, 148-181.

TAYLOR, G.I. (1920b): *Tidal Friction in the Irish Sea.* Phil. Trans. Roy. Soc. Lond. A,220, 1-33.

TELEKI, P.G., RABCHEVSKY , G.A. and WHITE, J.W. (1973): *On the Nearshore Circulation of the Gulf of Carpentaria, Australia - a Study in Uses of Satellite Imagery (ERTS) in Remotely Accessible Areas.* Proc. A.S.P. Symposium on Remote Sensing in Oceanog. 1973, Lake Buena Vista, Florida.

TEUBNER, M.D. (1976): *Tidal and Thermal Propagation in the Port River Estuary.* Ph. D. Thesis. U. of Adelaide.

WANG, J.D. and CONNOR, J.J. (1975): *Mathematical Modelling of Near Coastal Circulation.* MIT Rept. No. MITSG75-13.

WILLIAMS, N.V. (1972): *The Application of Resonators and Other Methods to Problems in Oceanography.* Ph. D. Thesis, U. of N.S.W.

The Admiralty Charts and the Australian National Tide Tables, published by the Hydrographer, R.A.N. were also used.